COBALT-SUPPORT COMPOUND FORMATION IN ALUMINA-SUPPORTED COBALT CATALYSTS

by

Bunjerd Jongsomjit

BS in Chemistry, Kasetsart University, Thailand, 1990

MS in Chemical Engineering, Colorado School of Mines, USA, 1998

Submitted to the Graduate Faculty of

the School of Engineering in partial fulfillment

of the requirements for the degree of

Doctor of Philosophy

University of Pittsburgh

2002

UNIVERSITY OF PITTSBURGH

School of Engineering

This dissertation was presented

by

Bunjerd Jongsomjit

It was defended on

May 10, 2002

and approved by

Dr. James G. Goodwin, Jr., Professor of Chemical Engineering

Dr. Irving Wender, Professor of Chemical Engineering

Dr. Shiao-Hung Chiang, Professor of Chemical Engineering

Dr. Joseph J. McCarthy, Assistant Professor of Chemical Engineering

Dr. Jayant Rajgopal, Associate Professor of Industrial Engineering

Dissertation Director: Dr. James G. Goodwin, Jr., Professor of Chemical Engineering Department

ABSTRACT

COBALT-SUPPORT COMPOUND FORMATION IN

ALUMINA-SUPPORTED COBALT CATALYSTS

Bunjerd Jongsomjit, Ph.D.

University of Pittsburgh, 2002

Supported cobalt (Co) catalysts are the preferred catalysts for Fischer-Tropsch synthesis (FTS) based on natural gas. However, Co-support compound formation (Co-SCF) can result in lower activity. It has been found that water vapor present during standard reduction affects the degree of reducibility.

The impact of water vapor on Co-SCF and the resulting characteristics of $Co/\gamma\text{-}Al_2O_3$ and $CoRu/\ \gamma\text{-}Al_2O_3$ catalysts were investigated to develop a better understanding of Co-SCF and the effect of Ru promotion on this formation. The degree of reduction was lower when additional water vapor was introduced during reduction, but to a lesser degree when the Ru promoter was present. It is suggested that the Co "aluminate" formed is not identical to $CoAl_2O_4$ (spinel) but is probably a surface compound deficient in Co. This Co-SCF is a major cause for differences seen in the degree of reducibility, H_2 chemisorption capacity, and Fischer-Tropsch synthesis (FTS) activity.

To minimize Co-SCF, the effect of reduction gas containing carbon monoxide (CO) was investigated. A H_2 flow containing CO (1-9 vol%) was used for standard reduction. After reduction, the pretreated catalyst samples were characterized and CO hydrogenation also performed. Both initial and steady-state rates went through a maximum for the addition of 3-5 vol% CO during standard reduction. It is concluded that the addition of CO during reduction has a significant effect on activity of the catalyst due to increases in both Co reducibility and dispersion. The effect of metal promoters, such as Cu and Zr on Co-SCF was also investigated. However, Cu addition was found to decrease FTS rate.

The impact of Zr modification of alumina had a significant impact on the catalyst properties: FTS rate per gram catalyst increased by a factor of two and reducibility also increased. The impact of Zr modification is likely due to stabilization of the alumina support, prevention or blockage of Co surface "aluminate" formation, and an increase in Co reducibility. Steady-state isotopic transient kinetic analysis (SSITKA) results for CO hydrogenation showed an increase in number of active surface intermediates (N_M) while the intrinsic activity ($1/\tau_M$) remained constant.

DESCRIPTORS

Catalyst Characterization

Catalyst Deactivation

Catalyst Morphology

Co-Aluminate

Co-Based Catalyst

CO Hydrogenation

Copper Promotion

Co-Support Compound Formation

Fischer-Tropsch Synthesis (FTS)

Impregnation

Metal-Support Interaction

Methanation

Modified Support

Ruthenium Promotion

Water Effect

Zirconium Promotion

ACKNOWLEDGMENTS

I would like to thank my advisor, Dr. James G. Goodwin, Jr. for his advice throughout this project. I will never forget his kindness and support during my student life at the University of Pittsburgh. I also would like to extend my thanks to my committee members, Dr. Irving Wender, Dr. Shiao-Hung Chiang, Dr. Joseph J. McCarthy, and Dr. Jayant Rajgopal for sharing their ideas and views for this project.

I would like to thank all my friends who supported me as well. I would like to thank the Energy International, Inc. (EI) for providing some materials used in this project. I also would like to thank the Royal Thai Government for the financial support and giving me the opportunity to further my Ph.D. (Chemical Engineering) at the University of Pittsburgh. I promise to do my best for our country.

Finally, most of all, I would like to thank my beloved parents and my three brothers, who have believed in me, inspired me, and supported me all of my life.

TABLE OF CONTENTS

LIST OF TABLES

LIST OF FIGURES

1.0 INTRODUCTION

Research in heterogeneous catalysis focuses on understanding the fundamental issues involved in the catalytic properties and reactions. Catalysts are chemically and physically complex. With this complexity, they require combined knowledge of chemistry, chemical engineering, physics, and material science to better understand the nature or properties of catalysts. Catalyst properties are divided into three parts: physical, chemical, and dynamic. Physical properties contain surface area, density, pore volume, pore size distribution, particle sizes, thermal and mechanical resistance. Chemical properties focus on the chemical state of active sites, chemical compositions, chemical structure and acidity. The dynamic properties include the catalytic behavior during reaction in terms of activity and selectivity. Understanding the impacts of the catalyst compositions and pretreatments on the catalytic behavior leads to more robust catalysts that can overcome the existing limitations.

In supported catalysts, there is usually three components: an active phase, a promoter, and a support or carrier. As mentioned before, the catalyst compositions, structure and pretreatments definitely affect the catalyst properties. For instant, in supported cobalt (Co) catalysts, compound formation between Co and the supports such as alumina or silica can occur leading to deactivation of the catalysts due to the loss in Co metal active sites.[1-14]* It is known that supported Co catalysts are the preferred catalysts for Fischer-Tropsch synthesis (FTS) based on natural gas because of their high activity for FTS[15], high selectivity to linear hydrocarbons,

* Parenthetical references placed superior to the line of text refer to the bibliography.

and low activity for the water-gas shift reaction.[16-17] In order to stabilize the catalyst activity, the amount of Co-support compound formation (Co-SCF) needs to be minimized.

This dissertation focuses on understanding the nature of Co-SCF in alumina-supported Co catalysts along with applying some strategies to minimize the amount of Co-SCF. The catalysts were prepared, pretreated, characterized, and then tested in the reaction. The first part of the dissertation addresses the nature or properties of Co-SCF and its effect on the characteristics of the catalysts. The obtained results are used as a bench mark for the identification of Co-SCF. Effect of ruthenium (Ru) was also investigated in this part.

The second portion of this dissertation focuses on the effect of reduction gas containing carbon monoxide (CO) on Co-SCF. It can be assumed that the presence of CO during FTS may prevent the Co catalysts from rapidly deactivating due to decreasing the impact of water vapor produced. It was found that the addition of CO had impacts on Co-SCF in some levels depending on the partial pressure of CO, H_2, and water vapor during reduction.

The remainder of the dissertation focuses on effect of copper (Cu) and zirconium (Zr) promotion on Co-SCF based on the hypothesis that the addition of these promoters may help to block Co-SCF. It was found that Cu itself is very active for H_2 chemisorption, but the rate during CO hydrogenation decreases with Cu promotion. Contrary to Cu, Zr itself is not active for H_2 chemisorption, but the rate increases with Zr promotion.

2.0 BACKGROUND

2.1 Fischer-Tropsch Synthesis (FTS)

Fischer-Tropsch synthesis (FTS) is a means to convert synthesis gas obtained from natural gas reforming and coal gasification, into mainly desirable long chain hydrocarbons. During the past decades, FTS has been developed continuously by many researchers, although the rise and fall in research intensity on this process has been highly related to the demands for liquid fuels and relative economics. This synthesis is basically the reductive polymerization (oligomerization) of carbon monoxide by hydrogen to form organic products containing mainly hydrocarbons and some oxygenated products in lesser amounts.[1] The main reactions of FTS are:

$$\mathbf{CO} + \left(1+\frac{m}{2n}\right)\mathbf{H_2} \rightarrow \left(\frac{1}{n}\right)\mathbf{C_nH_m} + \mathbf{H_2O} \qquad \mathbf{(1)}$$

$$\mathbf{CO + 3H_2 \rightarrow CH_4 + H_2O} \qquad \mathbf{(2)}$$

$$\mathbf{CO + H_2O \rightarrow CO_2 + H_2} \qquad \mathbf{(3)}$$

$$\mathbf{2CO \rightarrow C + CO_2} \qquad \mathbf{(4)}$$

Equations **(1)** is the formation of hydrocarbons higher than C_1, and the equation **(2)** is methanation. The water-gas shift reaction, which is undesirable for natural gas conversion, is shown in equation **(3)**. The Boudouard reaction, which results in carbon deposition on the catalyst surface, is shown in equation **(4)**.[2] Depending upon the type of catalyst used,

promoters, reaction conditions (pressure, temperature and H_2/CO ratios), and reactor, the distribution of the molecular weight of the hydrocarbon products can be noticeably varied.[3]

Normally, catalysts used for this synthesis are group VIII metals. By nature, the hydrogenation activity increases in order of Fe < Co < Ni < Ru. Ru is the most active. Ni forms predominantly methane, while Co yields much higher ratios of paraffins to olefins and much less oxygenated products such as alcohols and aldehydes than Fe does.[1]

With regards to the operating conditions, usually higher pressures will result in higher rates. Entrained bed reactors or slurry bubble column reactors are better than fixed-bed reactors for FTS since they can remove heat from this exothermic synthesis, allowing better temperature control.

The current main goal in using FTS is to obtain high molecular weight, straight chain hydrocarbons. However, methane and other light hydrocarbons are always present as less desirable products from the synthesis. According to the Anderson-Schulz-Flory (ASF) product distribution, typically 10 to 20% of products from the synthesis are usually light hydrocarbons (C_1-C_4). These light alkanes have low boiling points and exist in the gas phase at room temperature, which is inconvenient for transportation. Many attempts have been made to minimize these byproducts and increase the yield of long chain liquid hydrocarbons by improving chain growth probability. It would be more efficient to be able to convert these less desirable products into more useful forms, rather than re-reforming them into syngas and recycling them.

2.2 Co-Based Catalysts

Supported cobalt (Co) catalysts are the preferred catalysts for the synthesis of heavy hydrocarbons from natural gas based syngas (CO and H_2) because of their high Fischer-Tropsch (FT) activity, high selectivity for linear hydrocarbons, and low activity for the water-gas shift reaction.[3-4] It is known that reduced cobalt metal, rather than its oxides or carbides, is the most active phase for CO hydrogenation in such catalysts.[5] Investigations have been done to determine the nature of cobalt species on various supports such as alumina[6-14], silica[12-13,15-17], titania[12-13,16,18], magnesia[12-13,19], carbon[12-13,20], and zeolites.[21-22] The influence of various types of cobalt precursors used was also investigated.[23] It was found that the use of organic precursors such as Co (III) acetyl acetate resulting in an increase of CO conversion compared to that of cobalt nitrate.

2.3 Synthesis of Co-Based Catalysts

Basically, a typical heterogeneous metal catalyst may consist of three components: an active catalytic phase, a promoter, which increases activity and/or stability, and a high surface area support which is used to facilitate the dispersion and stability of the active catalytic phase. Transition metals and/or their oxides, sulfides, carbides, and nitrates are used as active catalytic phases because of their abilities to catalyze chemical reactions. This is because of their multiplicity of low energy surface electronic states, which can readily donate or accept electrons in the process of making or breaking bonds at a surface.[24] Catalyst supports are typically porous, high surface area, thermally stable carbon or metal oxides such as alumina, silica, titania,

zeolites, etc. Alumina and silica are two of the supports most commonly used commercially. In many cases, interaction between a support and a catalytic component can occur and can cause a decrease in the active catalytic phase, resulting in lower activity.

When cobalt-based catalysts are prepared mainly by incipient wetness impregnation, cobalt oxide is formed during calcination. Once standard reduction is carried out, most of the cobalt oxide will have been transformed to cobalt metal. The origins of TPR peaks observed for calcined alumina-supported cobalt catalysts have been discussed in several articles.[9,14,25] The lower temperature peak is usually assigned to reduction of crystalline Co_3O_4 particles. The higher temperature peak is attributed to the reduction of highly dispersed amorphous cobalt oxide, which is interacting strongly with the support. These reduction peaks are shifted to lower temperature by introducing a small amount of a noble metal, such as Ru, as a reduction promoter.[6,26-28]

In order to clarify the identity of the reduction peaks in TPR for CoRu/γ-Al_2O_3 catalysts, XRD measurements were conducted by Zhang et al.[29] with the catalyst at various stages during TPR. They found that the diffraction peak for CoO appears after completion of the lower temperature peak during TPR. This indicates that Co_3O_4 in the catalyst reduced to CoO during the generation of this peak. It was determined that hydrogen consumed during this peak in the absence of added water vapor is much larger than that required for the reduction of Co_3O_4 to CoO. It was suggested that reduction of some CoO to cobalt metal also took place during the lower temperature peak, probably Co existing in the large particles of cobalt oxide. Thermodynamics calculations were carried out to explain the effect of water vapor on the reducibility of the cobalt catalyst. The calculated results indicated that the degree of reduction decreases with increasing P_{H2O}/P_{H2} ratio and temperature. However, thermodynamically, the

effect of water vapor on the reduction of Co_3O_4 is very small. The near total reduction of bulk Co_3O_4 in H_2 is essentially feasible even in the presence of large amounts of water vapor. This is consistent with the results of TPR for unsupported Co_3O_4. Therefore the reduction of large particles of Co_3O_4 present on the CoRu/γ-Al_2O_3 catalyst has not been significantly affected by thermodynamic limitations even with the added water vapor.

2.4 Effects of Reduction Promoters

Generally, there are two types of promoters, textural and chemical promoters. Textural promoters are used to facilitate the dispersion of metal phase during preparation and/or reaction conditions. Chemical promoters are used to enhance the activity and/or selectivity of catalysts. Mostly, noble, alkali, and alkaline earth metals are considered to be chemical promoters, which play important roles on catalyst performances to date.

The effects of promoters such as Ru, Zr, La^{3+}, Rh, and Pt on Co catalysts were investigated.[27,30-34] It was found that metal promoters can increase the reducibility of Co[27,35], preserve the activity by preventing the carbon deposition[16], exhibit cluster and ligand effects, act as source of hydrogen spillover[26], and enhance Co reducibility and dispersion.[27-28]

2.5 Cobalt-Support Compound Formation (Co-SCF)

Compound formation between cobalt metal and the support can occur under pretreatment and/or reaction conditions, leading to catalyst deactivation. The compound formation of cobalt

metal with support materials, however, is difficult to predict because of the lack of sufficient thermodynamic data. Co-support compound formation can be detected evidentially.

2.5.1 Co-Aluminate Formation

Interaction of cobalt with its alumina support has been observed by many authors[6-14] using various techniques including TPR, XRD, EXAFS, and XPS (ESCA). The migration of cobalt ions into the alumina lattice sites of octahedral or tetrahedral symmetry is limited to the first few layers of the support under normal calcination conditions.[7] The reaction of Co with γ-Al_2O_3 can form a surface spinel in Co/γ-Al_2O_3 catalysts. The surface spinel structure can not be observed by X-ray diffraction because it does not have long range, three dimensional order.[7,36] It has been suggested that cobalt ions occupying surface octahedral sites of γ-Al_2O_3 are reducible while cobalt ions occupying tetrahedral sites are non-reducible[7], at least at temperatures $\leq$ 900°C. At lower calcination temperatures, filling of the octahedral sites is more favorable. Filling of the tetrahedral sites of γ-Al_2O_3 may be enhanced by an increase in calcination temperature.[7]

2.5.2 Co-Silicate Formation

The formation of cobalt silicates on Co/SiO_2 under hydrothermal conditions has been extensively studied by Kogelbauer et al.[27]. Hydrothermal treatment at 220°C led to a catalyst with lower reducibility due to the formation of both reducible and non-reducible (at temperatures $\leq$ 900°C) cobalt silicates. It was found that hydrothermal treatment of the reduced catalyst or hydrothermal treatment of the calcined catalyst in the presence of hydrogen produces cobalt

silicates, while hydrothermal treatment of the calcined catalyst in air does not result in their formation. Hydrothermal treatment of the calcined catalyst in inert gas also has little effect.

2.6 Impact of Water Vapor

Cobalt-support interaction and compound formation can occur during standard reduction, and temperature programmed reduction (TPR), especially in the presence of water. In a preliminary study for this presented research, Zhang et al.[29] investigated the reducibility of $CoRu/\gamma\text{-}Al_2O_3$ during standard reduction, TPR, and in the presence of water. The amount of cobalt able to be reduced during standard reduction at 350°C for 10 h was determined by pulse oxidation at 400°C. It was found that in a differential reactor and in the absence of added water vapor, 92% of the cobalt was able to be reduced during standard reduction with only 3.9% additionally reduced during TPR to 900°C. Introduction of water vapor decreased the degree of reduction of cobalt during standard reduction as well as the total amount able to be reduced up to 900°C. The degree of reduction decreased from 92% to 45% after introduction of 3% water vapor in the standard reduction process. Approximately 25% of cobalt could be additionally reduced during TPR to 900°C, while ca. 30% remained as non-reducible cobalt species. Introduction of water vapor to the system both during the ramping and the holding periods had a significant influence on the degree of reduction of cobalt. However, introduction of water vapor during either just the temperature ramp or the temperature holding period of the standard reduction procedure produced only a partial decrease in the reducibility. It can be concluded that water has a significant effect on the reduction behavior of $CoRu/\gamma\text{-}Al_2O_3$. Introduction of water vapor during standard reduction led to a decrease in the degree of reduction of the cobalt

probably in two ways: (i) inhibition of the reduction of well-dispersed CoO interacting with the alumina support possibly by increasing the cobalt-alumina interaction, and (ii) facilitation of migration of the cobalt ions into probable tetrahedral sites of γ-Al_2O_3 to form a non-reducible (at temperatures < 900°C) spinel. Such an irreversible spinel formation results in a decrease in the amount of reduced cobalt metal atoms available to catalyze reactions. Effect of water vapor on TPR profiles for unsupported Co_3O_4 is shown in Figure 2.1.[29] The effect of water vapor on reducibility at 30°-900°C for CoRu/γ-Al_2O_3 catalysts is also shown in Figure 2.2.[29]

2.7 Formation of Metal Aluminates from g-Alumina

The formation of metal aluminate spinel compounds at high temperatures (1200°C and above) has been studied.[37-41] Using metal oxide (MO)/Al_2O_3 indicated that the formation of MAl_2O_4 had a parabolic growth rate with the diffusion of M^{2+} into Al^{3+} ions. Bolt et al.[42] studied the rate of metal aluminate in MO/Al_2O_3 (M = Ni, Co, Cu, and Fe) at 500°-1000°C. The preparation method was based on chemical vapor deposition (CVD). The formation rate of MAl_2O_4 was determined using Rutherford back scattering spectroscopy and X-ray diffraction. The morphology of the samples was identified using scanning electron microscopy (SEM). They found that the formation rate of MAl_2O_4 was as follows: $CuAl_2O_4$ > $CoAl_2O_4$ > $NiAl_2O_4$ > $FeAl_2O_4$. The CuO/Al_2O_3 system was the fastest to form the spinel ($CuAl_2O_4$) because Cu ions penetrated more deeply into the substrate.

2.8 Metal Additive Modified Supports

In order to improve the catalyst performance, besides the addition of metal promoters into the metal catalytic phase, many studies have concentrated on the used to metal additives or mixed oxides to modify the interaction between the support or carrier and the metal active phase. It is known that the interaction between the active phase and the support has an impact on the chemical state and dispersion, which will cause any change in the catalyst performance. The effect of alkali cations on the dispersion of Ni, Co, and Mo supported on alumina has been studied by many authors.[43-47] The surface properties of Ni and Co supported on Ge^{4+}, Ga^{3+}, and Zn^{2+} modified aluminas have been investigated by many authors as well.[36,48-53] Stranick et al.[54] investigated the influence of boron on the chemical state and dispersion of Co/Al_2O_3 by bulk and surface spectroscopic techniques. They found that the presence of boron had an effect on the catalysts with Co loading in excess 1.5 wt% by increasing the overall Co dispersion and also a changing the chemical state of Co (as Co_3O_4, and tetrahedral or octahedral Co^{2+}). Rohr et al.[55] investigated the effect of adding zirconia to an alumina support in supported Co catalysts. They found that for methanation at 5 bar and H_2/CO of 9/1, zirconia-modified alumina supported Co exhibited an increase in the activity and selectivity to C_{5+} hydrocarbons. SSITKA also showed the same intrinsic activity. The use of Co/SiO_2-Al_2O_3 (a mixed oxide) for FTS was performed by Sharma et al..[56] It was found that the optimal selectivity to C_{5+} resulted.

2.9 Aluminate-Supported Copper Oxide

Alumina-supported copper (Cu) catalysts are used for an oxidation of methane to CO_2. However, Cu "aluminate" formation can occur resulting in the lower catalyst activity due to a loss in CuO for catalyzing the reaction. It is known that alumina is a spinel with cationic vacancies because of the trivalent state of the alumina ions. At high temperature, Cu^{2+} can migrate into the alumina matrix and form copper-aluminate[57] as well, resulting in catalyst deactivation. In order to prevent the reaction between copper and the alumina support, a use of an aluminate support (instead of an alumina support) was investigated. This is because Cu^{2+} ion migration is limited by the cationic vacancy occupancy. The catalytic combustion of methane on aluminate-supported copper oxide was studied by Artizzu et al..[58] In the study, in order to avoid copper-aluminate formation in CuO/Al_2O_3[58], copper oxide was deposited onto high surface area magnesium alumina spinel ($MgAl_2O_4$). They found that the deposition of CuO on $MgAl_2O_4$ led to an efficient catalyst for the total oxidation of methane with 100% selectivity to CO_2.

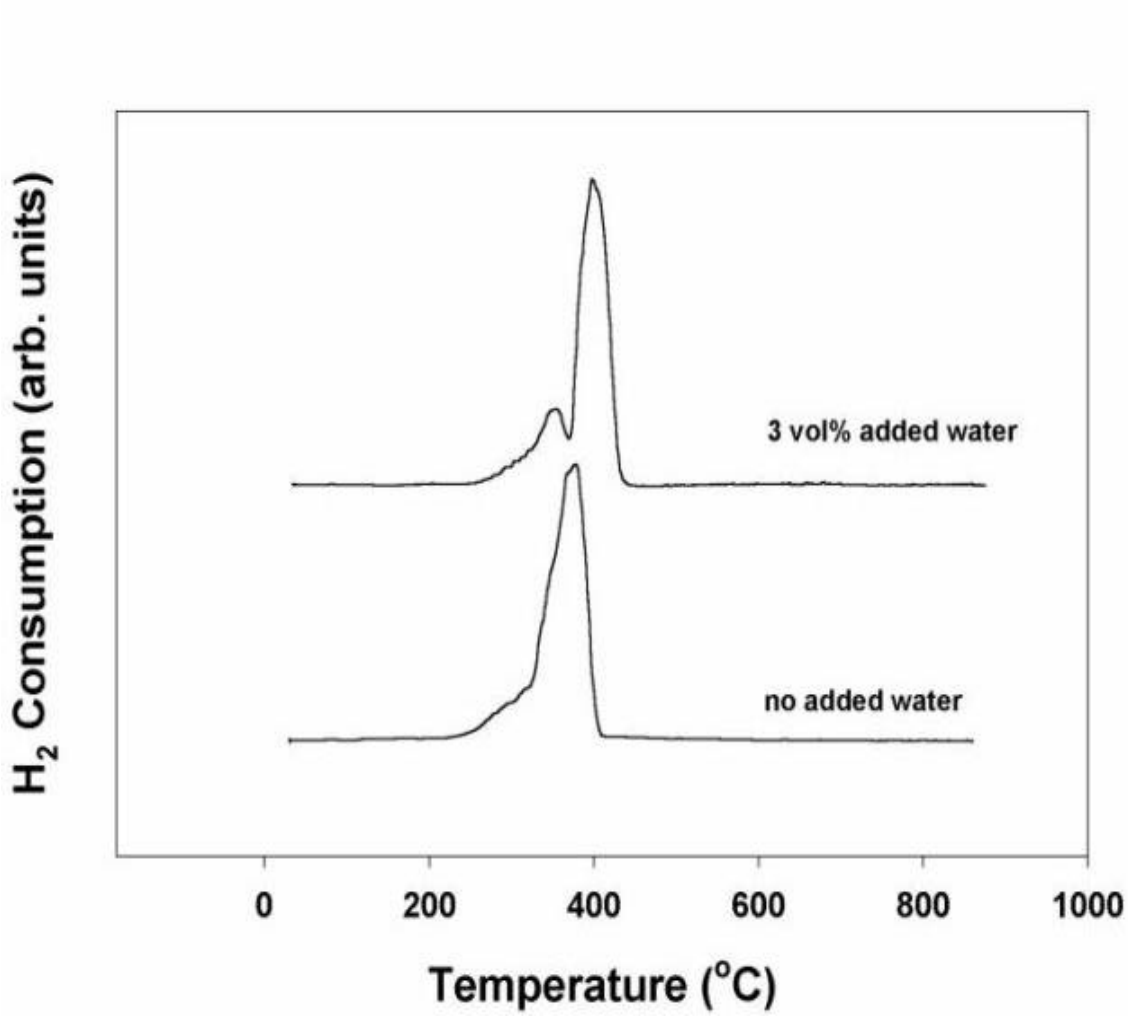

Figure 2.1 Effect of Water Vapor on TPR Profiles for Unpromoted Co_3O_4[29]

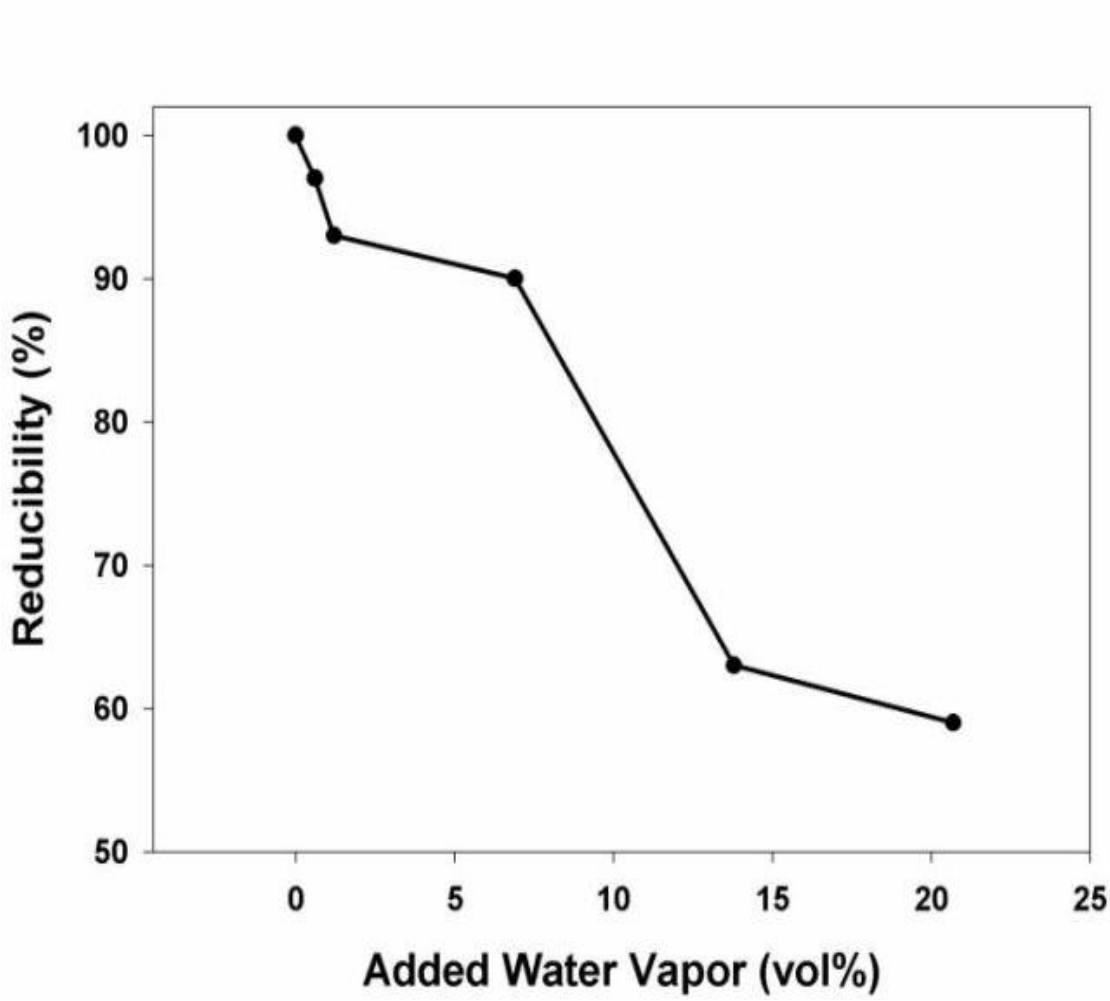

Figure 2.2 Effect of Added Water Vapor During TPR at 30^{o}-900^{o}C on the Reducibility of $CoRu/Al_2O_3$ Catalyst[29]

3.0 RESEARCH OBJECTIVES

The main objective of this research was first to develop a better understand of Co-support compound formation (Co-SCF) and then to apply some strategies to minimize the amount of this formation in order to, at least, stabilize the catalyst activity during Fischer-Tropsch synthesis (FTS). In details, this research was conducted in order to:

3.1 Develop a Better Understanding of Co-SCF

It is known that water vapor present as a byproduct of reduction and reaction causes an increase in the amount Co-SCF, leading to irreversible catalyst deactivation. In order to minimize the amount of Co-SCF, it is very important to first fully understand the nature of Co-SCF and its effect on the characteristics of catalysts using different characterization techniques such as BET surface area, XRD, Raman spectroscopy, H_2 chemisorption, SEM, EDX, and TPR.

3.2 Use of Strategies to Minimize Co-SCF

In order to stabilize the catalyst activity, the amount of Co-SCF must be minimized. This research also focused on how to use some strategies to decrease the amount of Co-SCF. These included the investigation of:

3.2.1 Effect of Reduction Gas Containing Carbon Monoxide (CO)

Reduction gas compositions can also affect the amount of Co-SCF. It can be observed that FTS at high conversion results in high partial pressures of water vapor as a byproduct without significant deactivation of Co catalysts. Thus, it is assumed that the present of CO may help to prevent the Co catalyst from rapidly deactivating due to Co-SCF. The effect of the presence of small quantities of CO during reduction was investigated.

3.2.2 Effect of Metal Promoters

Any means by which Co-support compound formation can be diminished could potentially lead to more robust catalysts. Catalyst additives, which preferentially form surface compounds with the support offer potentially opportunity to block Co-support compound formation. Metal modified supports might change the interaction between the active phase and the support as well. The effect of Ru, Zr, and Cu was investigated. Of course, the downside of any additives, i.e., interference with the catalytic properties of Co metal, was evaluated as well.

4.0 RESEARCH METHODOLOGY

A schematic of research methodology is illustrated in Figure 4.1. Basically, the research methodology applied was based on the following:

4.1 Catalyst Preparation

All catalyst samples were prepared as described in detail in each experimental chapter using the incipient wetness impregnation method. The base alumina-supported Co catalyst contained 20 wt% of Co in γ-Al_2O_3.

4.2 Catalyst Pretreatment

4.2.1 Calcination

Calcination was carried out at 300^{o}C in air for 2 h to decompose the various catalyst precursors, such as nitrates, and convert them to their oxide forms.

4.2.2 Reduction

Standard reduction for supported Co catalysts was carried out at 350^{o}C in H_2 for 10 h to convert oxides and/or catalyst precursor salts to metal.

4.2.3 Passivation

Passivation of metal catalysts after reduction is required prior to exposure to air due to the exothermicity of metal oxidation. This exothermicity can result in a significant increase in temperature of the catalyst resulting in a catalyst degradation and a potential fire hazard. Passivation is used to protect the surface of reduced catalysts from rapid oxidation. It is common to passivate metal by creating a layer of oxide on the surface with will decrease the activity of oxidation, thus, a decrease in the generated heat. Passivation of the reduced catalysts was carried out at room temperature with an O_2/He (5.2% of O_2) flow mixture for 2 h.

4.3 Catalyst Characterization

4.3.1 BET Surface Area

BET surface area was used to determine the total surface area of catalysts using N_2 adsorption at 77 K. It was performed using a Micromeritics ASAP 2010.

4.3.2 X-ray Powder Diffraction (XRD)

XRD was used to determine the bulk catalyst phases.

4.3.3 Raman Spectroscopy

Raman spectroscopy is a more surface sensitive technique compared to XRD. It was used to study the oxidation states and interactions of metal oxides.

4.3.4 Scanning Electron Microscopy (SEM)

SEM was performed to study the morphology of the catalysts.

4.3.5 Energy Dispersive X-ray Spectroscopy (EDX)

EDX was used to analyze the elemental distribution and concentrations.

4.3.6 H_2 Chemisorption

Static H_2 chemisorption at 100^oC on the reduced cobalt catalysts was used to determine the number of reduced surface cobalt metal atoms. This is usually related to the overall activity of the catalysts during FTS. It was performed using a Micromeritics ASAP 2010.

4.3.7 Temperature Programmed Reduction (TPR)

TPR was performed to determine the reduction behavior and reducibility of catalysts. It was carried out in an Altamira AMI-1 system.

4.4 Reaction (CO hydrogenation)

CO hydrogenation was performed to evaluate the catalyst performance in terms of activity and selectivity. CO hydrogenation was carried out in a fixed-bed reactor under differential conditions.

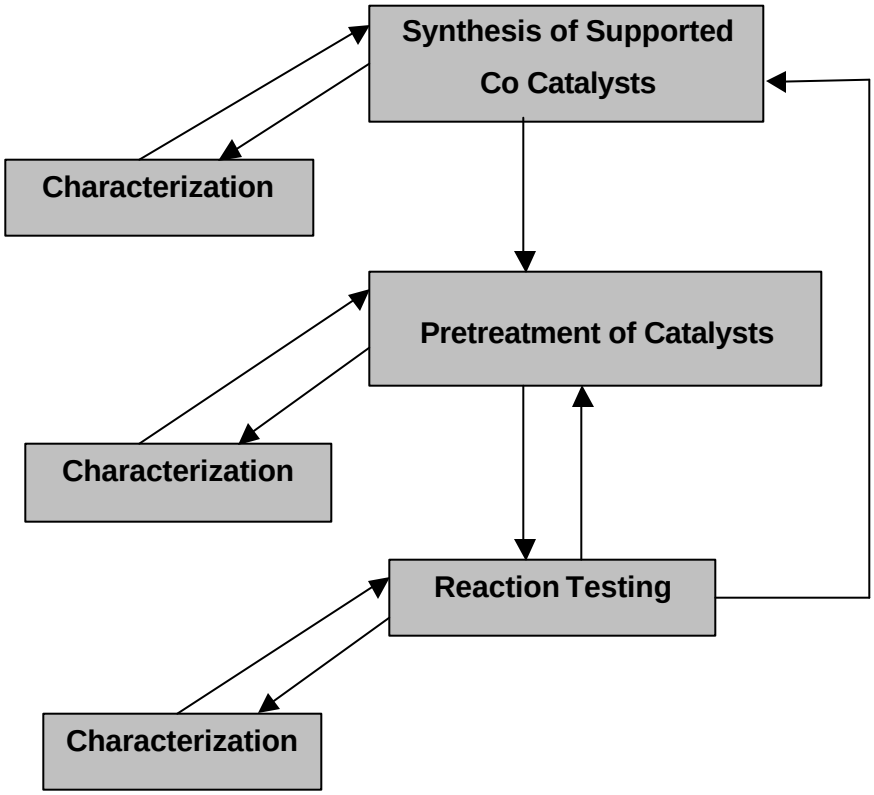

Figure 4.1 Illustration of a Schematic of Research Methodology

5.0 COBALT-SCF AND EFFECT OF RUTHENIUM PROMOTION

5.1 Introduction

The effects of noble metal promoters such as Ru[1-3], Rh[4,5] and Pt[6] on cobalt-based catalysts have been investigated. It has been proposed that these metal promoters can increase the reducibility and dispersion of Co[1,6-8], preserve the activity by preventing the formation of coke[9], exhibit cluster and ligand effects[10], and act as a source for hydrogen spillover.[11]

In a previous TPR study reported from our laboratory, Zhang et al.[12] investigated the reducibility of CoRu/γ-Al_2O_3 during standard reduction and during TPR in the presence of added water vapor. It was confirmed that water has a significant effect on the reduction behavior of CoRu/γ-Al_2O_3. Water vapor present during standard reduction was suggested to lead to a decrease in the degree of reduction of the cobalt in possibly two ways: (i) inhibition of the reduction of well-dispersed CoO interacting with the alumina support possibly by increasing the cobalt-alumina interaction, and (ii) facilitation of the migration of cobalt ions into probable tetrahedral sites of γ-Al_2O_3 to form a non-reducible (at temperatures $\leq 900°C$) spinel. This irreversible compound formation results in a decrease in the amount of reducible cobalt metal atoms using conventional reduction procedures. Although the effect of water vapor on the reducibility during standard reduction and TPR were studied, the nature of the Co-support compounds formed was not identified due to the limitations of the experimental techniques used.

It is known that water vapor is a byproduct of metal catalyst reduction. In a laboratory, the amount of water can be minimized; but, during reduction of the catalyst on an industrial

scale, this is more difficult. Thus, we need to understand the impact of water on cobalt-support compound formation and how it can be minimized during catalyst reduction and subsequent reaction.

The nature of Co-support compound formation and its effect on the characteristics of the catalysts were the focus of the present research. It is very important to fully understand the impact of water vapor on the formation of Co-support compounds and their nature in order to develop a strategy to minimize their formation. The main objectives of this study were to develop further knowledge about Co-support compound formation during reduction, to better identify the compounds formed, and to investigate the effect of noble metal (Ru) promotion on Co-support compound formation. In the present study, $Co/\gamma\text{-}Al_2O_3$ and $CoRu/\gamma\text{-}Al_2O_3$ catalysts were pretreated under various conditions and were then characterized using BET, XRD, SEM, EDX, Raman spectroscopy, TPR, and H_2 chemisorption.

5.2 Experimental

5.2.1 Catalyst Preparation

5.2.1.1 $Co/\gamma\text{-}Al_2O_3$. The $Co/\gamma\text{-}Al_2O_3$ catalyst was prepared by the incipient wetness impregnation of $\gamma\text{-}Al_2O_3$. The support precursor (Al_2O_3, Vista B) was first calcined at 500°C for 10 h before impregnation in order to put it in the form of $\gamma\text{-}Al_2O_3$ having a specific surface area of 209 m^2/g and average particle size ca. 60 μm. Cobalt nitrate [$Co(NO_3)_2 \bullet 6H_2O$] was dissolved in de-ionized water and impregnated into the support using incipient wetness to give a final reduced catalyst with 20 wt% cobalt. The catalyst was dried at 110°C for 12 h and calcined in air at 300°C for 2 h.

5.2.1.2 CoRu/γ-Al_2O_3. The CoRu/γ-Al_2O_3 catalyst was also prepared by the incipient wetness co-impregnation method. The same γ-Al_2O_3 support as mentioned before was used. Cobalt nitrate and ruthenium (III) nitrosyl nitrate [$Ru(NO)(NO_3)_3$] were dissolved in de-ionized water and co-impregnated into the support to produce a reduced catalyst with 20 wt% cobalt and 0.5 wt% ruthenium. The catalyst was also dried at 110°C for 12 h and calcined in air at 300°C for 2 h.

5.2.1.3 $CoAl_2O_4$ (spinel), CoO, and Co_3O_4 (spinel). In order to identify the Raman bands and XRD peaks of the samples, cobalt aluminate (spinel) [98% $CoAl_2O_4$, 39-41% Co], cobalt (II) oxide [95% CoO] from Alfa Aesar and cobalt (II, III) oxide [99.5% Co_3O_4] from Strem Chemicals, Inc. were used as reference materials.

5.2.2 Catalyst Pretreatment

The catalysts were characterized following three pretreatments. These were as follows:

(i) after the original calcination step,

(ii) after standard reduction of the calcined catalysts in a high space velocity (16,000 h^{-1}) of H_2 at 350°C for 10 h and passivation with an O_2/He (5.20% of O_2) mixture at room temperature for 2 h,

(iii) after standard reduction of the calcined catalysts in a high space velocity (16,000 h^{-1}) of H_2 with 3% of added water vapor at 350°C for 10 h followed by passivation with an O_2/He (5.20% of O_2) mixture at room temperature for 2 h.

While the concentration of water vapor during reduction without added water vapor was certainly not zero, it was very low due to the high space velocity used.

5.2.3 Catalyst Nomenclature

The nomenclature used for samples in this study is the following:

C: the calcined catalyst samples

RP: the reduced and passivated catalyst samples

$\boldsymbol{R_WP}$***:*** the catalyst samples reduced in H_2 with 3% added H_2O vapor and then passivated

5.2.4 Catalyst Characterization

5.2.4.1 BET Surface Area. BET surface area measurements were performed to determine if the total surface area changes following different pretreatment conditions. The surface area was determined using N_2 adsorption at 77 K in a Micromeritics ASAP 2010.

5.2.4.2 X-ray Powder Diffraction (XRD). XRD was performed to determine the bulk crystalline phases of the catalysts following different pretreatment conditions. X-ray powder diffraction patterns of samples were collected using a Philips X'pert X-ray diffractometer with monochromatized Cu-K_α radiation (λ = 1.54439 Å). The spectra were scanned at a rate of 2.4 degree/min from 2θ = 20 to 80 degrees.

5.2.4.3 Raman Spectroscopy. The Raman spectra of the samples were collected by projecting a continuous wave laser of Argon ion (Ar^+) green (514.532 nm) through the samples exposed to air at room temperature. A scanning range between 0 to 1000 cm^{-1} with a resolution of 2 cm^{-1} was

applied. The data were analyzed using the Renishaw WiRE (Windows-based Raman Environment) software, which allows Raman spectra to be captured, calibrated, and analyzed using system 2000 functionality via the Galactic GRAMS interface with global imaging capacity.

5.2.4.4 SEM and EDX. Particle microstructure and elemental distribution were determined using scanning electron microscopy (SEM) and energy dispersive X-ray spectroscopy (EDX), respectively. SEM and EDX analysis were performed using a Philips XL30 FEG electron microscope. SEM micrographs were further analyzed using Scion Beta 2 image analysis software for determination of areas and perimeters of particle projections. Elemental distribution data were further analyzed using EDAX software.

5.2.4.5 Hydrogen Chemisorption. Static H_2 chemisorption at 100°C on the reduced cobalt catalysts (re-reduced at 350°C) was used to determine the number of reduced surface cobalt metal atoms. This is related to the overall activity of the catalysts during FTS. Gas volumetric chemisorption at 100°C was performed using the method described by Reuel and Bartholomew.[13] The experiment was performed in a Micromeritics ASAP 2010 using ASAP 2010C V3.00 software.

5.2.4.6 Temperature Programmed Reduction (TPR). TPR was performed to determine the reducibilities of the catalyst samples. TPR was carried out in an Altamira AMI-1 system. It was conducted using 50 mg of catalyst and a temperature ramp from 30ºC to 900ºC at 5ºC/min. The carrier gas was 5% H_2 in Ar. A cold trap (-70ºC) was placed before the detector to remove water

produced during the reaction. A thermal conductivity detector (TCD) was used to determine the amount of hydrogen consumed. The hydrogen consumption was calibrated using TPR of silver oxide (Ag_2O) at the same conditions. The *RP* and *RWP* catalyst samples were re-calcined at the original calcination conditions before performing TPR.

5.2.5 Reaction

FTS was carried out at 220°C and 1 atm total pressure. A flow rate of H_2/CO/Ar = 60/30/10 cc/min in a fixed-bed reactor under differential conditions was used. Thermocouples at the top and the bottom of the catalyst bed assured precise temperature control during pretreatment and reaction. Typically, 0.2 g of the pretreated catalyst sample was re-reduced *in situ* in flowing H_2 (50 cc/min) at 350°C for 10 h prior to FTS. In order to avoid exotherms and hot spots that lead to rapid catalyst deactivation, the reaction was initiated in a controlled manner by gradually increasing the reactant concentrations over a period of 2 h. After the start-up, samples were taken at 3-h intervals and analyzed by GC. Steady state was reached after 24 h in all cases.

5.3 Results

5.3.1 BET Surface Area

BET surface areas of the Co catalysts after various pretreatments were all slightly less than that of the alumina support (209 m^2/g). Since all the surface areas of the catalyst samples in this study ranged between 171-188 m^2/g (Table 5.1), there was no significant change in surface areas after the various pretreatments within experimental error.

5.3.2 X-ray Diffraction

XRD patterns of the Co and CoRu catalysts following different pretreatment conditions are shown in Figure 5.1. The calcined samples of Co-*C* and CoRu-*C* had identical XRD patterns. The diffraction peaks at 31.3°, 36.8°, 59.4°, and 65.4° are those of Co_3O_4. The XRD patterns of reduced and passivated samples of Co-*RP*, Co-R_WP, CoRu-*RP* and CoRu-R_WP were also essentially identical. The diffraction peaks at 42.6° and 61.8° in both catalyst series were due to CoO. No peaks for Co metal were seen in any of the XRD patterns due to overlap with those for γ-Al_2O_3. For reference, XRD of the alumina support, CoO, $CoAl_2O_4$ (spinel), and Co_3O_4 (spinel) was carried out, and their XRD patterns are also shown in Figure 5.1. No peaks for $CoAl_2O_4$ (spinel) were detected for any of the catalyst samples.

5.3.3 Raman Spectroscopy

Raman spectra for Co and CoRu catalysts after different pretreatment conditions are shown in Figure 5.2. Strong Raman bands for Co-*C* and CoRu-*C* were observed at 694, 528, and 488 cm^{-1} which can be assigned to Co_3O_4.[14,15] Raman bands for Co_3O_4 were not apparent for Co-*RP*, Co-R_WP, CoRu-*RP* and CoRu-R_WP because of its reduction to CoO and Co metal. Broad Raman bands between 400-750 cm^{-1} can be observed in the reduced and passivated samples of Co-*RP*, Co-R_WP, CoRu-*RP*, and CoRu-R_WP. However, the peak area in that region was significant more apparent when 3% added water vapor was present during standard reduction. For the same pretreatment conditions, the broad peak in that region was apparently diminished when Ru promotion was used. In order to identify the Raman bands of the samples, Raman spectra of bulk CoO, Co_3O_4 (spinel), and $CoAl_2O_4$ (spinel) were collected and are also shown in Figure 5.2. It indicates that $CoAl_2O_4$ (spinel) has strong Raman bands at 198, 412, 480, 519,

619, 690, and 753 cm^{-1}. The broad Raman bands of the catalyst samples between 400-750 cm^{-1} are clearly not identical with those of $CoAl_2O_4$ (spinel), CoO, or Co_3O_4.

5.3.4 Scanning Electron Microscopy

SEM micrographs of Co and CoRu after various pretreatment conditions are shown in Figures 5.3 to 5.6. The term "granule" is used here to refer to the overall catalyst particles composed of Co, Ru (for CoRu), and γ-Al_2O_3. The term "patches" will be used to refer to entities rich in Co supported on the catalyst granules. In all the SEM figures, the white or light spots on the catalyst granules represent high concentrations of cobalt and its compounds while the darker areas of the granules indicate the support with minimal/no cobalt present. Figures 5.3 and 5.4 show SEM micrographs of the catalysts after initial calcination (Co-*C* and CoRu-*C*) on the carbon tapes used for holding the catalyst samples (the dark background). Figure 5.3 shows the typical overall shapes of the granules of the catalysts studied. It can be seen in Figure 5.4 that Co on the CoRu catalyst granules was more dispersed (i.e., smaller SEM-visible patches/particles) than on the unpromoted Co catalyst. The morphologies of the catalyst granules changed insignificantly for the most part after the different reduction conditions (not shown here). However, the most dramatic change is shown in Figure 5.5. As can be seen, there was a significantly greater number of small Co patches/particles on Co-*RP* granules than on Co-R_WP ones. This same phenomenon was also observed for CoRu-*RP* and CoRu-R_WP as shown in Figure 5.6.

5.3.5 Temperature Programmed Reduction

TPR profiles of bulk Co_3O_4 and the Co and CoRu catalysts after different pretreatment conditions are shown in Figure 5.7. As can be seen in the figure, one reduction peak envelop for bulk Co_3O_4 was obtained. This can be assigned to the two-step reduction of Co_3O_4 to CoO and then to Co^0.[6,12,,16]

There were three major reduction peaks for Co-*C* located at ca. 200°C, 300°C, and between 400-750°C (max. at 600°C). These peaks have been related to the following steps: decomposition of residual Co nitrate, $Co_3O_4 \rightarrow CoO$, $CoO \rightarrow$ Co metal, and Co_XO_Y-$Al_2O_3 \rightarrow$ Co metal.[1,6,17-18] However, after reduction, passivation, re-calcination and TPR, there were only two peaks left for Co-*RP* and Co-R_WP located at ca. 350°C and between 400-750°C.

For the CoRu catalyst after different pretreatment conditions, there were always only two peaks. For CoRu-*C*, these were located at ca. 200°C and between 250-550°C (max. at 400°C). After reduction, passivation, re-calcination and TPR, two peaks of reduction were still observed for CoRu-*RP* and CoRu-R_WP. However, they were located at slightly higher temperatures: ca. 250°C and between 300-600°C.

The reducibilities of the catalyst samples after different pretreatments are shown in Table 5.2. They ranged from 83 to 50% for the Co catalyst and 98 to 80% for CoRu. The reducibilities of catalyst samples decreased with the introduction of 3% additional water vapor during reduction and increased with the addition of the Ru promoter.

5.3.6 Hydrogen Chemisorption

The H_2 chemisorption results for Co and CoRu after different pretreatment conditions are shown in Table 5.2. The overall dispersion of reduced Co in the catalyst samples and the

average reduced Co metal particle sizes are also given. The results indicate that the overall dispersion increases with the addition of Ru promoter (5.7 to 7.8%) and decreases with the introduction of water vapor during reduction, especially in the absence of the Ru promoter (5.7 to 3.8%).

5.3.7 Reaction Rate

The rate of CO conversion on the pretreated catalyst samples is shown in Table 5.2 and Figure 5.8. It can be seen that the rate of CO conversion during FTS decreased with the addition of water vapor during reduction. Since only Co metal has significant activity for FTS, these results are consistent with both the reducibility and H_2 chemisorption results. No significant change in product distribution was observed.

5.4. Discussion

The BET surface areas of the catalysts in this study did not change significantly after the various pretreatments. It is clear that the various pretreatments in this study had little effect on surface area of the alumina support. Thus, changes in catalyst characteristics in this study were not caused by any change in total surface area of the catalysts.

In order to determine the bulk crystalline phases of the catalysts, XRD was performed. As seen in Figure 5.1, the XRD peaks of the alumina support were present in all catalyst samples as broad peaks. The XRD patterns for Co and CoRu catalysts were identical for the same pretreatments, as shown in Figure 5.1. Diffraction peaks of Co_3O_4 were observed for Co-*C* and CoRu-*C*. No XRD peaks of the Ru promoter were detected because Ru was present in such a small amount (0.5 wt%) and was well dispersed on the catalyst surface. After reduction and

passivation, the diffraction peaks of Co_3O_4 were not apparent for Co-*RP*, Co-R_W*P*, CoRu-*RP*, or CoRu-R_W*P*. The diffraction peaks for CoO were, however, present. This indicates that Co_3O_4 in the calcined samples was reduced to Co metal and CoO during standard reduction at 350°C. Any Co_3O_4 formed during passivation was present in only very thin surface layers and was consequently XRD invisible. Because both $CoAl_2O_4$ and Co_3O_4 have a spinel structure, the XRD patterns for both materials are almost identical, as shown in Figure 5.1. No evidence for $CoAl_2O_4$ was detectable for either Co or CoRu after any of the reduction pretreatment conditions. The diffraction peaks of cobalt metal could not be seen due to overlap with those for γ-Al_2O_3. XRD patterns were identical for both Co and CoRu after the same pretreaments where additional water vapor was and was not introduced during reduction, as shown in Figure 5.1.

Raman spectroscopy provided additional results about the Co species present. The strong Raman bands of Co_3O_4 in Co-*C* and CoRu-*C* can be observed in Figure 5.2. They confirm the XRD results that Co_3O_4 was present in the calcined catalyst samples. After reduction, the strong Raman bands of Co_3O_4 totally disappeared. Broad Raman bands between 400-750 cm^{-1} were observed in all reduced and passivated samples (including both *RP* and R_W*P* samples). However, these broad Raman bands were not identical with those of CoO, Co_3O_4 (spinel) or $CoAl_2O_4$ (spinel). Thus, the broad Raman bands between 400-750 cm^{-1} can not be attributed to either the support, Co_3O_4, CoO, Co metal, or $CoAl_2O_4$ (spinel). It is suggested that these broad Raman bands represent a surface Co compound species related to Co strongly interacting with the alumina as a Co "aluminate". The identified Co "aluminate" is suggested to be different from $CoAl_2O_4$ (spinel) due to it being a non-stoichiometric surface Co "aluminate" compound. This highly dispersed Co "aluminate" (Co-Al_XO_Y) may be formed, possibly, by Co atom migration into the alumina matrix and is detectable using Raman spectroscopy but not with XRD.

It is known that there are two steps for the reduction of bulk Co_3O_4.[6,16-20] The first step is the reduction of Co_3O_4 to CoO and then that of CoO to Co metal. However, the two reduction steps may not always be observed as separate peaks in TPR[17-20], as seen in Figure 5.7 for the reduction of bulk Co_3O_4. They can, however, be separated for bulk Co_3O_4 by adding water vapor during TPR.[12] In addition, it has been found that often, due to interactions between Co_3O_4 and support materials such as silica or alumina, TPR of supported Co_3O_4 can also manifest a separation of the two reduction steps.[13,20]

TPR profiles of the catalyst samples are shown in Figure 5.7. There were three reduction peaks located at ca. 200°C, 300°C, and between 400-750°C (max. at 600°C) for Co-*C*. It has been suggested that the reduction peak at ca. 200°C is due to the decomposition of residual Co nitrate to Co_3O_4.[1,17-18] However, XRD and Raman spectroscopic results (shown in Figures 5.9 and 5.10) for dried $Co(NO_3)_2/\gamma\text{-}Al_2O_3$ prior to calcination (the precursor for Co-*C*) show no detectable amounts of $Co(NO_3)_2$ remaining and only the existence of Co_3O_4. Previous results from our lab have proved that this peak for $Co/\gamma\text{-}Al_2O_3$ is due to decomposition of residual $Co(NO_3)_2$.[1]

TPR peak locations are affected by reduction kinetics. The kinetics of reduction can be affected by a wide range of variables including particle size, support interaction, and reduction gas composition. The effects of particle size and support interaction can superimpose on each other. Thus, while a decrease in metal oxide particle size can result in faster reduction due to a greater surface area/volume ratio, smaller particles may interact more with the support slowing reduction.

The reduction of the unpromoted Co catalyst after various pretreatments can be suggested to occur as shown in Figure 5.11. For Co-*C*, the first reduction peak (at ca. 200°C) can be

assigned to the decomposition of $Co(NO_3)_2$[1,17-18], as has previously been shown for catalysts similar to this one.[1] The second reduction peak (at ca. 300°C) is assigned to the reduction of Co_3O_4 to CoO and Co^0. The reduction peak at 400-750°C (max. at 600°C) was clearly related to the reduction of Co strongly interacting with the support (Co_XO_Y-Al_2O_3)[18,21-24], which can only be reduced at higher temperature.

The first low temperature peak is not observed for a Co-*C* type catalyst if a longer calcination period of 14 h is used.[1] Prolonged calcination or reduction and re-calcination results in complete decomposition of any $Co(NO_3)_2$ present. As a result, the low temperature (ca. 200°C) peak disappears after such treatments and only the second peak at ca. 350°C remains for Co-*RP* and Co-R_W*P*. Reduction and re-calcination probably causes sintering of Co_3O_4 and/or increased interaction with the support resulting in a shift in the TPR peak to ca. 350°C for both Co-*RP* and Co-R_W*P*. The reduction peak at ca. 600°C for Co-*RP* and Co-R_W*P* was also about 20°C higher than that for Co-*C* due to stronger interaction between Co and the support induced by reduction and water effects on the Co_XO_Y-Al_2O_3 species.

The reduction of the Ru promoted Co catalysts can be suggested to occur as shown in Figure 5.12. For CoRu-*C*, the two main reduction peaks were located at ca. 200°C and between 250-550°C (max. at 400°C). A lower temperature shoulder on the 200°C peak was observed due to the reduction of Ru_2O_3 to Ru^0 at ca. 160°C.[25-26] The reduction of Co_3O_4 to CoO and Co^0 then occurred around 200°C, along with some possible decomposition of residual Co nitrate. The higher temperature peak can be assigned to the reduction of Co strongly interacting with the support (Co_XO_Y-Al_2O_3) to Co^0.

For CoRu-*RP* and CoRu-R_W*P*, two reduction peaks were also seen. However, the lower temperature peak was shifted about 60°C higher compared to that for CoRu-*C* probably due to

sintering and/or increased interaction with the support caused by the reduction and re-calcination prior to TPR measurement. It also had a low temperature shoulder due to the initial reduction of Ru. The higher temperature peak located at ca. 380°C for CoRu-*RP* and at ca. 500°C for CoRu-R_WP can again be assigned to the reduction of Co_XO_Y-Al_2O_3 to Co^0. This peak for CoRu-R_WP at a higher temperature than that for CoRu-*RP* was undoubtably caused by an increase in the interaction of Co with Al_2O_3 due to the presence a higher partial pressure of water vapor during reduction.

It can be observed that with Ru promotion, the reduction peaks of Co on alumina shifted to lower temperatures. This has been shown previously to be due to the Ru reducing at a lower temperature and then facilitating the reduction of Co.[1-3]

The reducibilities during TPR from 30-900°C for the catalysts studied are shown in Table 5.2. The results indicate that the reducibility of samples increased with the addition of the Ru promoter and decreased with the introduction of additional water vapor during reduction. This indicates that a larger amount of the non-reducible Co "aluminate" (at temperatures ≤ 900°C) was formed during reduction in the presence of a "relatively" high partial pressure of water vapor (when 3% water vapor was added) leading to a lower reducibility. The addition of the Ru promoter resulted in an increase in reducibility of the catalyst. This might be explained in possibly one of two ways: (i) some of the Co strongly interacting with the alumina (Co_XO_Y-Al_2O_3) can be reduced at lower temperature when Ru is present and/or (ii) the Ru promotion can prevent the formation of the Co "aluminate" by minimizing the impact of water vapor on the formation of such compounds.

The results from H_2 chemisorption show that Ru promotion also results in an increase the dispersion of the Co on the catalyst. This has been noted previously for noble metal promoted

Co catalysts in general.[1-3,6] The overall dispersion was found to decrease with the introduction of additional water vapor during reduction. This may be related to the loss of smaller Co patches/particles as seen by SEM.

SEM and EDX gave information about the morphology and the elemental distribution of the alumina-supported cobalt catalysts after different pretreatments. It is confirmed that with the addition of Ru, Co is more dispersed on the catalyst surface. Comparing the particle size of Co obtained by SEM and H_2 chemisorption, it is obvious that the average particle size of Co^0 metal obtained from H_2 chemisorption (ca. 11-22 nm) is significantly smaller than the patches/particles able to be seen by SEM (ca. 1-5 microns). In addition, SEM does not differentiate between Co metal, Co oxide, Co "aluminate". Thus, with SEM only large dense patches of particles of Co metal and compounds can be detected. However, it must be noted that, after reduction with and without added water vapor, significant differences were observed using SEM, as shown in Figures 5.5 and 5.6. The disappearance of large numbers of smaller Co patches/particles can be seen after the introduction of additional water vapor during reduction. There are two possibilities: either water vapor can facilitate the migration of small Co particles resulting in particle agglomeration (sintering) or it increases the diffusion of Co atoms from the smaller Co particles into the alumina. Considering, the SEM, H_2 chemisorption, TPR, and Raman results, it would appear that both phenomena probably occur, with the latter being especially important and resulting in significant Co "aluminate" formation.

It was seen that the addition of water vapor during reduction also decreased the overall activity of the Co catalysts for FTS, which is related to the decrease in the reducibility and H_2 chemisorption of the catalysts. This is probably due to the fact that water vapor causes an

increase in the amount of Co "aluminate" formation resulting in a decrease in the amount of active Co metal available for the reaction.

5.5 Conclusions

Water vapor present during reduction has a major impact on alumina supported Co catalysts resulting in an increase in the amount of non-reducible Co "aluminate" (at temperatures ≤ 900°C) formed. This Co "aluminate" formation causes changes in the characteristics of Co catalysts, especially their reducibilities and overall activity during FTS. It is concluded that water vapor present during reduction possibly increases the amount of Co able to migrate into the alumina matrix forming a highly dispersed Co "aluminate" resulting in two broad Raman peaks between 400-750 cm^{-1}. This surface Co "aluminate" formed is different from $CoAl_2O_4$ (spinel).

The addition of Ru promoter to Co catalysts increases both the overall Co^0 dispersion and the reducibility. It is suggested that the Ru promoter not only facilitates the reduction of Co at lower temperatures, but also decreases the formation of Co strongly interacting with the alumina (Co_XO_Y-Al_2O_3) and non-reducible Co "aluminate" by minimizing the impact of water vapor on this formation. It is highly possible that this minimization is due to the effect of reduction at lower temperatures.

Table 5.1 BET Surface Area of Co and CoRu Catalysts

Catalyst Samples	**BET Surface Area (m^2/g)**
γ-Al_2O_3	209
Co-***C***	175
Co-***RP***	183
Co-$\boldsymbol{R_WP}$	175
CoRu-***C***	178
CoRu-***RP***	171
CoRu-$\boldsymbol{R_WP}$	188

Table 5.2 Reducibility, H_2 Chemisorption, and Reaction Rate

Catalyst Samples	Reducibility[a] (30 to 900°C) (%)	Total H_2 Chemisorption[b] (mmole H_2/g cat)	Overall Dispersion (%)	Co^0 d_p[c] (nm)	Rate[d] (mmole/g cat/s)	
					Initial	SS
Co-***C***	83	-	-	-	3.0	2.2
Co-***RP***	58	97	5.7	15	2.6	1.4
Co-$\boldsymbol{R_WP}$	50	64	3.8	22	2.2	0.6
CoRu-***C***	98	-	-	-	-	-
CoRu-***RP***	86	132	7.8	11	-	-
CoRu-$\boldsymbol{R_WP}$	80	120	7.1	12	-	-

[a] The ***RP*** and $\boldsymbol{R_WP}$ samples were re-calcined at 300°C in air for 2 h before TPR measurement.

[b] Error = ±5% of measurement of H_2 chemisorption.

[c] Particle size is based upon H_2 chemisorption and the amount of reduced cobalt [$d_p = 5/(S_{Co} \times \rho_{Co})$, where S_{Co} is the surface area of reduced Co/g. of reduced Co and ρ_{Co} is the density of Co catalyst].

[d] FTS was carried out at 220°C, 1 atm, and $H_2/CO = 2$ (H_2/CO/Ar = 60/30/10 cc/min).

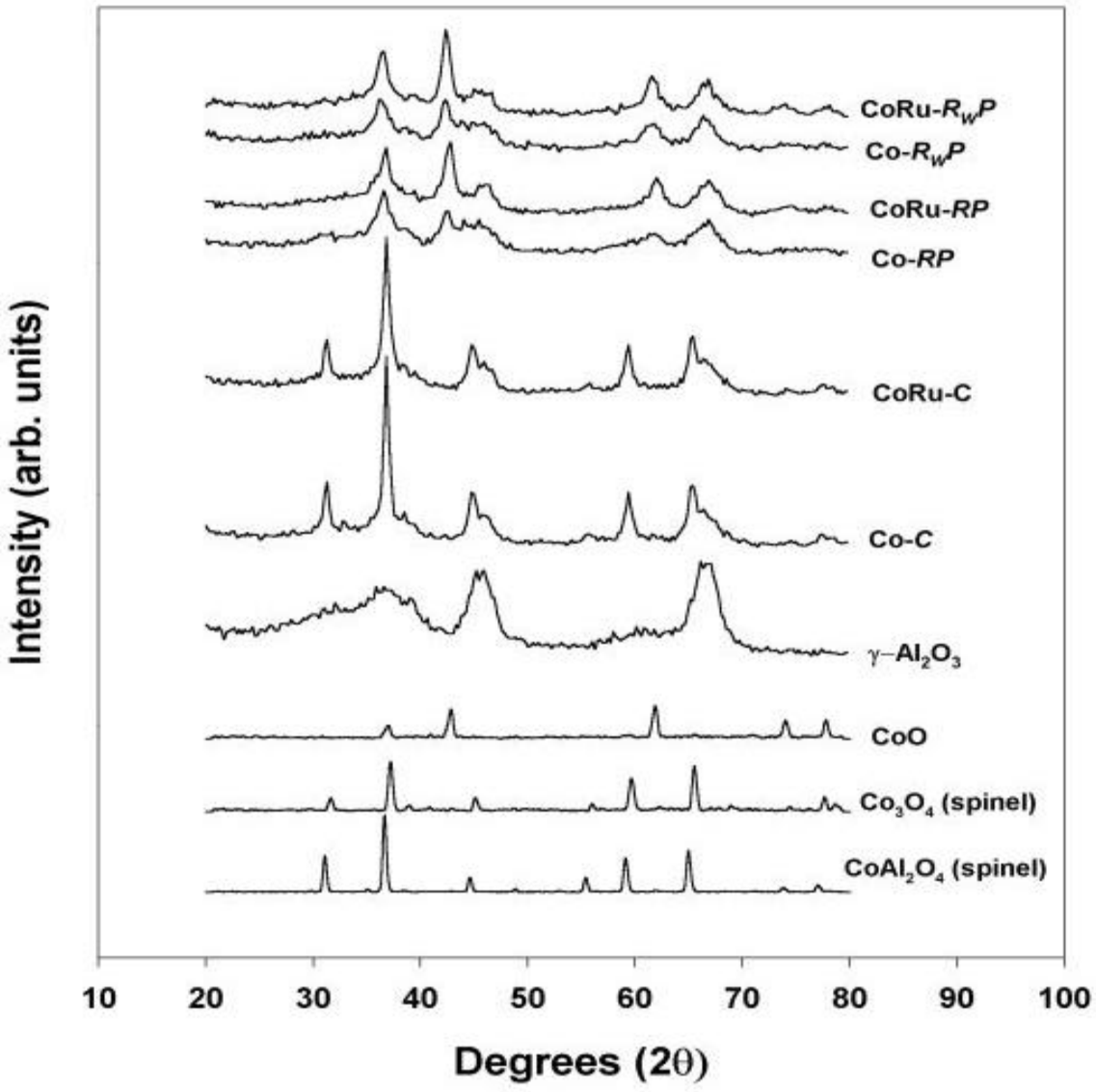

Figure 5.1 XRD Patterns for γ-Al_2O_3, CoO, Co_3O_4 (spinel), $CoAl_2O_4$, and Co/γ-Al_2O_3, and CoRu/γ-Al_2O_3 after various Pretreatments

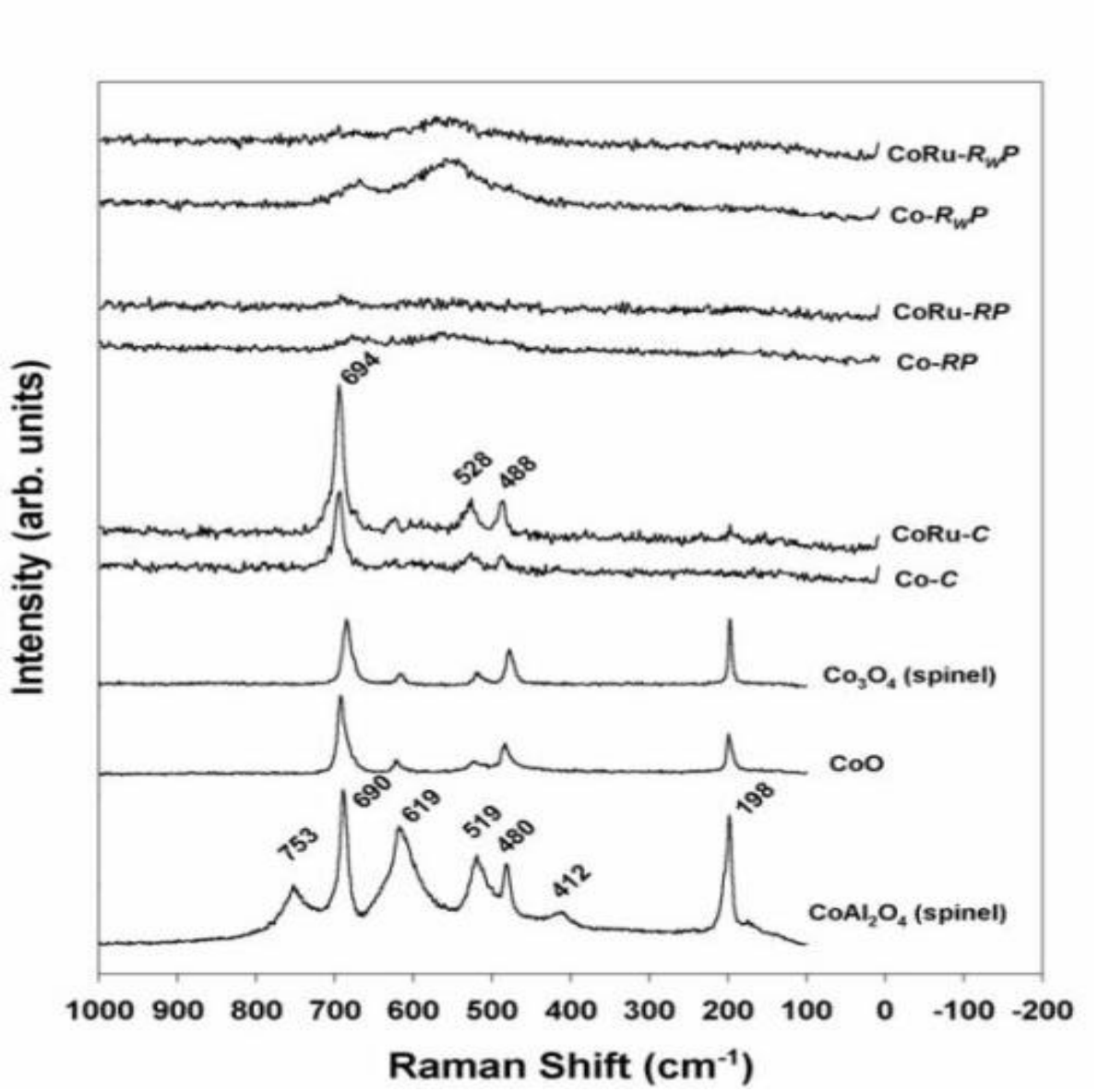

Figure 5.2 Raman Spectra of Co/γ-Al_2O_3 and CoRu//γ-Al_2O_3 after Various Pretreatments, CoO, Co_3O_4 (spinel), and $CoAl_2O_4$ (spinel)

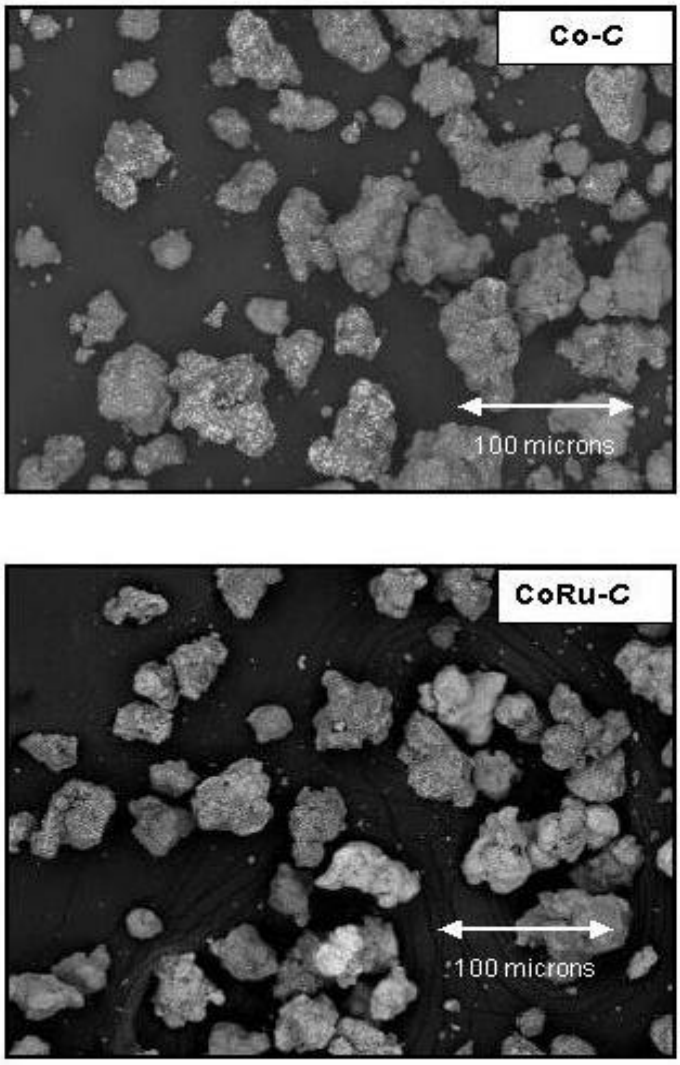

Figure 5.3 SEM Micrographs of the Calcined Co and CoRu Catalysts

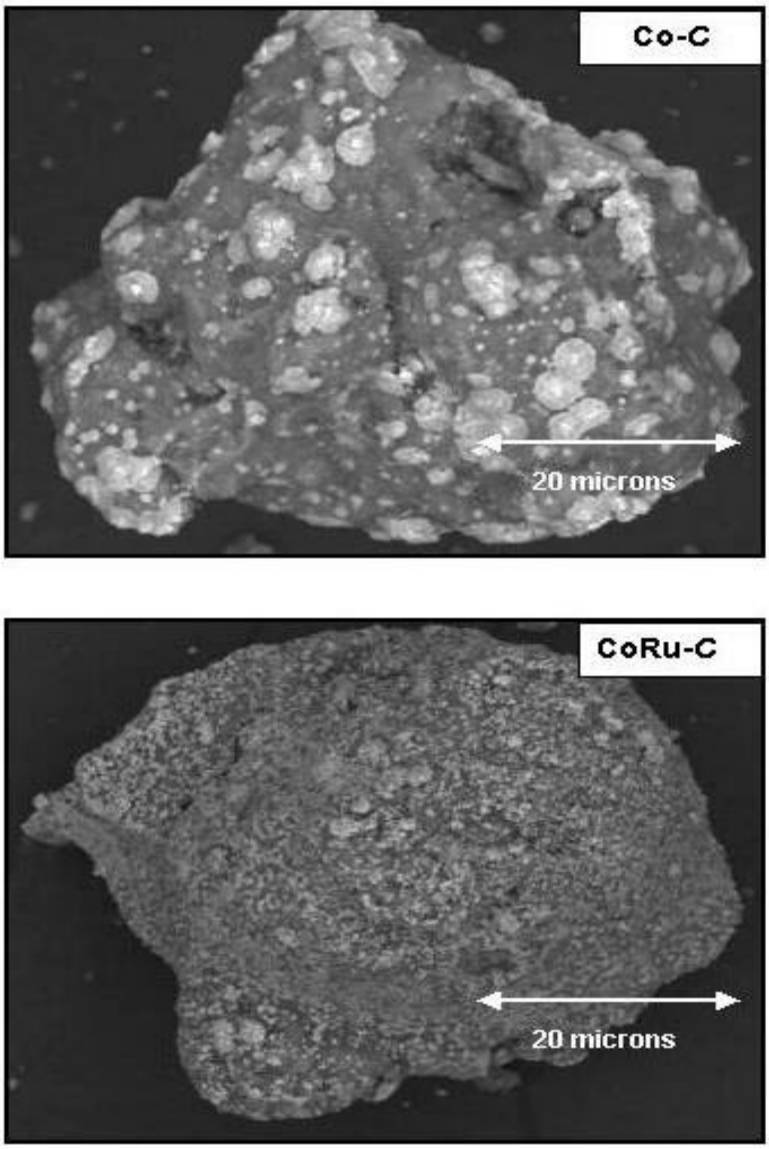

Figure 5.4 SEM Micrographs of the Calcined Co and CoRu Catalyst Granules (external surface)

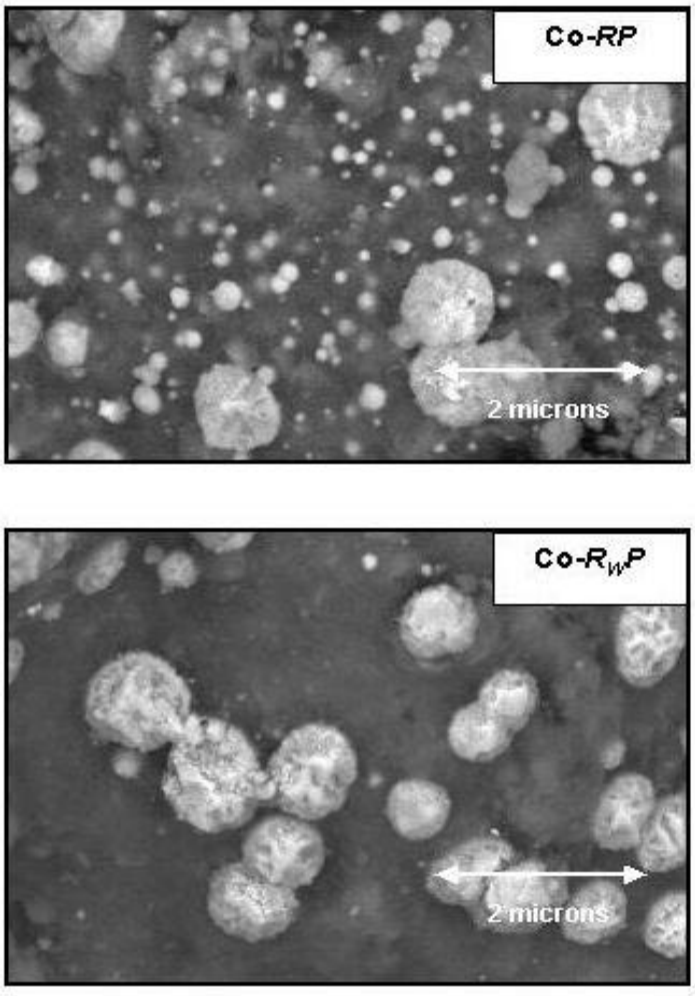

Figure 5.5 SEM Micrographs of the Reduced and Passivated Co Catalysts at 6700X Magnification (external surface)

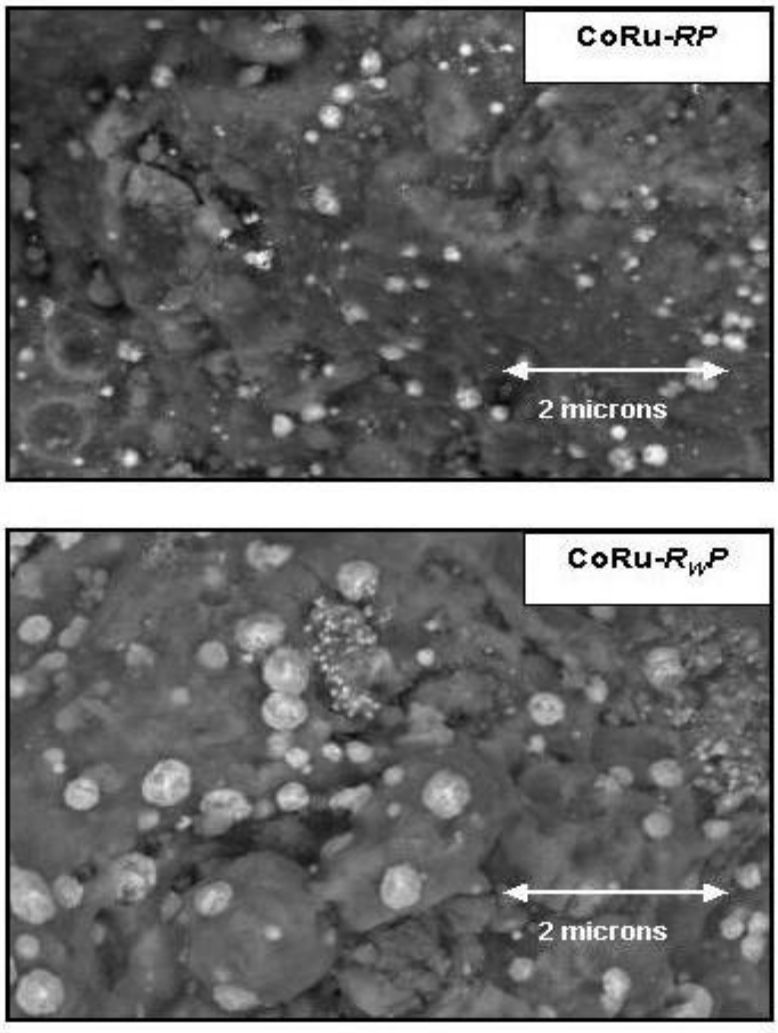

Figure 5.6 SEM Micrographs of the Reduced and Passivated CoRu Catalysts at 6700X Magnification (external surface)

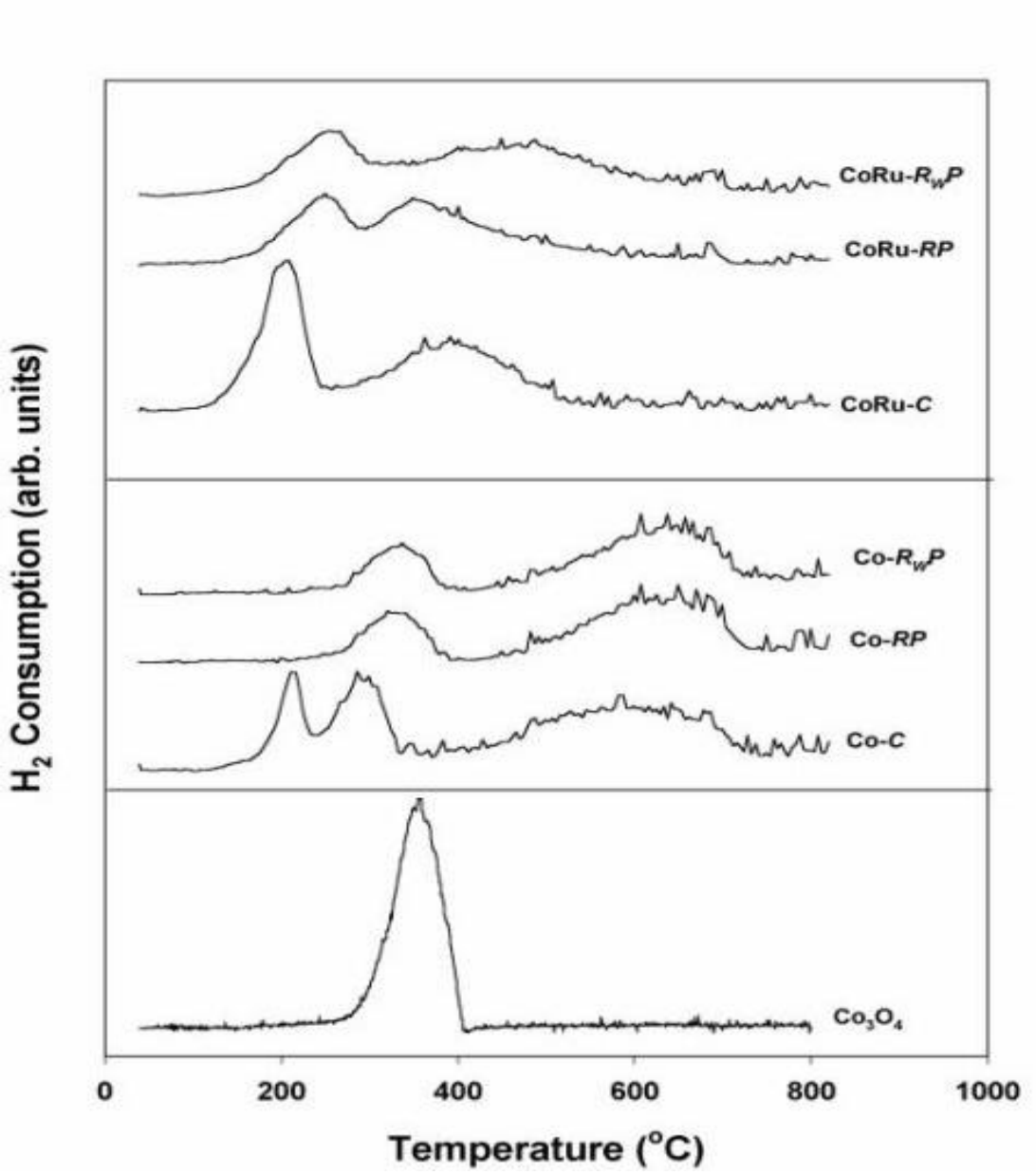

Figure 5.7 TPR Profiles of Co_3O_4, Co/γ-Al_2O_3 and CoRu/γ-Al_2O_3 Catalysts

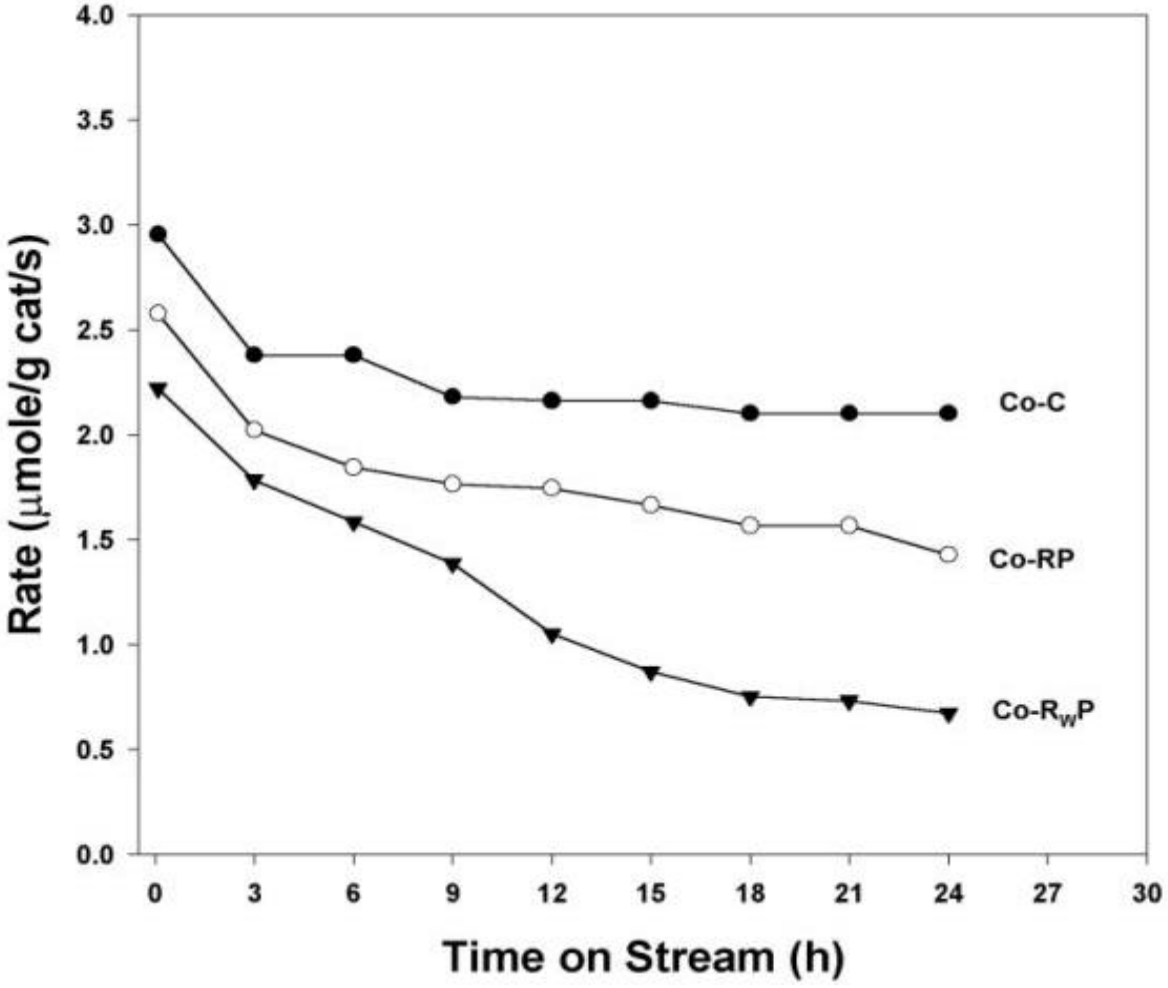

Figure 5.8 Effect of Various Pretreatments on Reaction Rate for Co Catalysts

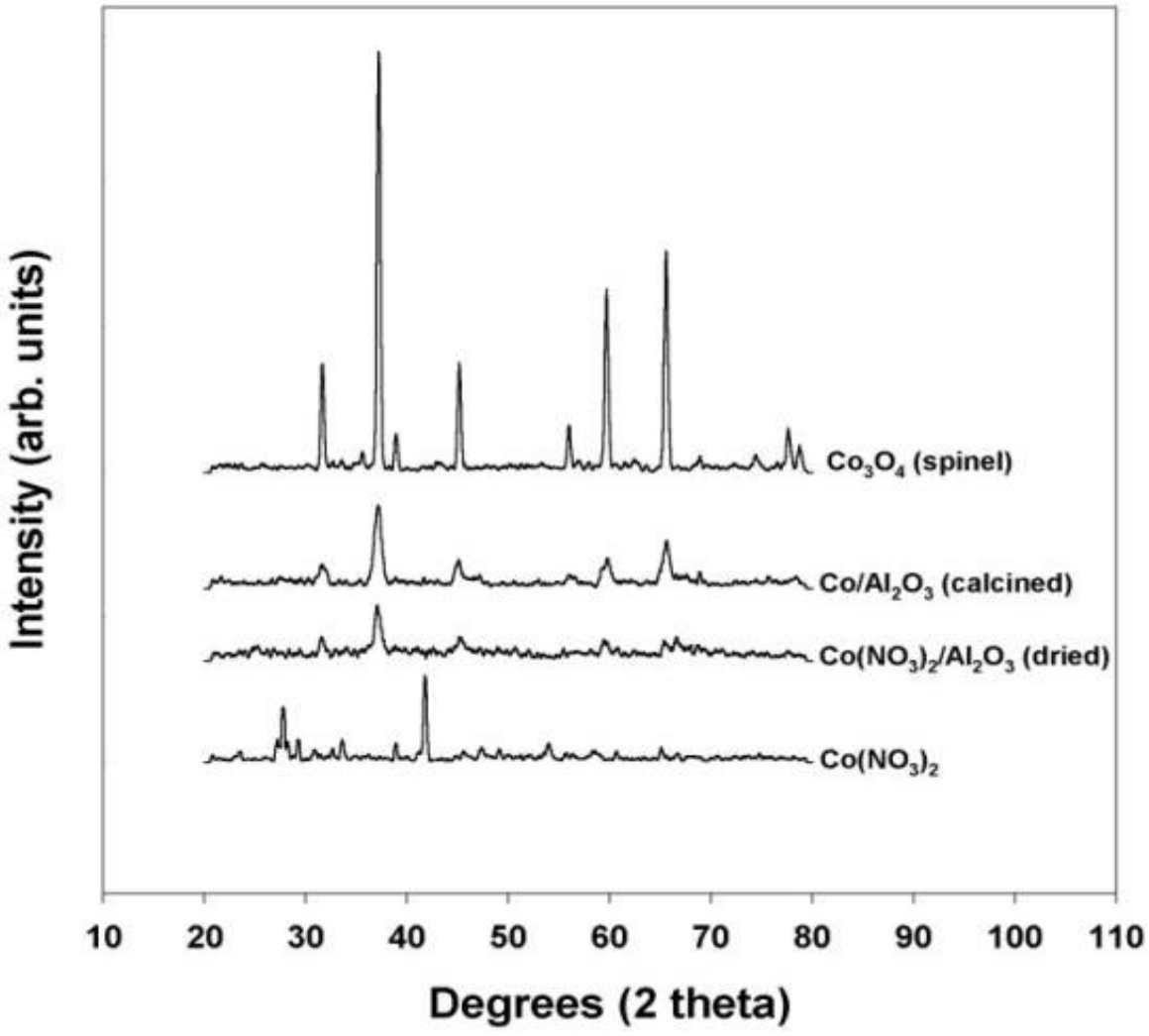

Figure 5.9 XRD Patterns of $Co(No_3)_2$, Co_3O_4 (spinel), Dried $Co/\gamma\text{-}Al_2O_3$ and Calcined $Co/\gamma\text{-}Al_2O_3$

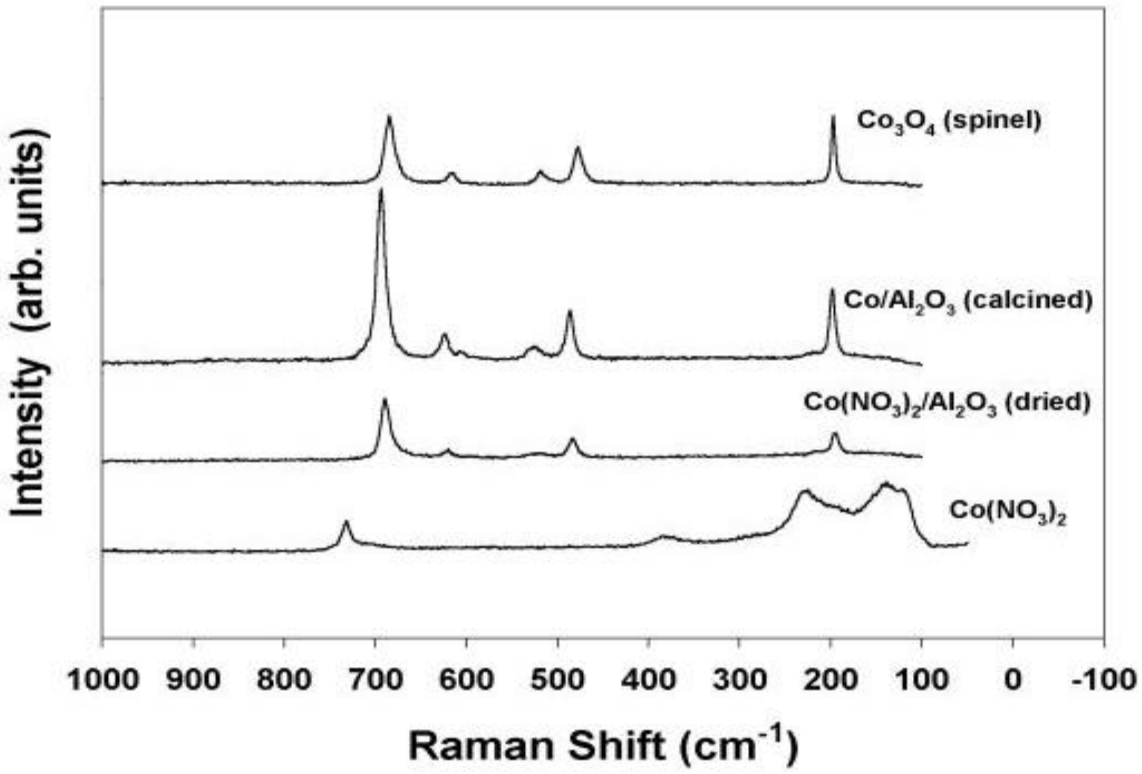

Figure 5.10 Raman Spectra of $Co(NO_3)_2$, Co_3O_4 (spinel), Dried $Co/\gamma\text{-}Al_2O_3$, and Calcined $Co/\gamma\text{-}Al_2O_3$

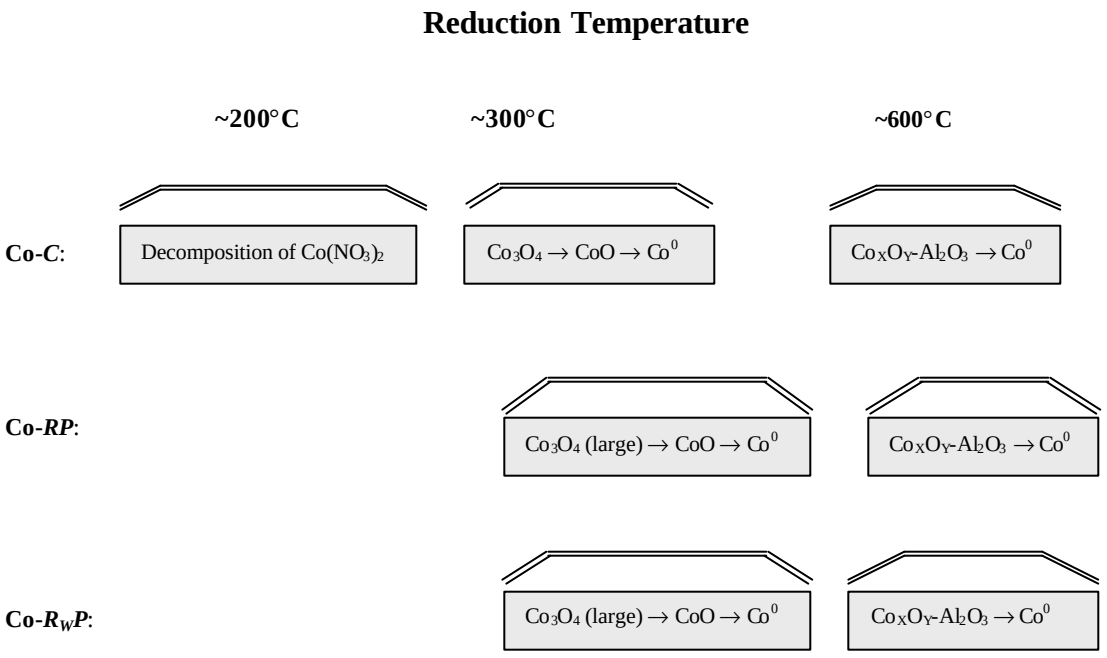

Figure 5.11 Suggested Reduction Behavior of Unpromoted Co Catalysts after Various Pretreatments

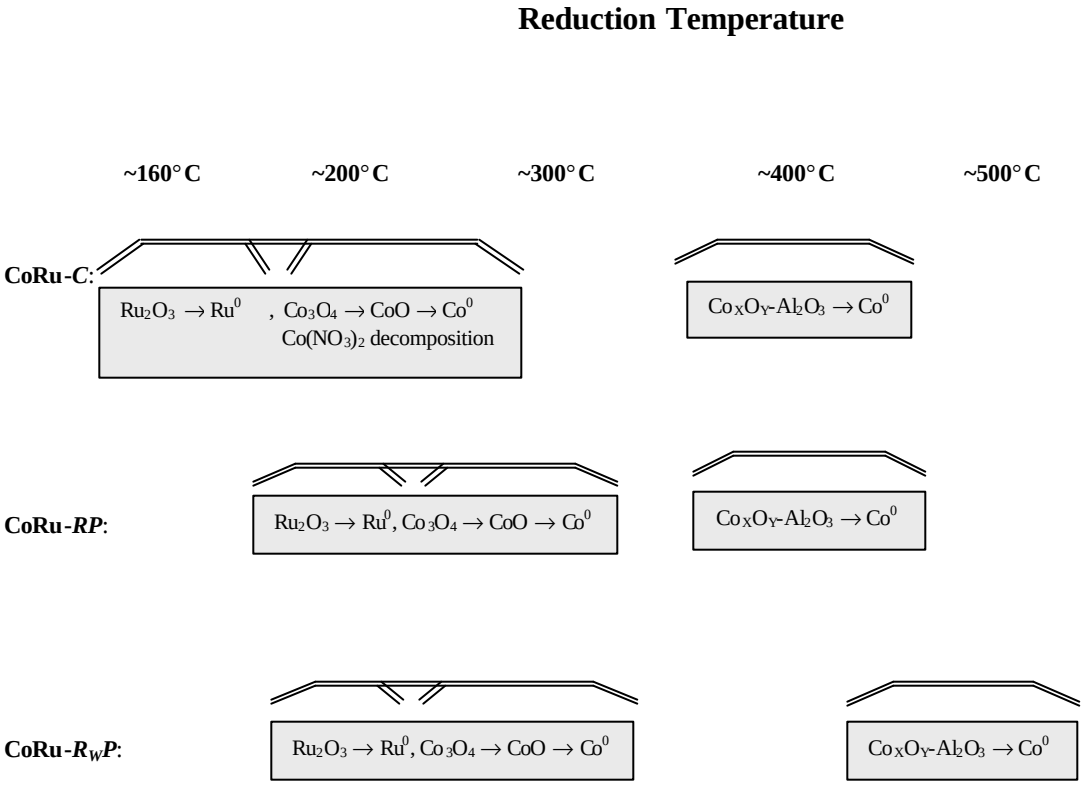

Figure 5.12 Suggested Reduction Behavior of Ru Promoted Co Catalysts after Various Pretreatments

6.0 COBALT-SCF AFTER ACID LEACHING

6.1 Introduction

Although the impact of water vapor on the reducibility during standard reduction and TPR were studied, it did not give the information about the nature of Co-SCF or how to identify the formation. In order to monitor how the impact of water can be minimized, it is very important to fully understand the nature of Co-SCF and how this formation affects the characteristics of the catalysts as mentioned in chapter 5.

It has been proposed that Co metal is the active form of supported Co catalysts for FTS. After calcination, Co-oxides are obtained. Prier to FTS, the catalyst precursors must be reduced in order to change them to Co metal atoms. However, based upon the impact of water vapor produced during reduction, a strong interaction between Co and the supports can be induced and thus, Co-SCF is formed. It is considered that only a weakly interacted Co species (i.e. Co_3O_4, CoO, and Co^0 metal) can be removed using strong acid leaching (such as concentrated hydrochloric acid)[(1)], but a strongly interacted Co species (i.e. Co-SCF) are considered to be residues on the support. This can provide a promising way to identify the nature and characteristics of Co-SCF after acid leaching followed by using other characterization techniques. The main objective of this study was to develop a better understanding of the nature and characteristics of Co-SCF using strong acid leaching followed by various characterization techniques such as inductively coupled plasma (ICP), XRD, SEM/EDX, and Raman spectroscopy.

6.2 Experimental

6.2.1 Catalyst Preparation

6.2.1.1 Co/γ-Al_2O_3. The Co/γ-Al_2O_3 catalyst was prepared by the incipient wetness impregnation of γ-Al_2O_3. The support precursor (Al_2O_3, Vista B) was calcined at 500°C for 10 h before impregnation in order to put it in the form of γ-Al_2O_3 having a specific surface area of 209 m^2/g and average particle size ca. 60 µm. Cobalt nitrate [$Co(NO_3)_2 \bullet 6H_2O$] was dissolved in de-ionized water and impregnated into the support using incipient wetness to give a final reduced catalyst with 20 wt% cobalt. The catalyst was dried at 110°C for 12 h and calcined in air at 300°C for 2 h.

6.2.1.2 CoRu/γ-Al_2O_3. The CoRu/γ-Al_2O_3 catalyst was also prepared by the incipient wetness co-impregnation method. The same γ-Al_2O_3 support as mentioned before was used. Cobalt nitrate and ruthenium (III) nitrosyl nitrate [$Ru(NO)(NO_3)_3$] were dissolved in de-ionized water and co-impregnated into the support to produce a reduced catalyst with 20 wt% cobalt and 0.5 wt% ruthenium. The catalyst was also dried at 110°C for 12 h and calcined in air at 300°C for 2 h.

6.2.2 Catalyst Pretreatment

6.2.2.1 Reduction. The catalysts were characterized following two pretreatments. These were as follows:

(i) after standard reduction of the calcined catalysts in a high space velocity (16,000 h^{-1}) of H_2 at 350°C for 10 h and passivation with an O_2/He (5.20% of O_2) mixture at room temperature for 2 h,

(ii) after standard reduction of the calcined catalysts in a high space velocity (16,000 h^{-1}) of H_2 with 3% of added water vapor at 350°C for 10 h followed by passivation with an O_2/He (5.20% of O_2) mixture at room temperature for 2 h.

6.2.2.2 Acid Leaching. In order to study on the strongly interacted Co "aluminate", acid leaching was performed on the reduced and passivated catalysts as mentioned before. A 30% hydrochloric solution (pH = 1) was used to treat the catalysts for 48 h. After Co^0, CoO, and weak interacted Co species were dissolved, the residues were filtered and rinsed with deionized water for several times to remove all dissolved components. After filtration, the residue was dried under vacuum at room temperature for overnight in order to avoid any further reaction caused by heating. The acid leaching catalyst was then collected and characterized.

6.2.3 Catalyst Nomenclature

The nomenclature used for the catalyst samples in this study is the following:

RP: the reduced and passivated catalyst samples

R_WP: the catalyst samples reduced in H_2 with 3% added H_2O vapor and then passivated

RPA: the *RP* catalyst sample after acid leaching

R_WPA: the *R_WP* catalyst sample after acid leaching

6.2.4 Catalyst Characterization

6.2.4.1 Elemental Analysis. Inductively coupled plasma (ICP) spectroscopy was performed by Galbraith Laboratories, Inc. in order to analyze the amount of Co remains in the catalyst samples after acid leaching.

6.2.4.2 X-ray Powder Diffraction (XRD). XRD was performed to determine the bulk crystalline phases of the catalysts following different pretreatment conditions. X-ray powder diffraction patterns of samples were collected using a Philips X'pert X-ray diffractometer with monochromatized Cu-K_α radiation (λ = 1.54439 Å). The spectra were scanned at a rate of 2.4 degree/min. from 2θ = 20 to 80 degrees.

6.2.4.3 Raman Spectroscopy. The Raman spectra of the samples were collected by projecting a continuous wave laser of Argon ion (Ar^+) green (514.532 nm) through the samples exposed to air at room temperature. A scanning range between 100 to 1000 cm^{-1} with a resolution of 2 cm^{-1} was applied. The data were analyzed using the Renishaw WiRE (Windows-based Raman Environment) software which allows Raman spectra to be captured, calibrated, and analyzed using system 2000 functionality via the Galactic GRAMS interface with global imaging capacity.

6.2.2.4 SEM and EDX. SEM and EDX were performed to study on the morphology of catalysts and elemental distribution, respectively. A Hitachi S3500N SEM was used having the back scattering electron (BSE) mode at 15 kV and working distance (the distance between a sample

and the electron beam) of 15 mm. After the catalyst micrographs were taken, EDX was then performed to analyze the elemental concentration on catalyst surface (using INCA software).

6.3 Results and Discussion

The amount of Co concentration on the catalysts before and after acid leaching obtained by ICP was shown in Table 6.1. It can be observed that the amount of cobalt remains in the catalyst samples after acid leaching increased with added water vapor during reduction and decreased with Ru promotion. The amount of Co remains in the catalyst samples after acid leaching was related to the amount of the strongly interacted Co-aluminate and ranged between 2.9 to 4.6 wt% based on the amount of the original Co present (ca. 20 wt% Co in the catalyst samples). It can be seen that the amount of Co remains after acid leaching in Co-$R_W PA$ was highest at 4.6 wt%.

The XRD patterns of the catalysts before and after acid leaching was shown in Figure 6.1. It was clear that the weak interacted Co species (i.e. Co^0 and CoO) were totally removed after acid leaching due to a disappearance of the XRD peaks at 36.8°, 42.6° and 61.8°. The XRD patterns of all catalyst samples after acid leaching were identical to those for γ-Al_2O_3. It indicated that the strongly interacted Co species (i.e. Co-aluminate) remains in the samples after acid leaching could not be detected by XRD due to they were in a highly dispersed form.

Raman spectra of the catalysts were shown in Figure 6.2 (shown only Co-$R_W PA$ and CoRu-$R_W PA$). They all were identical. No peaks of Co "aluminate"[(2)] and other Co species could be detected probably due to only a small amount of them were present. Thus, the XRD and Raman spectroscopic results were obviously related.

Pictures of Co-*RP* sample before and after acid leaching obtained from a digital camera are shown in Figure 6.3. The color changed from black to white after acid leaching. Some of the catalyst micrographs after various pretreatments are shown in Figures 6.4 to 6.7. The term "granule" is used here to refer to the overall catalyst particles composed of Co, Ru (for CoRu), and γ-Al_2O_3. The term "patches" will be used to refer to the entities rich in Co supported on the catalyst granules. In all SEM figures, the white or light spots on the catalyst granules represent high concentrations of cobalt and its compound while the darker areas of the granules indicate the support with minimal/no cobalt present. Figure 6.4 shows the Co-*RP* (top) and CoRu-*RP* (bottom) catalyst granules before acid leaching. The Co-*RP* catalyst granule after acid leaching is shown in Figures 6.5 (external surface) and 6.6 (cross section). It indicates that a small amount of Co "aluminate" remains could be seen after acid leaching. These Co parches can not be attributed to Co metals or Co oxide due to they were removed after acid leaching as seen in XRD and Raman spectroscopic results. Thus, only Co "aluminate" remains after acid leaching were seen. It should be mentioned that SEM does not differentiate the Co species patches and $CoAl_2O_4$ (spinel) as shown in Figure 6.7.

EDX result indicates that Co species can be detected after acid leaching. The EDX mappings are shown in Figures 6.8 (before acid leaching) and 6.9 (after acid leaching). It can be seen that all elements are well distributed all over the catalyst granules. However, after acid leaching, only a small amount of Co could be detected in all samples and was assigned to the Co "aluminate" remains. The concentration and distribution of Al and O were essentially not affected by acid leaching.

Considering the acid leaching technique, it is a practical procedure for removing the minimal/no interacted Co species with the support such as Co metal, CoO, and Co_3O_4 as seen in

XRD and Raman spectroscopy. Thus, only Co species strongly interacted with the supported, i.e. Co "aluminate" is remains and easy to identify using various characterization techniques. Co "aluminate" remains can be seen by SEM and EDX mapping techniques. However, ICP is the most powerful technique used directly to analyze the amount of Co "aluminate" remains in the catalyst samples. It must be remembered that besides the pretreatment conditions and Ru promotion, the amount of Co "aluminate" remains depends upon the acid leaching conditions, such as the pH and soaking period, which was not the focus of this investigation.

6.4 Conclusions

This study indicates that the characteristics of the strongly interacted Co "aluminate" can be identified using acid leaching treatment followed by ICP, XRD, Raman spectroscopy, and SEM/EDX. XRD and Raman spectroscopic results proved that Co metal, CoO, and Co_3O_4 were mainly removed after acid leaching. The strongly interacted Co "aluminate" can be detected by ICP and SEM/EDX. It is suggested that the amount of Co remains, which is related to the amount of Co "aluminate" formed is affected by the pretreatment conditions and Ru promotion based on the ICP results. It can be concluded that the amount of Co "aluminate" formed increases with the addition of 3% water vapor during reduction and decreases with Ru promotion.

Table 6.1 Co Remains after Acid Leaching of the Reduced Co Catalysts

Catalyst Samples	**Co Remains after Acid Leaching (wt %)[a,b]**
Co-***RP[A]***	4.3
Co-$\boldsymbol{R_WP[A]}$	4.6
CoRu-***RP[A]***	2.9
CoRu-$\boldsymbol{R_WP[A]}$	3.2

[a] The amount of Co remains after acid leaching was obtained using ICP by Galbraith Laboratories, Inc.

[b] The amount of Co remains is based on the amount of Co originally present in the reduced catalyst samples before acid leaching (ca. 20 wt% of Co in the catalyst sample).

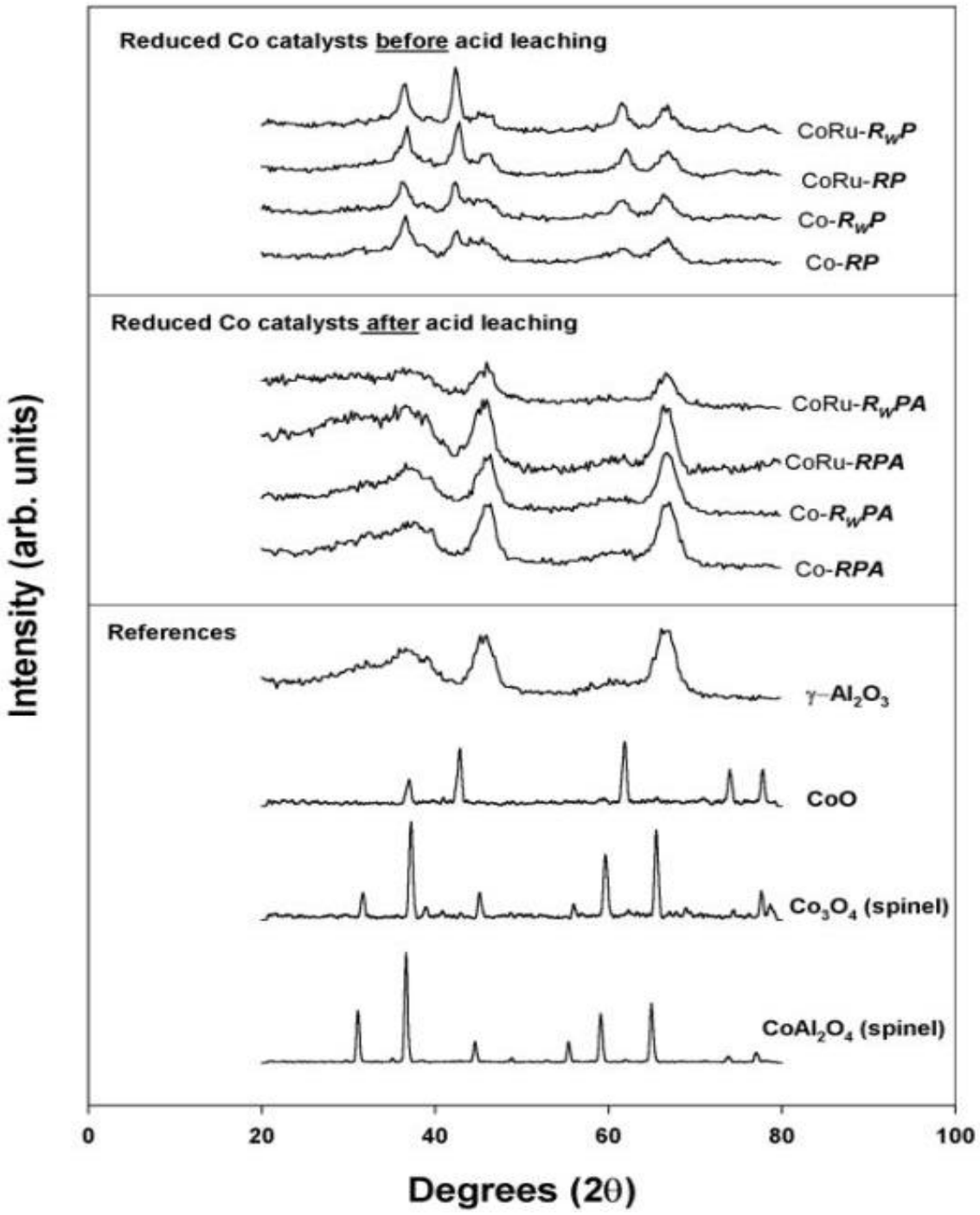

Figure 6.1 XRD Patterns of γ-Al_2O_3, Co/γ-Al_2O_3, and CoRu/γ-Al_2O_3 after Various Pretreatments

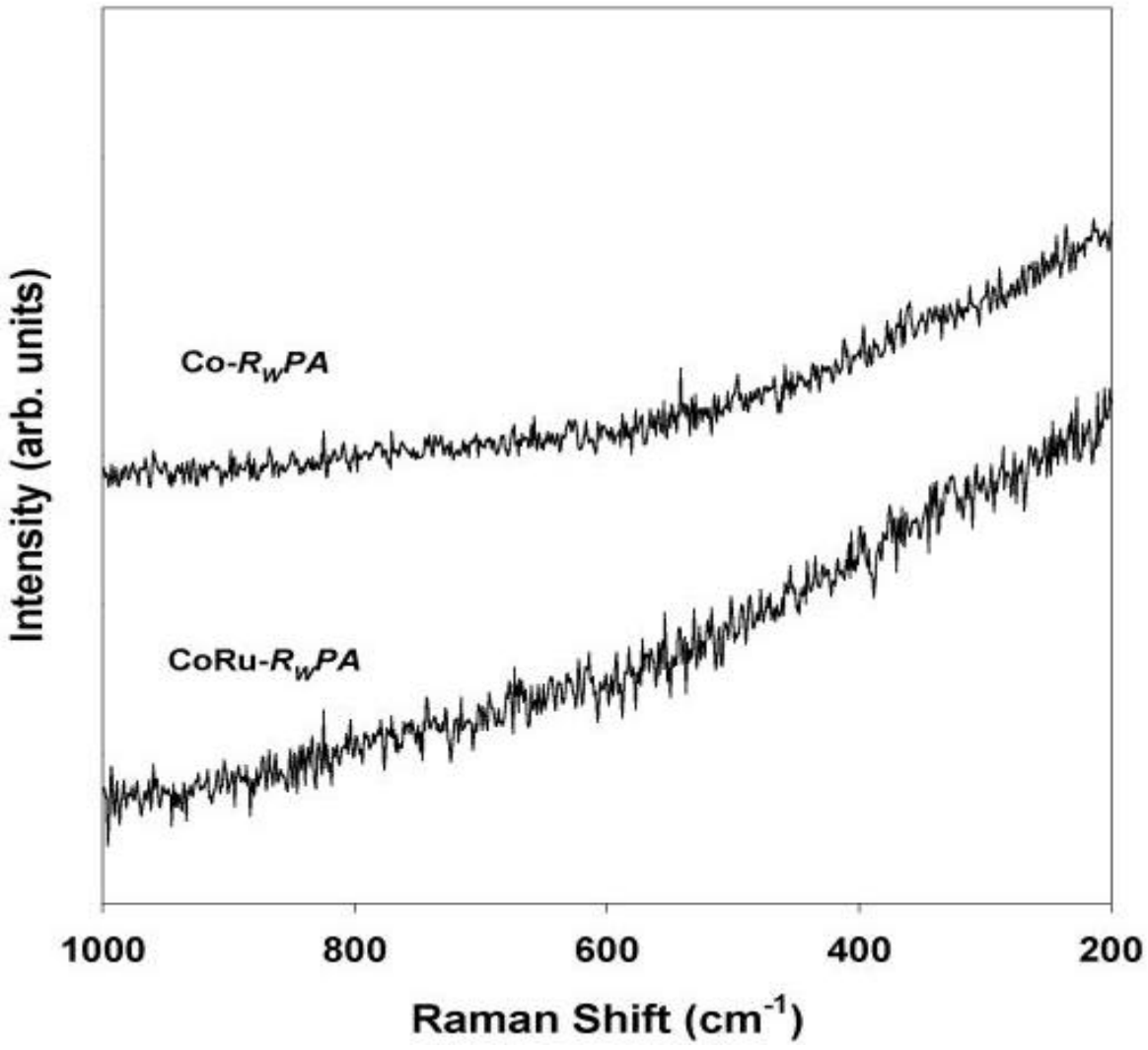

Figure 6.2 Raman Spectra of Co-R_W*PA* and CoRu-R_W*PA*

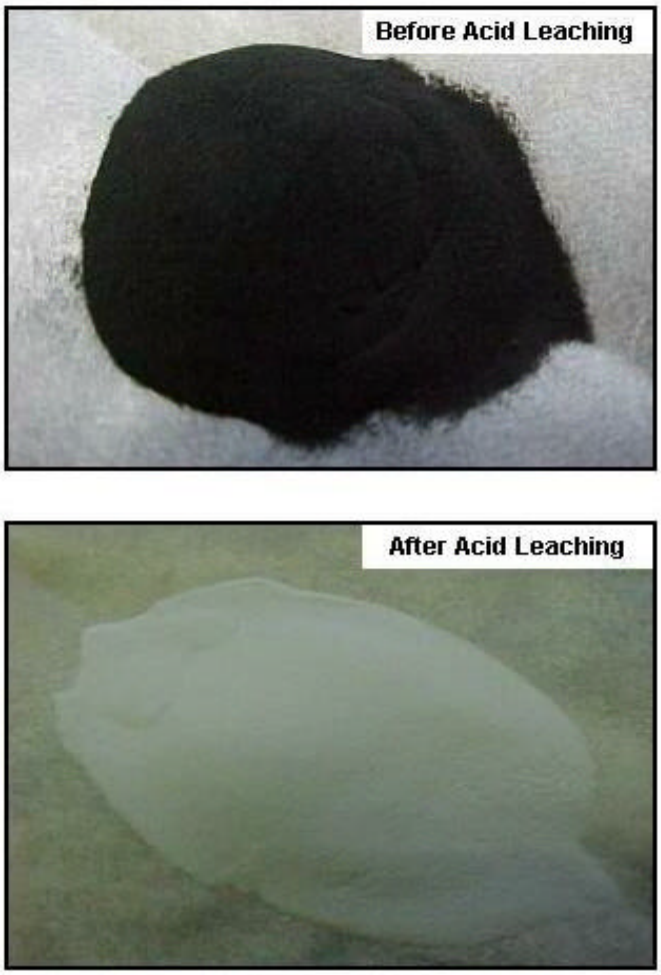

Figure 6.3 Pictures of Co-*RP* Catalysts Powder (10X) Obtained from a Digital Camera

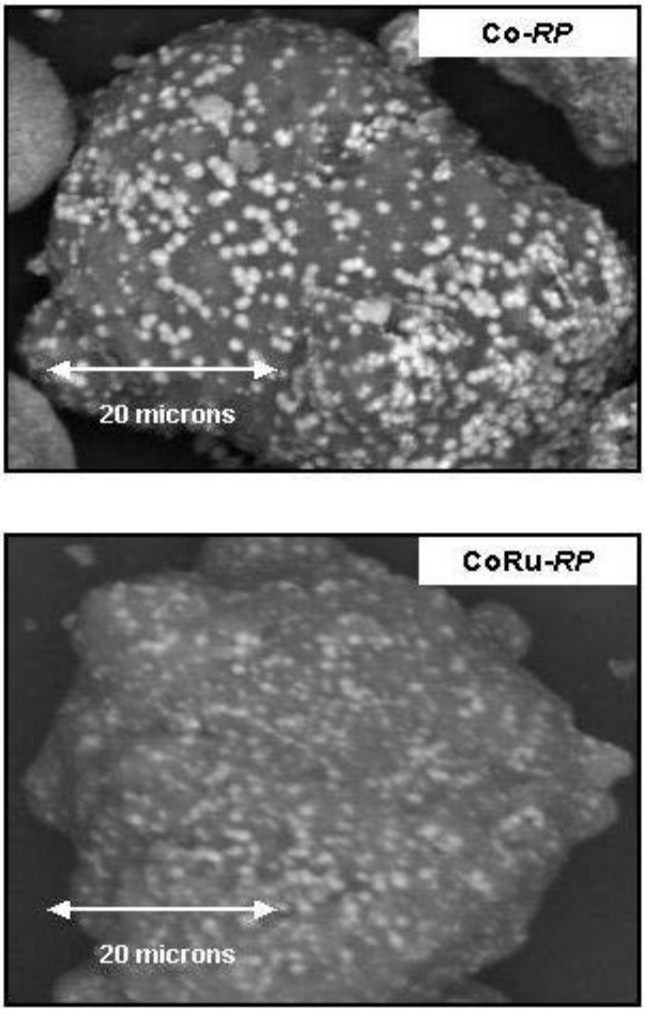

Figure 6.4 SEM of Co-*RP* and CoRu-*RP* Catalyst Granules (external surface)

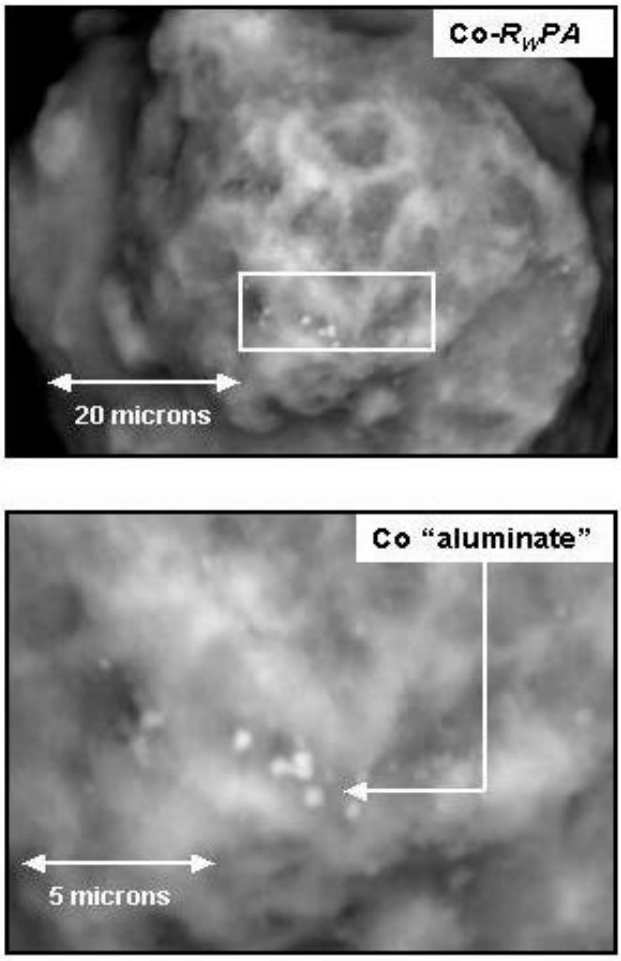

Figure 6.5 SEM of Co-R_W*PA* (after acid leaching) Catalyst Granule (external surface)

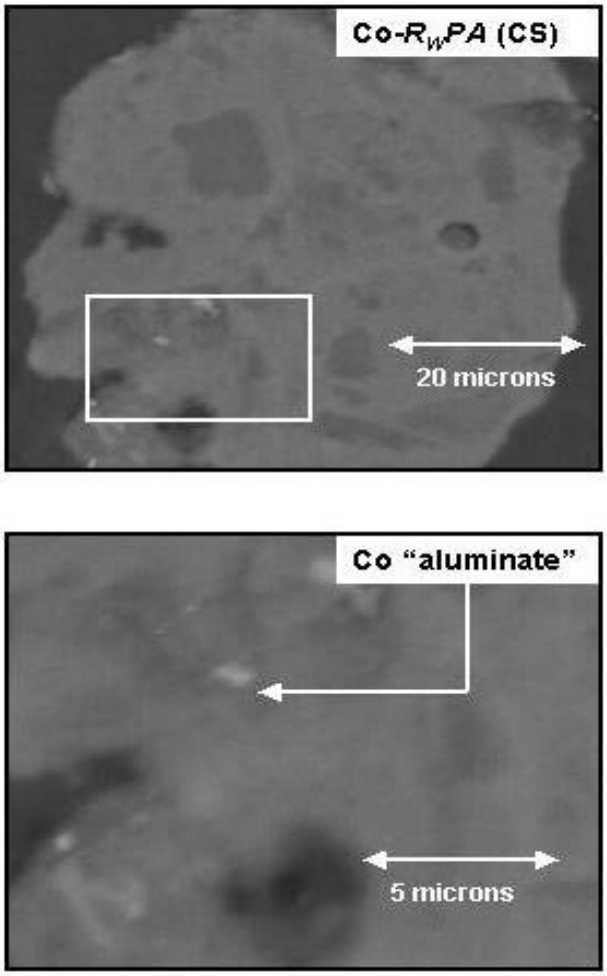

Figure 6.6 SEM of Co-R_W*PA* Catalyst Granules (cross-section)

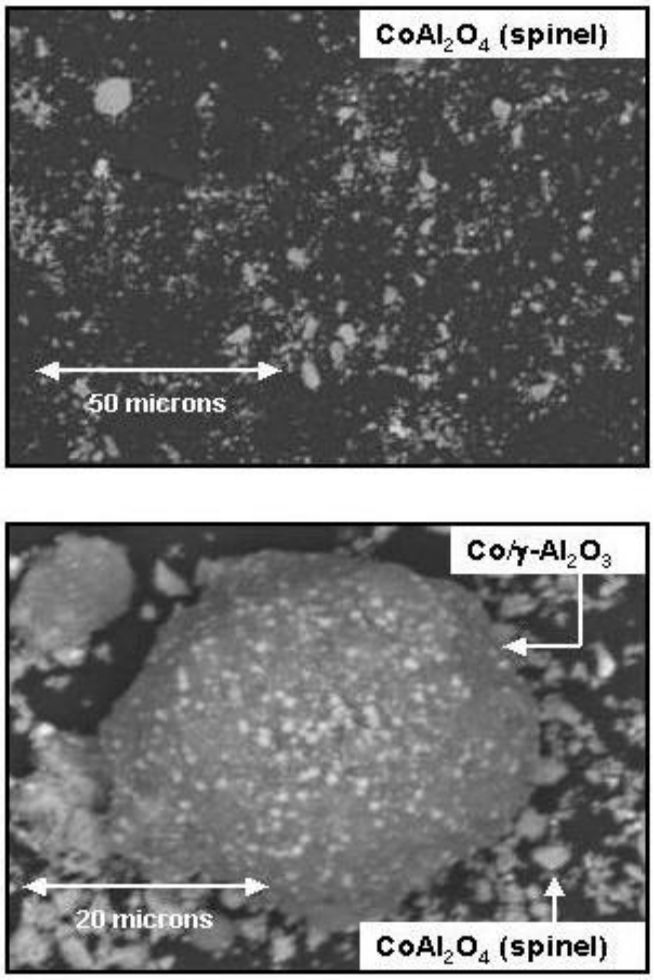

Figure 6.7 SEM of $CoAl_2O_4$ and a Mixture of $Co/\gamma\text{-}Al_2O_3$ and $CoAl_2O_4$ (external surface)

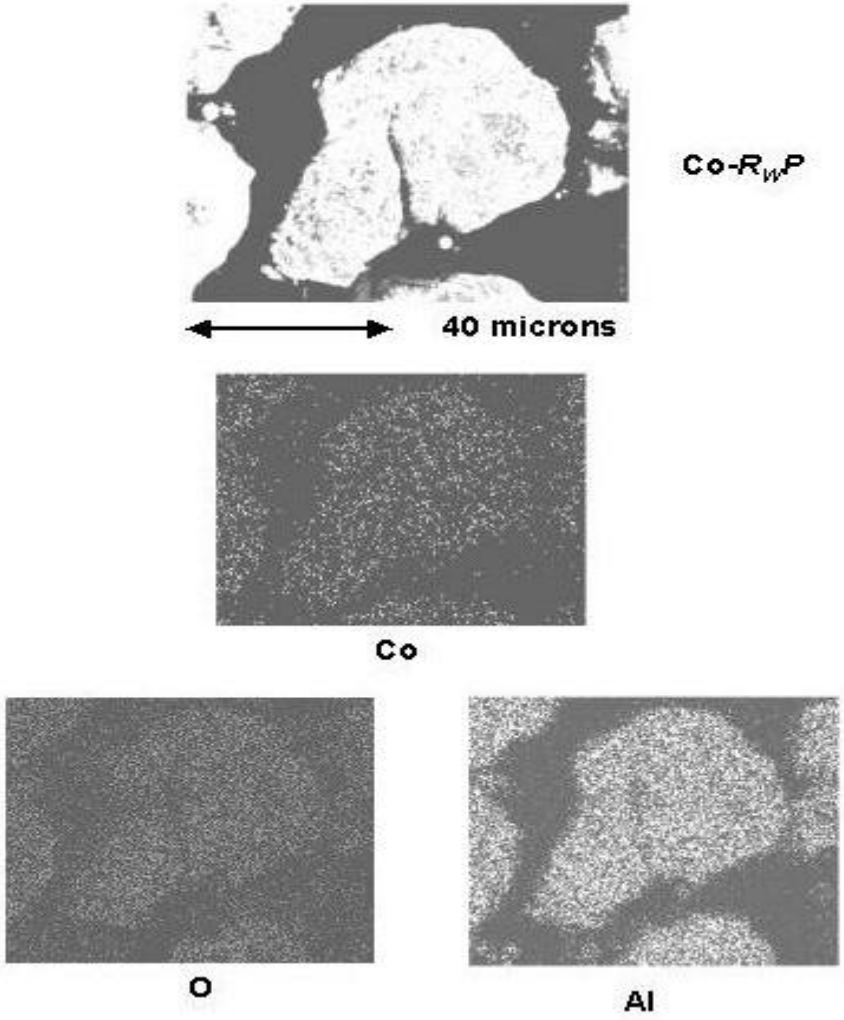

Figure 6.8 EDX Mapping for Co-R_WP Catalyst Granule

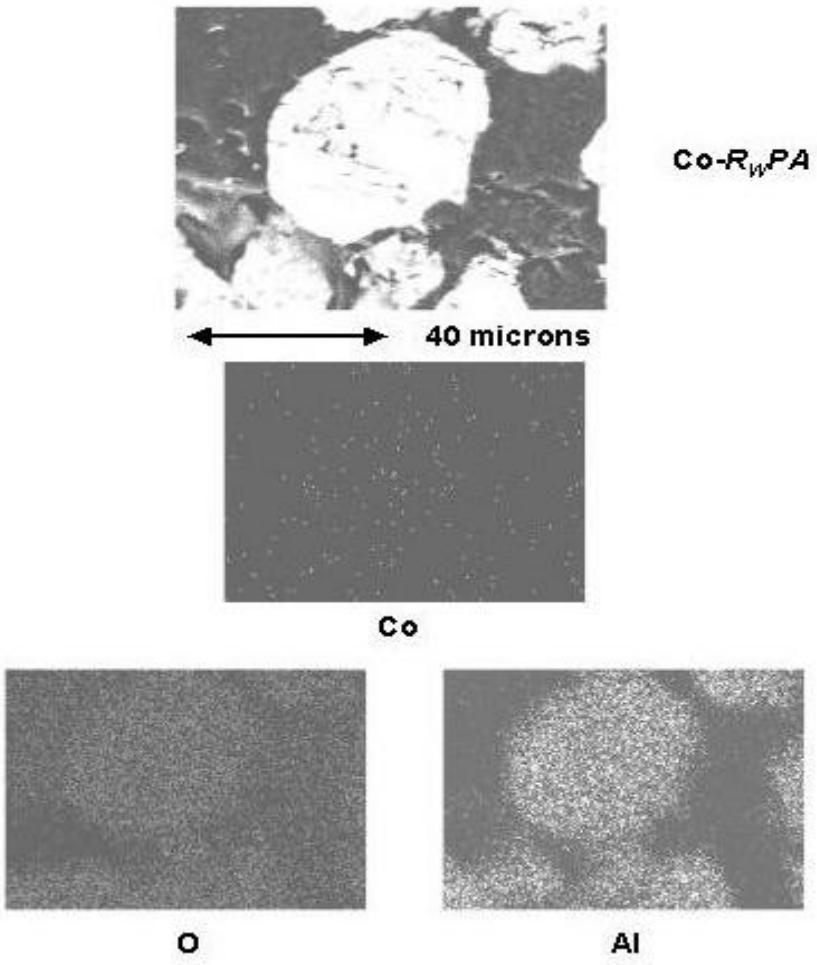

Figure 6.9 EDX Mapping for Co-R_W*PA* Catalyst Granule

7.0 EFFECT OF REDUCTION GAS CONTAINING CARBON MONOXIDE

7.1 Introduction

Water vapor is a byproduct of metal catalyst reduction and has also been shown to have a major impact on Co-SCF. In a previous study reported by our laboratory[1], water vapor was found to increase the amount of non-reducible (at temperatures ≤ 900°C) Co "aluminate" formed during reduction of $CoRu/\gamma\text{-}Al_2O_3$. It was suggested that water vapor decreases the reducibility of the cobalt in possibly two ways: (i) inhibition of the reduction of well-dispersed CoO interacting with the alumina support possibly by increasing the cobalt-alumina interaction, and/or (ii) facilitation of the migration of cobalt ions into probable tetrahedral sites of $\gamma\text{-}Al_2O_3$ to form a non-reducible (at temperatures ≤ 900°C) Co "aluminate". This irreversible Co "aluminate" formation results in a decrease in the amount of cobalt able to be reduced using conventional reduction procedures. However, it is uneconomic to decrease water vapor partial pressure to low enough levels during reduction of Co catalysts for industrial scale processes to avoid facilitation of Co-SCF. Thus, in order to decrease the amount of non-reducible Co-SCF, a way needs to be found to minimize the impact of water vapor during reduction.

FTS at high conversions results in high partial pressures of water vapor as a byproduct without significant deactivation of Co catalysts. Thus, it is assumed that the presence of CO may help to prevent Co catalysts from rapidly deactivating due to Co-SCF. This study reported the results of a study of the effect of CO partial pressure on Co-SCF during reduction of a $Co/\gamma\text{-}$

Al_2O_3 catalyst. Since water vapor can have a significant impact on Co-SCF, the effect of CO on the H_2 reduction of Co/γ-Al_2O_3 at low and relatively high partial pressures of water vapor was investigated. Noble metal promotion of the Co/γ-Al_2O_3 was not used in this study in order to maximize the amount of Co-SCF.[2]

7.2 Experimental

7.2.1 Materials

7.2.1.1 Co/γ-Al_2O_3. The Co/γ-Al_2O_3 catalyst was prepared by the incipient wetness impregnation of γ-Al_2O_3 having a specific surface area of 209 m^2/g and an average particle size ca. 60 μm. The support precursor (Vista B boehmite) was first calcined at 500°C for 10 h before impregnation in order to put it in the form of γ-Al_2O_3. Cobalt nitrate ($Co(NO_3)_2 \cdot 6H_2O$) was dissolved in de-ionized water and impregnated into the support using incipient wetness to give a final catalyst with 20 wt% cobalt. The catalyst was dried at 110°C for 12 h and calcined in air at 300°C for 2 h.

7.2.1.2 CoO, Co_3O_4 (spinel), and $CoAl_2O_4$ (spinel). In order to identify the XRD peaks and Raman bands of the samples, cobalt (II) oxide [95% CoO] from Alfa Aesar, cobalt (II, III) oxide (spinel) [99.5% Co_3O_4] from Strem Chemicals, Inc., and cobalt aluminate (spinel) [98% $CoAl_2O_4$, 39-41% Co] from Alfa Aesar were used as reference materials.

7.2.2 Catalyst Pretreatment

Standard reduction of the calcined catalyst was carried out in a fixed-bed flow reactor under differential conditions at 1 atm using a temperature ramp from ambient to 350^{o}C at 1^{o}/min and holding at 350^{o}C for 10 h in a gas flow having a space velocity of 16,000 h^{-1} and consisting of H_2 or a mixture of H_2 and 3 vol% added water vapor. Various amounts of CO between 0 to 9 vol% (P_{CO}/P_{H2} = 0-0.10) were also introduced into the reduction gas from the beginning. The reduced catalyst was then passivated at room temperature for 2 h with a mixture of O_2/He (5.2% of O_2). The high space velocity of the H_2 flow without water vapor added insured that the partial pressure of water vapor in the catalyst bed produced by Co oxide reduction would be essentially zero in this case.

7.2.3 Catalyst Nomenclature

The nomenclature used for the catalyst samples in this study is the following:

Co-***R***: The catalyst samples reduced in H_2 and then passivated.

Co-$\boldsymbol{R_{[W]}}$: The catalyst samples reduced in a mixture of H_2 with 3% water vapor added and then passivated.

Co-$\boldsymbol{R_{[C\text{-}n]}}$: The catalyst samples reduced in H_2 and n% (0-9%) of CO, and then passivated.

Co-$\boldsymbol{R_{[WC\text{-}n]}}$: The catalyst samples reduced in a mixture of H_2 with 3% added water vapor and n % (0-9%) of CO, and then passivated.

7.2.4 Catalyst Characterization

7.2.4.1 X-ray Powder Diffraction (XRD). XRD was performed to determine the bulk crystalline phases of the catalyst following different pretreatment conditions. X-ray powder diffraction patterns of samples were collected using a Scintag XDS-2000 X-ray diffractometer with monochromatized Cu-K_α radiation (λ = 1.54439 Å). The spectra were scanned at a rate of 2.4 degree/min from 2θ = 20 to 80 degrees.

7.2.4.2 Raman Spectroscopy. The Raman spectra of the samples were collected by projecting a continuous wave laser of helium-neon (He-Ne) red (632.816 nm) through the samples exposed to air at room temperature. A scanning range between 100 to 1000 cm^{-1} with a resolution of 2 cm^{-1} was applied. The data were analyzed using Renishaw WiRE (Windows-based Raman Environment) software which allows Raman spectra to be captured, calibrated, and analyzed using system 2000 functionality via the Galactic GRAMS interface with global imaging capacity.

7.2.4.3 SEM and EDX. SEM and EDX were performed to study the morphology of the catalyst and elemental distribution, respectively. A Hitachi S3500N SEM was used in the back scattering electron (BSE) mode at 15 kV with a working distance (the distance between a sample and the electron beam) of 15 mm. After the SEM micrographs were taken, EDX was performed to determine the elemental concentration on the catalyst surface (using INCA software).

7.2.4.4 Hydrogen Chemisorption. Static H_2 chemisorption on the reduced cobalt catalysts was used to determine the number of reduced surface cobalt metal atoms. This is related to the

overall activity of the catalyst during FTS. Gas volumetric chemisorption at 100°C was performed using the method described by Reuel and Bartholomew.[3] Chemisorption was conducted in a Micromeritics ASAP 2010 using ASAP 2010C V3.00 software. Prior to H_2 chemisorption, the passivated catalyst samples were evacuated to 10^{-6} mm Hg at 100°C for 15 min, reduced in H_2 flow at 100°C for 15 min, reduced at 350°C for 10 h, and then evacuated at 350°C for 90 min to desorb any hydrogen.

7.2.4.5 Temperature Programmed Reduction (TPR). TPR was performed to determine the reducibility and reduction behavior of the catalyst samples. TPR was carried out in an Altamira AMI-1 system using 50 mg of catalyst and a temperature ramp from 30ºC to 900ºC at 5ºC/min. The reduction gas was 5% H_2 in Ar. A cold trap (-70ºC) was placed before the detector to remove water produced during the reaction. A thermal conductivity detector (TCD) was used to determine the amount of hydrogen consumed. The amount of hydrogen consumption was calibrated using TPR of silver oxide (Ag_2O) at the same conditions. The reduced and passivated catalyst samples were re-calcined in-situ at 300°C for 2 h before performing TPR.

7.2.5 Reaction

The catalyst samples reduced in various reduction gas compositions were tested for their initial and steady-state activity. Hydrogenation of CO was carried out at 220°C and 1.8 atm. A flow rate of H_2/CO/He = 20/2/8 cc/min in a fixed bed flow reactor under differential conditions was used. Thermocouples at the top and at the bottom of the catalyst bed assured precise temperature control during pretreatment and reaction. Typically, 15 mg of a reduced and passivated catalyst sample was re-reduced *in situ* in flowing H_2 (30 cc/min) at 350°C for 10 h

prior to the reaction. Reactor effluent samples were taken at 1-h intervals and analyzed by GC. In all cases, steady state was reached within 5 h.

7.3 Results

7.3.1 XRD

XRD patterns for representative catalyst samples reduced at various reduction gas phase compositions are shown in Figure 7.1. Reference patterns for γ-Al_2O_3, CoO, Co_3O_4 (spinel), and $CoAl_2O_4$ (spinel) are also shown. The XRD results for all the catalyst samples reduced with the various gas compositions used in this study were identical after passivation. For all the samples, only XRD peaks of CoO at 37°, 42.6° and 61.8° as well as those for γ-Al_2O_3 were evident. No XRD peaks of $CoAl_2O_4$ (spinel) were detected for any of the catalyst samples.

7.3.2 Raman Spectroscopy

Raman spectra of the catalyst samples are shown in Figures 7.2 to 7.4. Raman bands for all Co-$R_{[C\text{-}n]}$ were identical and different from that for Co-*R* as shown in Figure 7.2. Only two very broad Raman bands at ca. 690 and 560 cm^{-1} were detected for Co-*R* and this has been correlated to the formation of a highly dispersed Co "aluminate" [2]. Strong Raman bands at 690 and 480 cm^{-1} were observed for the Co-$R_{[C\text{-}n]}$ samples. As can be seen in Figure 7.3, as previous reported[2], the addition of water vapor during reduction resulted in an enhancement for Co-$R_{[W]}$ of the Co "aluminate" bands, without any other bands being evident. However, for the Co-$R_{[WC\text{-}9]}$ sample at the highest concentration of added CO, there were obvious Raman bands at 690, 619, 519, 480, and 198 cm^{-1}. These bands can be assigned to Co_3O_4 (see Figure 7.4) present on

catalyst surface after the samples were exposed to air rather than CoO (detected in the bulk by XRD) since Raman is more of a surface technique. Samples reduced at lower concentrations of CO also exhibited similar peaks as well as a broad peak from 520-620 cm^{-1} that obscured the weak band at 619 and 519. The broad Raman band between 450-620 cm^{-1}, which represents Co "aluminate" as seen for Co-$R_{[W]}$, was thus apparently present for the Co-$R_{[WC-n]}$ samples where $n \leq 7$. No peaks for $CoAl_2O_4$ (spinel) were detected in any of the samples.

7.3.3 SEM and EDX

There was no significant change in morphology of the catalyst samples after the various reduction conditions used in this study. The typical morphology of a sample is shown in Figures 7.5 and 7.8. In all figures, the white or light spots represent high concentrations of Co and its compounds and the gray areas represent the alumina support with no/minimal Co. Figures 7.5 and 7.7 shows the external catalyst granule surface of sample Co-$R_{[C-n]}$ and Co-$R_{[WC-n]}$, whereas Figures 7.6 and 7.8 shows a cross section of a catalyst granule of the same samples. Co patches were well distributed over the external surface and throughout the interior of all the catalyst granules.

EDX gave useful information about elemental distribution in the pretreated catalyst granules. EDX mapping indicated that all elements in the catalyst samples were well distributed (Figure 7.9 shows typical elemental distributions for a cross section of a catalyst granule). EDX was also able to detect the presence of carbon for those samples exposed to CO addition > 3 vol%. Average elemental compositions on the external catalyst granule surfaces of the samples are given in Table 7.1.

7.3.4 TPR

TPR was preformed to determine the reduction behavior and reducibility of the catalysts. TPR profiles of the catalyst samples after various pretreatment conditions are shown in Figures 7.10 and 7.11. Reduction was observed for all catalyst samples to occur in two major peaks. The first peak is due to a two-step reduction of Co_3O_4 (with no/minimal interaction with the support) to Co metal[2,4-7] and occurred at ca. 320°C for both Co-$R_{[C-n]}$ and Co-$R_{[WC-n]}$ samples. This peak occurred about 20°C lower than those for Co-R and Co-$R_{[W]}$. The second observable peak (very broad and made up of multiple overlapping peaks) is due to the reduction of Co species strongly interacting with the support ($Co\text{-}Al_XO_Y$)[2,4-7] and occurred between 400-700°C (max. at 650°C) for both Co-$R_{[C-n]}$ and Co-$R_{[WC-n]}$ samples. The reducibilities (at temperatures up to 900°C) of the catalysts were calculated and are given in Table 7.2 and figure 7.12. The reducibilities for TPR between 30-400°C (related to the reducibilities of the samples during standard reduction at 350°C[6]) ranged between 16-29% for Co-$R_{[C-n]}$ samples and 14-20% for Co-$R_{[WC-n]}$ samples. For Co-$R_{[C-n]}$, the reducibility increased from 17% (for Co-R) up to a maximum of 29% for 5 vol% added CO before decreasing when greater amounts of CO were added. For Co-$R_{[WC-n]}$, the reducibility appeared to also go through a maximum (for 3-5 vol% CO) with increasing amount of added CO, but the difference was less dramatic (14% to 20%). The results for reducibilities during TPR from 30-900°C for the two catalyst sample series manifested similar trends as for 30-400°C, but were greater.

7.3.5 H_2 Chemisorption

H_2 chemisorption was performed to determine the overall Co metal dispersion after different reduction conditions. The Co metal dispersions of the samples are shown in Table 7.2

and ranged from 2.8 to 7.9%. For Co-$R_{[C\text{-}n]}$ samples, the Co metal dispersion increased from 3.2% to 7.9% with increasing CO concentration up to the maximum investigated of 9 vol%. However, Co metal dispersion for the Co-$R_{[WC\text{-}n]}$ samples passed through a maximum of 6.2% for 3 vol% added CO.

7.3.6 Reaction

CO hydrogenation (H_2/CO = 10/1) was performed to determine the overall activity of the catalyst samples reduced at various reduction gas compositions. The results are shown in Table 7.3 and Figures 7.13 (no water vapor added during reduction) and 7.14 (with water vapor added during reduction). A plot of rate and CO addition is also shown in Figure 7.15. It can be seen that for Co-$R_{[C\text{-}n]}$, the addition of CO during standard reduction of the Co catalyst caused the rate (both initial and steady-state) of CO hydrogenation to go through a maximum for the case of 5 vol% CO addition. However, the rate after the addition of 9 vol% CO during reduction was lower than that of Co-*R*, the base case.

A similar trend was found for Co-$R_{[WC\text{-}n]}$, except the maximum rate occurred after 3 vol% CO addition and the rate after 9 vol% CO addition was still significantly higher than for Co-$R_{[W]}$. The selectivity to CH_4 during CO hydrogenation was found to be ca. 80-90%. Although the Co-$R_{[C\text{-}n]}$ results would appear to suggest that the CH_4 selectivity went to a minimum with CO addition during reduction, the Co-$R_{[WC\text{-}n]}$ results suggest little variation in selectivity. At this time we are not prepared to conclude that there was any significant different in selectivity for any of the samples.

7.4 Discussion

The addition of CO during standard reduction had a significant impact on the reaction rate during CO hydrogenation (H_2/CO = 10/1). It was found that an optimal concentration of CO (3-5 vol%) added to H_2 during reduction at low or high partial pressures of water vapor produced specific activities four times greater than when the catalyst was reduced without CO addition. One thing that might explain higher activity is increased reducibility.

It is known that three reduction peaks located at ca. 200°, 300°, and between 400° and 750°C (max. at 600°C) can be seen for calcined Co/γ-Al_2O_3 (calcined at 300°C for 2 h).[2,4] The first peak at ca. 200°C has been assigned to the decomposition of residual Co nitrate. The second peak at ca. 300°C has been assigned to the reduction of Co_3O_4 to CoO and Co^0 and the highest reduction temperature peak is related to the reduction of Co species strongly interacting with the alumina support to Co metal. Due to the sequential pretreatments (calcination, reduction, passivation, and recalcination) prior to TPR measurement, only two reduction steps are observed during TPR from 30-900°C (Figures 7.10 and 7.11) of the samples. The pretreatments used prior to TPR measurement were able to decompose all residual Co nitrate resulting in the absence of a peak at 200°C. Based on the similar TPR profiles in this study, it is suggested that CO addition during reduction did not have a significant impact on the reduction characteristics (peak locations) of the samples with the possible exception of an increase in the kinetics of reduction for the peak ca. 340°C that was shifted -20°C. However, the % reducibilities were much more dramatically affected by the CO addition.

It was observed that, for standard reduction at low partial pressure of water vapor (Co-$R_{[C-n]}$), the reducibility of these catalysts[1] went through a maximum with increasing amount of CO added during standard reduction. For reduction at high partial pressure of water vapor (Co-

$R_{[WC-n]}$), the results were much less dramatic, probably due to the impact of water vapor, but similar. It is possible that the addition of an optimum amount of CO resulted in an increase in reducibility due to CO helping to prevent the formation of Co species strongly interacting with the support. However, higher concentrations of CO possibly resulted in lower reducibilities as a result of H_2 being more difficult to activate on carbon-blocked Co surfaces and Co oxide being more difficult to reduce under deposited carbon (Table 7.1), especially graphitic carbon.

It is known that cobalt carbide can be formed during carburization of cobalt metal using CO.[8] However, there was no evidence of carbide formation, possibly due to the very high ratio of H_2/CO used. In this study, after the use of high concentrations of CO, it is not surprising that carbon deposition was found (Table 7.1). The amount of deposited carbon increased with increasing amount of CO added during reduction. However, for the same amount of CO added, there was less carbon deposited when water vapor was also added. This would appear to be due to an impact of water vapor on CO dissociation. The carbon deposited can exist in two forms: active carbon and graphite. Active carbon can react with hydrogen to form methane (CH_4) or oxygen to form CO or CO_2, whereas graphite is very non-reactive and difficult to remove.

If the deposited carbon were in the form of active carbon, it could have reacted with H_2 resulting in an increase in the amount of H_2 consumed during TPR. In order to determine the impact of this on the % reducibility obtained, the Co-$R_{[C-9]}$ and Co-$R_{[WC-9]}$ samples were analyzed for carbon content (Table 7.4). Both samples were chosen based on the fact that they contained the highest amount of carbon. After reduction and passivation, the carbon content was found to be ca. 0.9 and 0.6 wt%, respectively. After re-reduction and passivation, only ca. 0.4 and 0.2 wt% remained (57-64% of the carbon was removed). However, after recalcination prior to TPR measurement, the carbon content was found to be ca. 0.2 wt% (61-76% of the carbon was

removed). After TPR the same amount of carbon appeared to still remain for Co-$R_{[C\text{-}9]}$. This suggests that the form of carbon left was graphite, which did not have an effect on the amount of H_2 consumed during TPR. However, for Co-$R_{[WC\text{-}9]}$, the amount of carbon removed during TPR was at most ca. 0.1 wt%, and may have been zero given experimental error. Based on calculation, if 0.1 wt% active carbon reacted with H_2 during TPR, this would account for at most only 3% of the total possible 100% reducibility for the 20 wt% Co catalyst. This suggests that the pretreatment used prior to TPR measurement was able to remove most of the active carbon in the samples and any error introduced in the measurement of Co reducibility was minimal.

Besides Co reducibility, Co dispersion is critical in determining catalytic activity. There was an increase in Co dispersion upon CO addition during reduction (as determined by H_2 chemisorption) possibly because there was a decrease in sintering of the Co metal. However, the chemisorption results cannot be taken at face value. Clearly, if one looks at the values of TOF calculated, one sees a lot of variation. CO hydrogenation is well known to be a structure insensitive reaction. As such, TOF should not vary greatly with Co dispersion. If one considers the base samples (Co-*R* and Co-$R_{[W]}$), their initial TOF's are ca. 1 x 10^{-2} sec^{-1} - typical for Co catalysts under these conditions.[9-10] Since H_2 chemisorption on Co is highly activated, it must be carried out at 100°C in order to come close to adsorbing hydrogen on all the available surface metal atoms in a reasonable time.[3] Reduction in the presence of added CO results in carbon deposition on the catalyst samples. Such carbon may bias the chemisorption results by (i) reacting with some H_2 to form CH_4, (ii) providing adsorption sites for H atoms that spill over from Co sites at 100°C, and (iii) providing a bridge for H atoms to spill over onto the support. Any of these would, thus, result in an amount of hydrogen atoms "chemisorbed" greater than the number of reduced Co metal surface atoms. On the other hand, it is also possible that carbon

could block some Co metal surface sites and, if spillover did not happen, would result in exposed Co metal sites being counted accurately. Although, based on steady-state isotopic transient kinetic analysis (SSITKA) results, it is known that the number of active intermediates on a Co surface during CO hydrogenation is only a small fraction of the number of Co metal surface atoms[9-10], this fraction remains fairly constant for a wide variety of Co dispersions. It can be suggested that Co-$R_{[C-9]}$ exhibited a large amount of hydrogen chemisorbed, but a low TOF based on its low rate. One might imagine that, for this sample at the highest concentration of added CO, spillover of hydrogen must have occurred. It should be noted that this catalyst also had the highest concentration of deposited carbon. All the rest of the samples gave reasonable TOF's (within a factor of 2, as is often seen).[9]

It should also be mentioned that XRD did not detect any difference upon CO addition during reduction. The XRD results are typical for reduced Co/γ-Al_2O_3 catalysts.[1-2] However, Raman spectroscopic results were clearly different. In our previous investigation of Co-SCF[2], it was found that Raman spectroscopy is one of the most powerful techniques besides TPR able to identify Co "aluminate" formation (two broad Raman bands at ca. 690 and 560 cm^{-1}). The identified Co "aluminate" is suggested to be different from $CoAl_2O_4$ (spinel) due to it being a non-stoichiometric surface Co "aluminate" compound. In the present study, dramatic changes in the characteristics of the Raman bands for the reduced and passivated catalyst samples were observed with the addition of CO during standard reduction. Basically, the Co "aluminate" bands disappeared more and more with increasing amount of CO added. The Raman bands for the passivated samples of apparently Co_3O_4 at 690 and 480 cm^{-1} became more dominant. This suggests that the addition of CO during reduction may have helped to decrease the amount of Co "aluminate" formed. It should be noted that the characteristics of Raman bands for Co-$R_{[C-n]}$ and

Co-$R_{[WC-n]}$ were different. This is based on the fact that water vapor increases the amount of Co "aluminate" formed. Since Co catalysts in general and Co/Al_2O_3 in particular are not good water-gas-shift catalysts, CO is not able to react with the water to decrease its concentration.

It is clear that CO addition during reduction had effects on Co reducibility and dispersion of the catalyst samples. Based on all the evidence presented, it is suggested that the increase in specific activity (per gram basis) seen was primarily due to an increase in Co reducibility along with an increase in the number of Co metal surface atoms as determined by H_2 chemisorption.

7.5 Conclusions

The addition of CO during standard H_2 reduction of a 20 wt% Co/γ-Al_2O_3 catalyst produced specific activities about four times greater than when the catalyst reduced without CO addition. Most of this increase appears to have been due to increases in Co reducibility and dispersion. In general, initial and steady-state rates of CO hydrogenation, Co reducibility, and Co dispersion went through a maximum for 3-5 vol% CO added during H_2 reduction. Carbon deposition was detected upon increasing the amount of added CO. The effect of CO addition may be due to one or more of possibly three reasons: (i) CO may help to prevent the formation of Co species strongly interacting with the support, thereby facilitating its reduction, (ii) CO may decrease sintering of the Co metal resulting an increase in Co dispersion, and (iii) CO may block Co "aluminate" formation by minimizing the impact of water vapor even at low partial pressures.

Table 7.1 Elemental Concentrations from EDX

Catalyst Samples	Elemental Concentration (wt%)[a]				
	C	**O**	**Al**	**Co**	**Total**
Co-$R_{[C\text{-}1]}$	-	42.1	39.8	18.1	100
Co-$R_{[C\text{-}3]}$	0.9	45.7	34.6	18.8	100
Co-$R_{[C\text{-}5]}$	1.2	44.1	34.5	20.2	100
Co-$R_{[C\text{-}9]}$	2.5	41.2	38.2	18.1	100
Co-$R_{[WC\text{-}1]}$	-	47.0	32.4	20.6	100
Co-$R_{[WC\text{-}3]}$	-	37.1	43.1	19.8	100
Co-$R_{[WC\text{-}5]}$	0.7	42.8	35.6	20.9	100
Co-$R_{[WC\text{-}7]}$	0.7	44.9	33.2	21.2	100
Co-$R_{[WC\text{-}9]}$	1.5	40.9	35.5	22.1	100

[a] EDX was performed at the external surface of catalyst samples and the elemental concentration was calculated from the average value of 20 spots all over the catalyst granule.

Table 7.2 TPR and H_2 Chemisorption Results

Catalyst Samples	Reduction Conditions			Reducibility [a, b,c] (%)		Total H_2 Chemisorption [e] (mmole H_2/g cat)	Overall Co metal Dispersion [f] (%)	Co^0 d_p [g] (nm)
	P_{CO}/P_{H2} (at feed)	Added CO (vol%)	P_{H2O}/P_{H2} (at feed)	30-900°C [d]	30-400°C			
Co-*R*	0	0	0	58	17	54	3.2	26
Co-$R_{[C-1]}$	0.01	1	0	62	17	85	5.0	17
Co-$R_{[C-3]}$	0.03	3	0	80	28	117	6.9	12
Co-$R_{[C-5]}$	0.05	5	0	93	29	120	7.1	12
Co-$R_{[C-7]}$	0.07	7	0	96	25	132	7.8	11
Co-$R_{[C-9]}$	0.10	9	0	61	16	134	7.9	11
Co-$R_{[W]}$	0	0	0.03	50	14	49	2.9	29
Co-$R_{[WC-1]}$	0.01	1	0.03	58	16	95	5.6	15
Co-$R_{[WC-3]}$	0.03	3	0.03	61	20	105	6.2	14
Co-$R_{[WC-5]}$	0.05	5	0.03	57	20	85	5.0	18
Co-$R_{[WC-7]}$	0.08	7	0.03	54	16	64	3.8	22
Co-$R_{[WC-9]}$	0.10	9	0.03	49	18	47	2.8	29

[a] All catalyst samples were re-calcined at 300°C in air for 2 h before TPR measurement.

[b] The reducibility was based on a calibration with Ag_2O (100% reducibility).

[c] Measurement error = ±5%.

[d] The reducibility during TPR at 30-400°C is related to the reducibility of the catalysts during standard reduction.[(1)]

[e] Error = ±5% of measurement of H_2 chemisorption.

[f] Co metal dispersion (%) = [2 x (total H_2 chemisorption/g cat)/(no. μmole Co tot./g cat)] x 100%.

[g] Average particle size (d_p) is based upon H_2 chemisorption and the amount of reduced cobalt [$d_p = 5/(S_{Co} \times \rho_{Co})$, where S_{Co} is the surface area of reduced Co/g of reduced Co, and ρ_{Co} is the density of cobalt]. Surface area occupied by 1 reduced Co atom assumed to be 6.62 Å^2.[(11)]

Table 7.3 Reaction Rate of CO Hydrogenation

Catalyst Samples	CO Conversion [a] (%)		Rate[d] (mmole/g cat/s)		CH_4 Selectivity (%)		TOF_H [e] x 10^3 (s^{-1})	
	Initial [b]	SS [c]	Initial	SS	Initial	SS	Initial	SS
Co-*R*	1.1	0.8	1.1	0.8	93	94	10.0	7.4
Co-$R_{[C-3]}$	2.0	1.4	1.9	1.3	84	85	8.1	5.6
Co-$R_{[C-5]}$	5.8	4.6	5.5	4.4	86	76	23.0	18.0
Co-$R_{[C-9]}$	0.7	0.6	0.7	0.5	96	92	2.6	1.9
Co-$R_{[W]}$	0.9	0.5	0.8	0.5	84	82	8.2	5.1
Co-$R_{[WC-3]}$	3.6	3.3	3.3	3.0	92	88	16.0	14.0
Co-$R_{[WC-5]}$	3.3	2.7	3.0	2.5	85	84	18.0	15.0
Co-$R_{[WC-9]}$	2.4	1.5	2.2	1.4	86	80	23.0	15.0

[a] CO hydrogenation was carried out at 220°C, 1.8 atm, and H_2/CO = 10 (H_2/CO/He = 20/2/8 cc/min).

[b] After 5 min of reaction.

[c] After 5 h of reaction.

[d] Error ±5%.

[e] Based on total H_2 chemisorption.

Table 7.4 Carbon Content on the Co Catalysts at Various Pretreatments

Catalyst Samples	Carbon Content (wt%)[a]			
	After Reduction[b] (*C-R-P*)	After Re-reduction[c] (*C-R-P-R-P*)	After Re-calcination[d] (*C-R-P-C*)	After TPR[e] (*C-R-P-C-TPR*)
Co-$R_{[C\text{-}9]}$	0.86	0.37	0.21	0.20
Co-$R_{[WC\text{-}9]}$	0.61	0.22	0.24	0.14

C= Calcination, ***R***= Reduction, ***P***= Passivation

[a] Carbon content on the various pretreated catalyst samples was analyzed using combustion/coulometric titration by Galbraith Laboratories, Inc.

[b] Reduction on the calcined catalyst was done at 350^{o}C for 10 h with the various reduction gas mixtures.

[c] Re-reduction on the reduced catalyst was also done at 350^{o}C for 10 h with H_2 prior to FTS.

[d] Re-calcination of the reduced catalyst was done at 300^{o}C for 2 h prier to TPR measurement.

[e] TPR was performed at 30-900^{o}C.

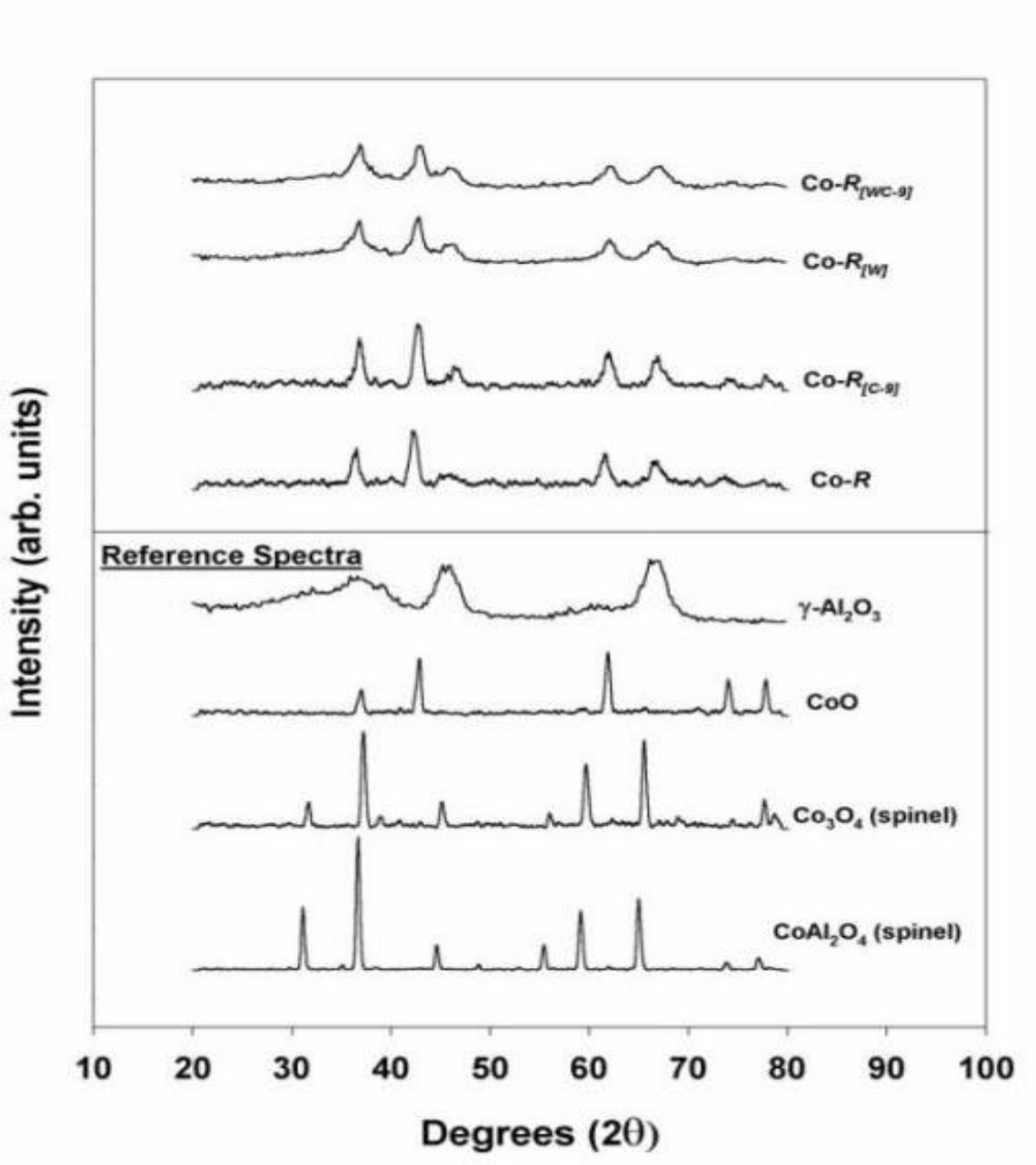

Figure 7.1 XRD Patterns of Co/γ-Al_2O_3 after Various Reduction Conditions, $CoAl_2O_4$ (spinel), Co_3O_4 (spinel), CoO, and γ-Al_2O_3

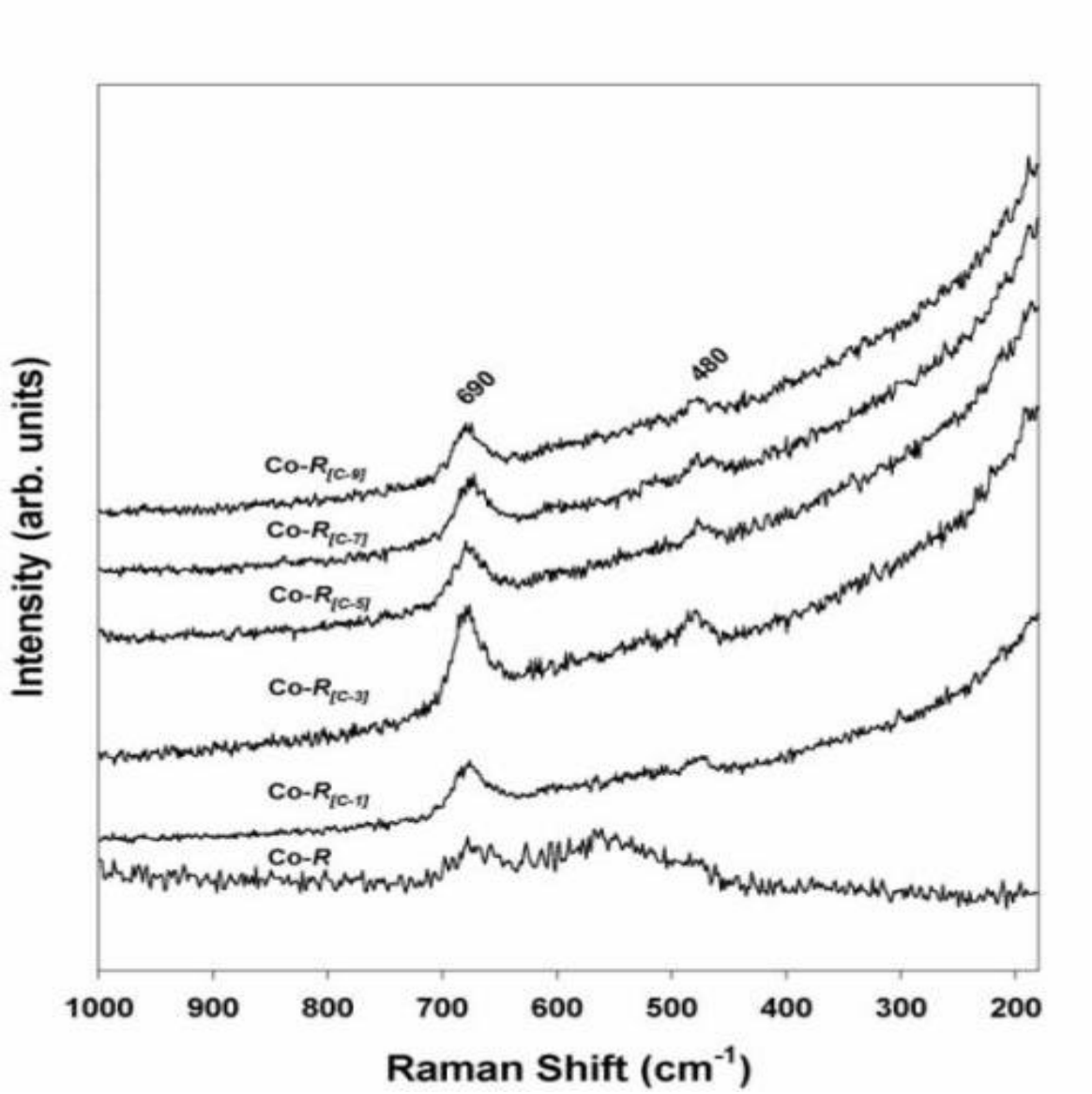

Figure 7.2 Raman Spectra of Co-*R* and Co-$R_{[C-n]}$ Samples

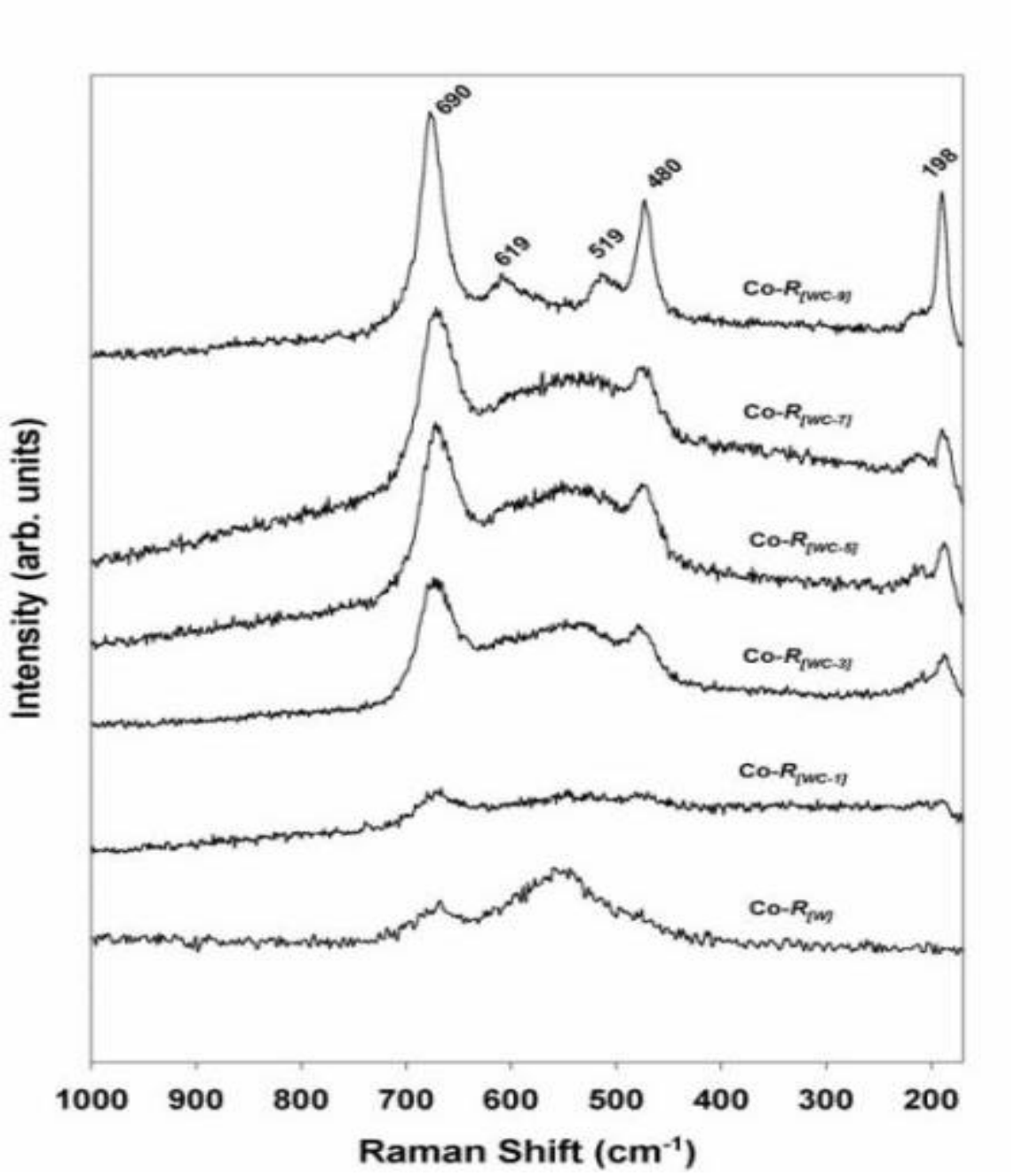

Figure 7.3 Raman Spectra of Co-$R_{[W]}$ and Co-$R_{[WC\text{-}n]}$ Samples

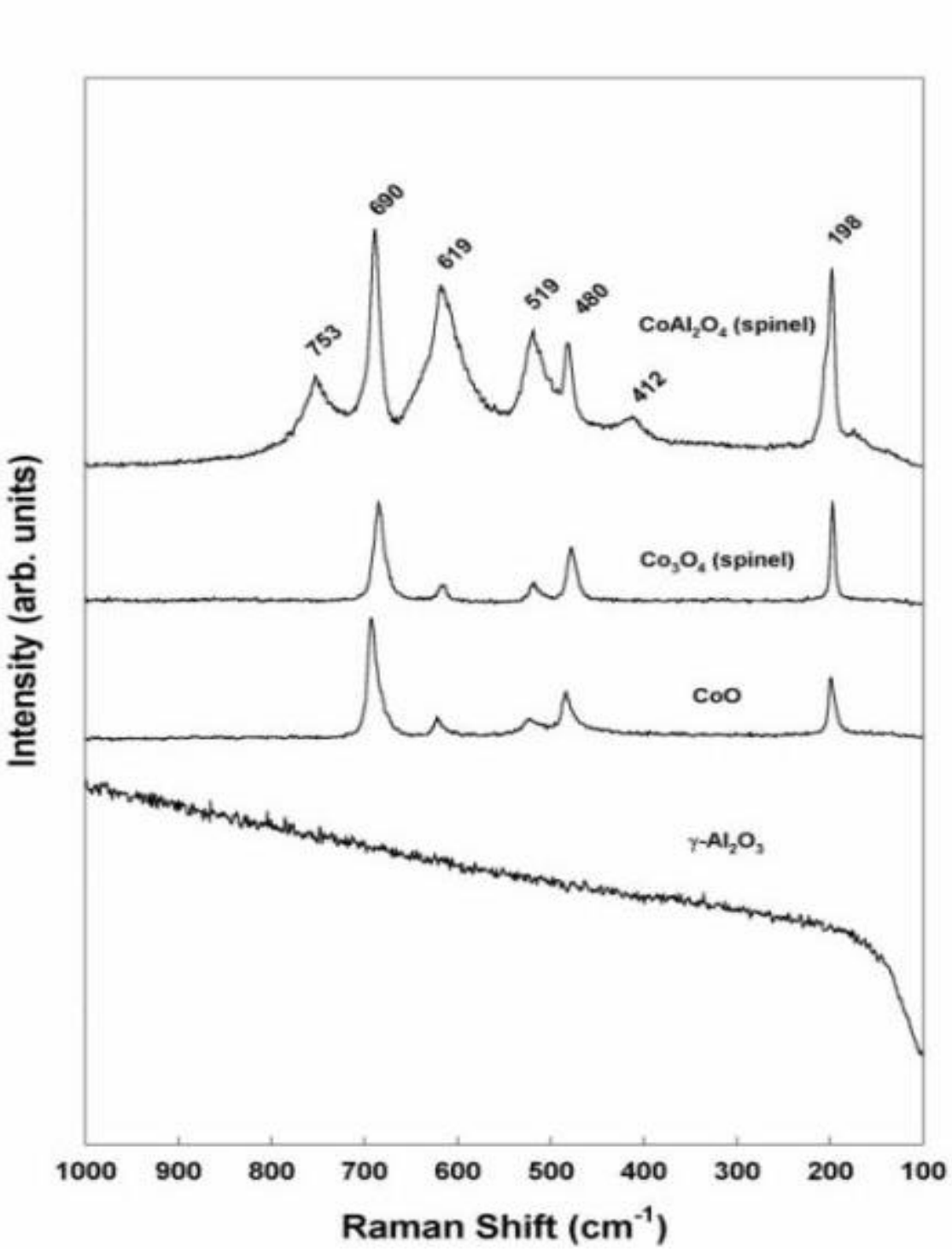

Figure 7.4 Raman Spectra of γ-Al_2O_3, CoO, Co_3O_4, and $CoAl_2O_4$

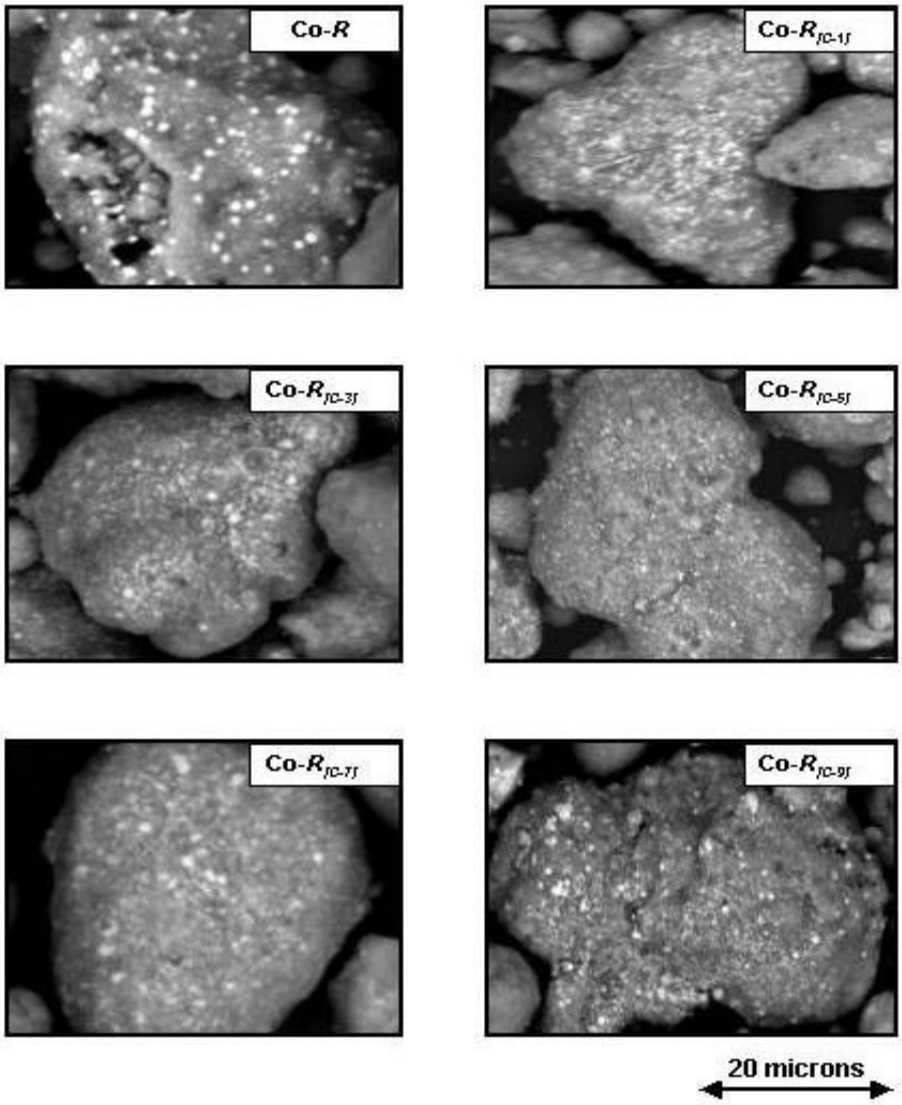

Figure 7.5 SEM Micrographs of Co-$R_{[C-n]}$ Catalyst Granules (external surface)

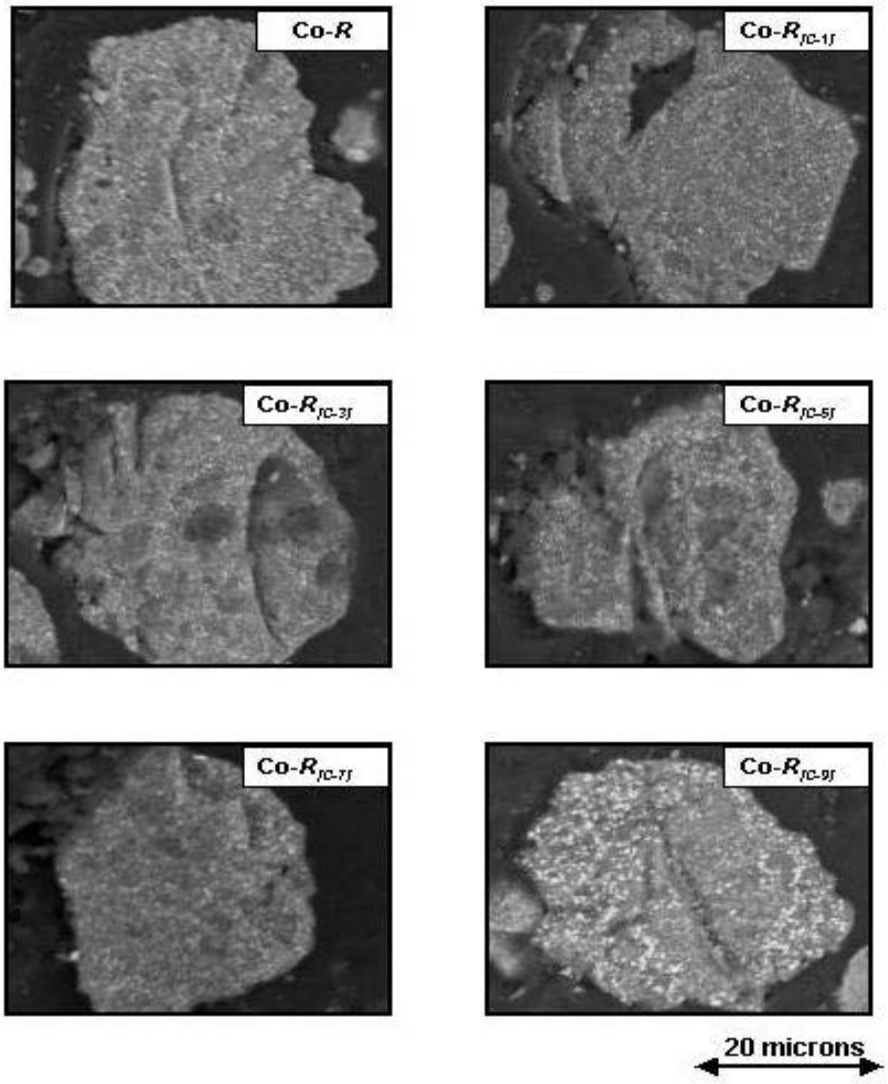

Figure 7.6 SEM Micrographs of Co-$R_{[C\text{-}n]}$ Catalyst Granules (cross section)

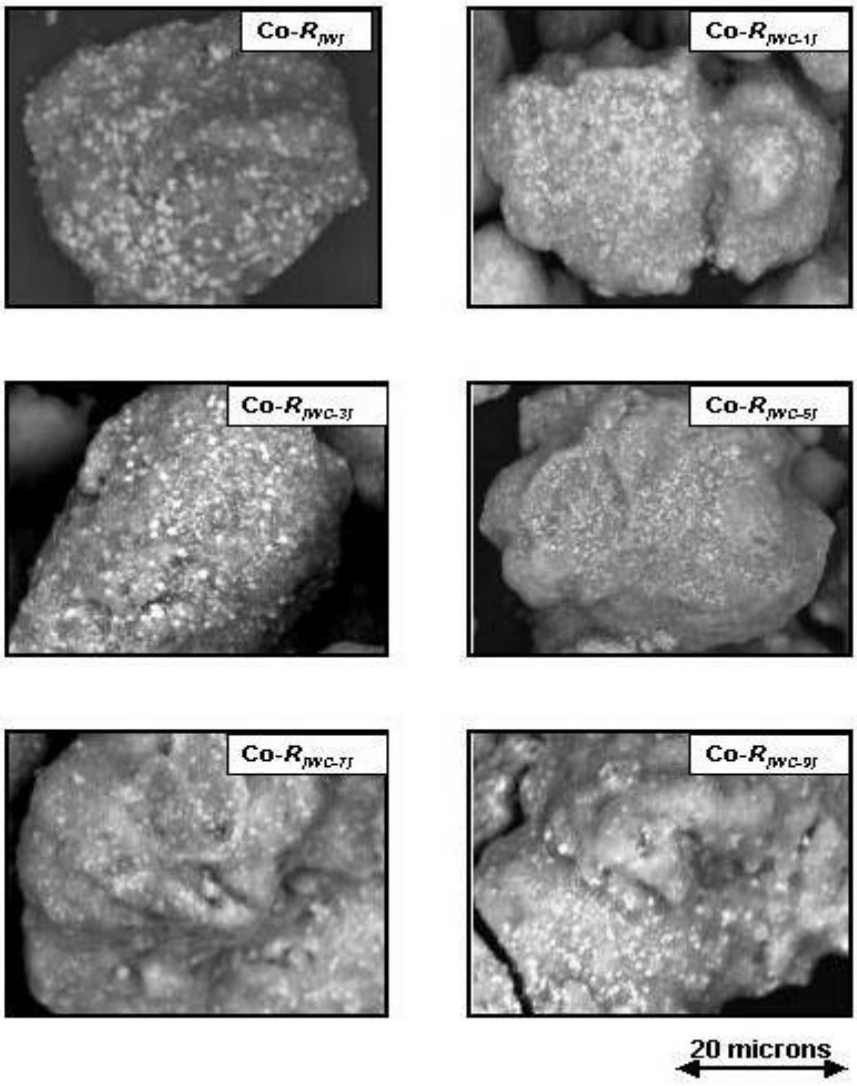

Figure 7.7 SEM Micrographs of Co-$R_{[WC-n]}$ Catalysts Granules (external surface)

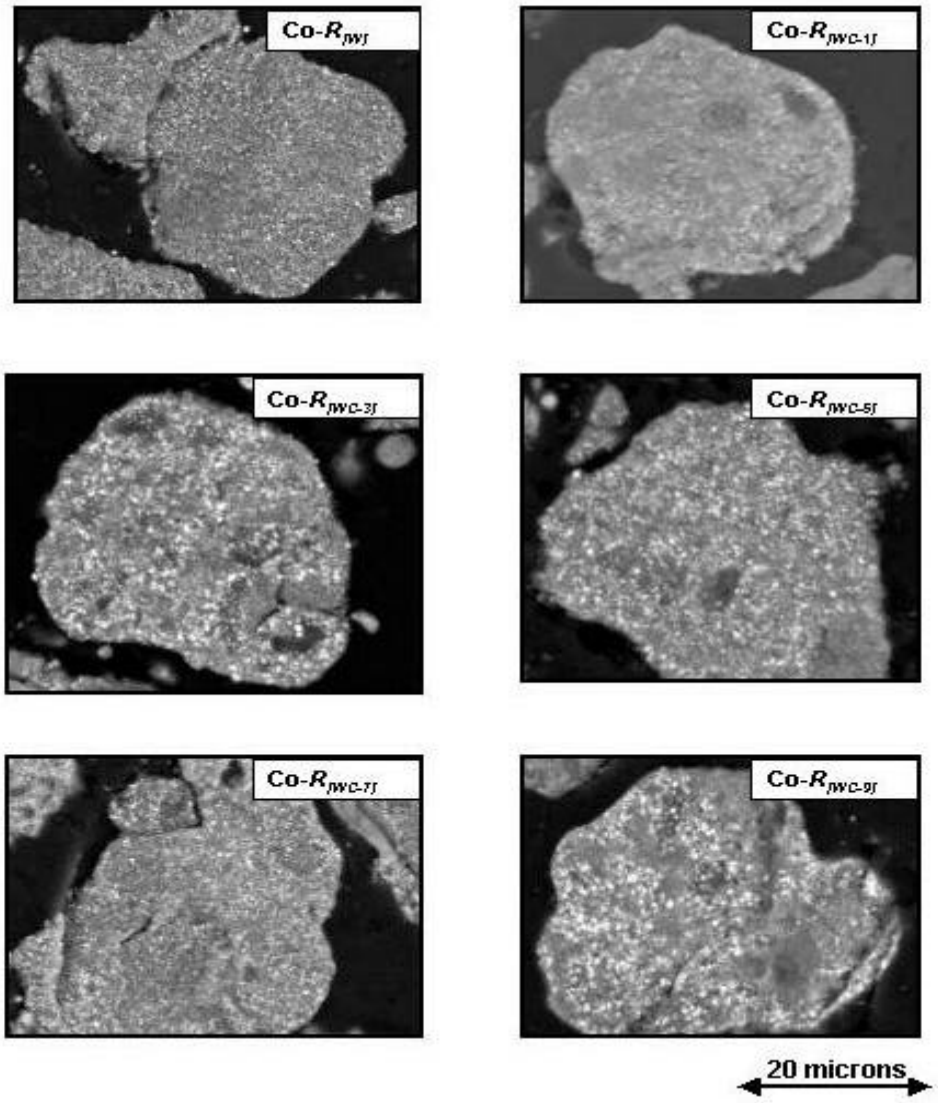

Figure 7.8 SEM Micrographs of Co-$R_{[WC-n]}$ Catalyst Granules (cross section)

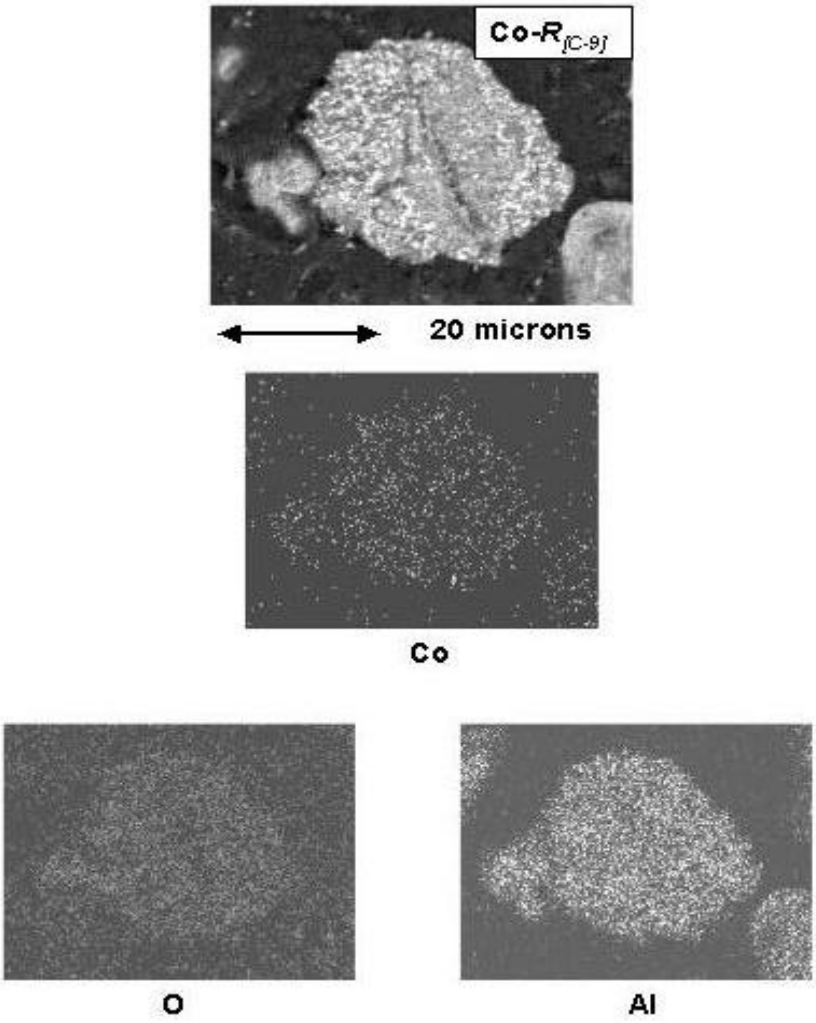

Figure 7.9 Elemental Distribution of Co-$R_{[C-9]}$ Obtained by EDX

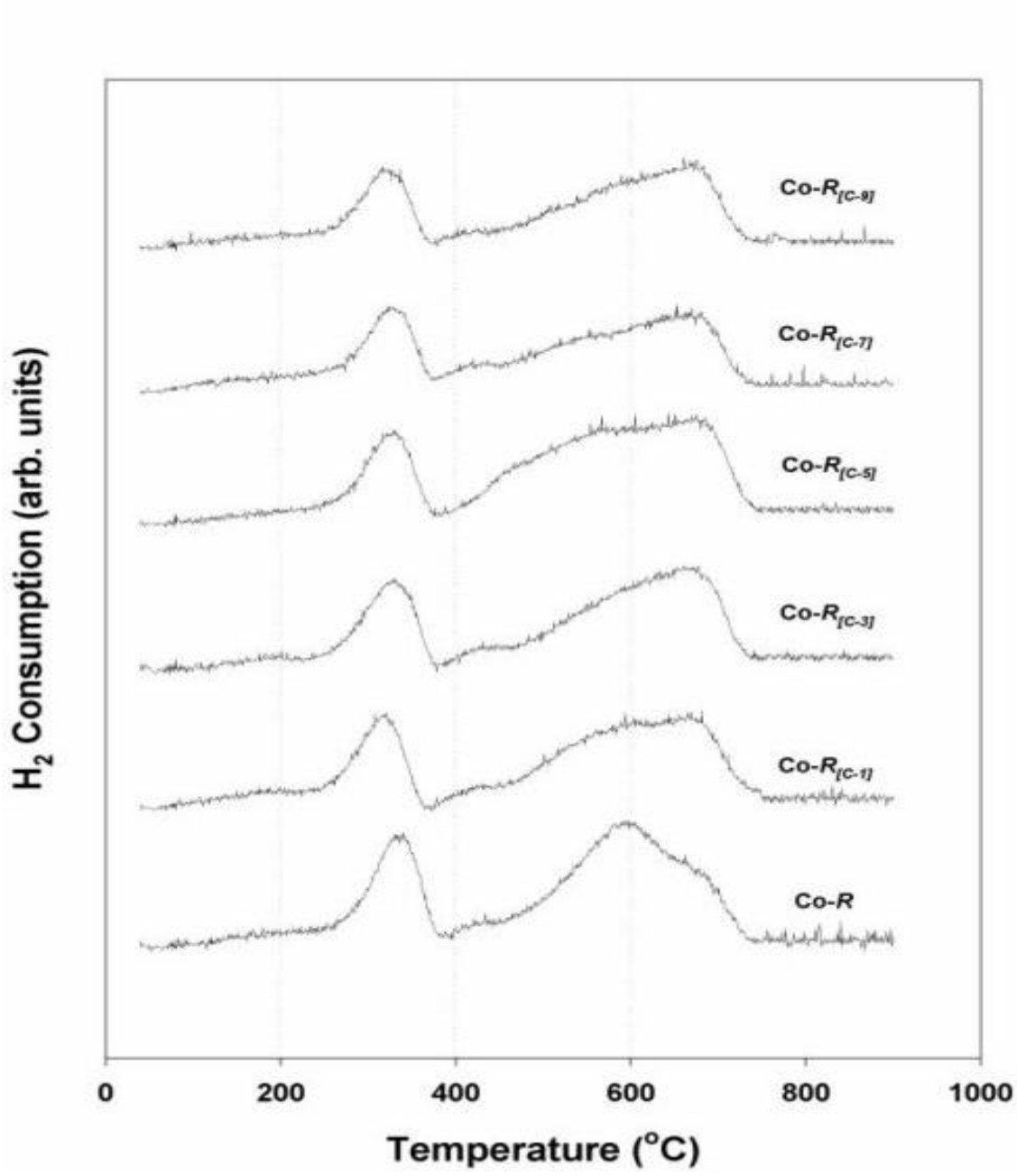

Figure 7.10 TPR Profiles of Co-*R* and Co-$R_{[C-n]}$ Samples

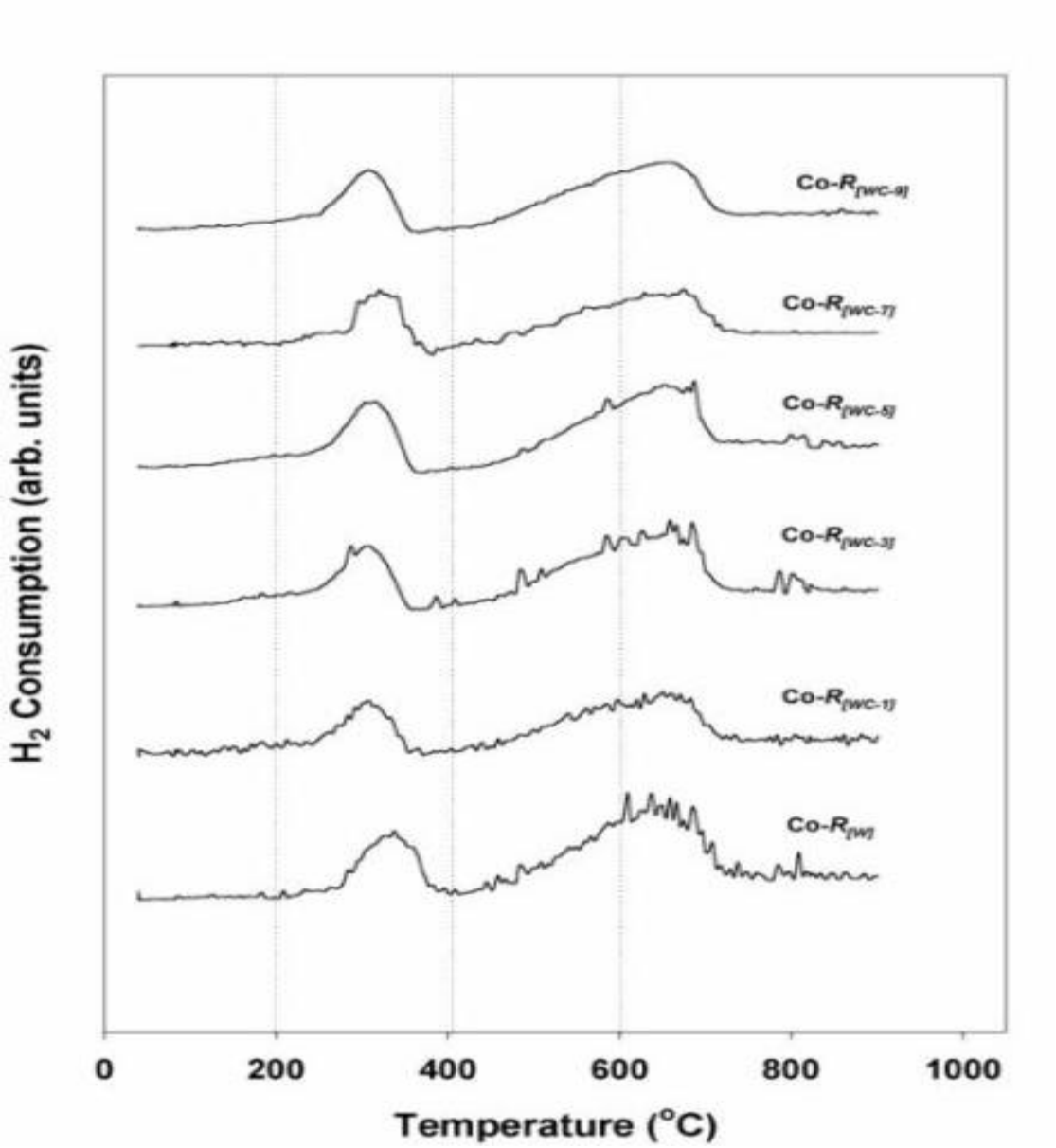

Figure 7.11 TPR Profiles of Co-$R_{[W]}$ and Co-$R_{[WC-n]}$ Samples

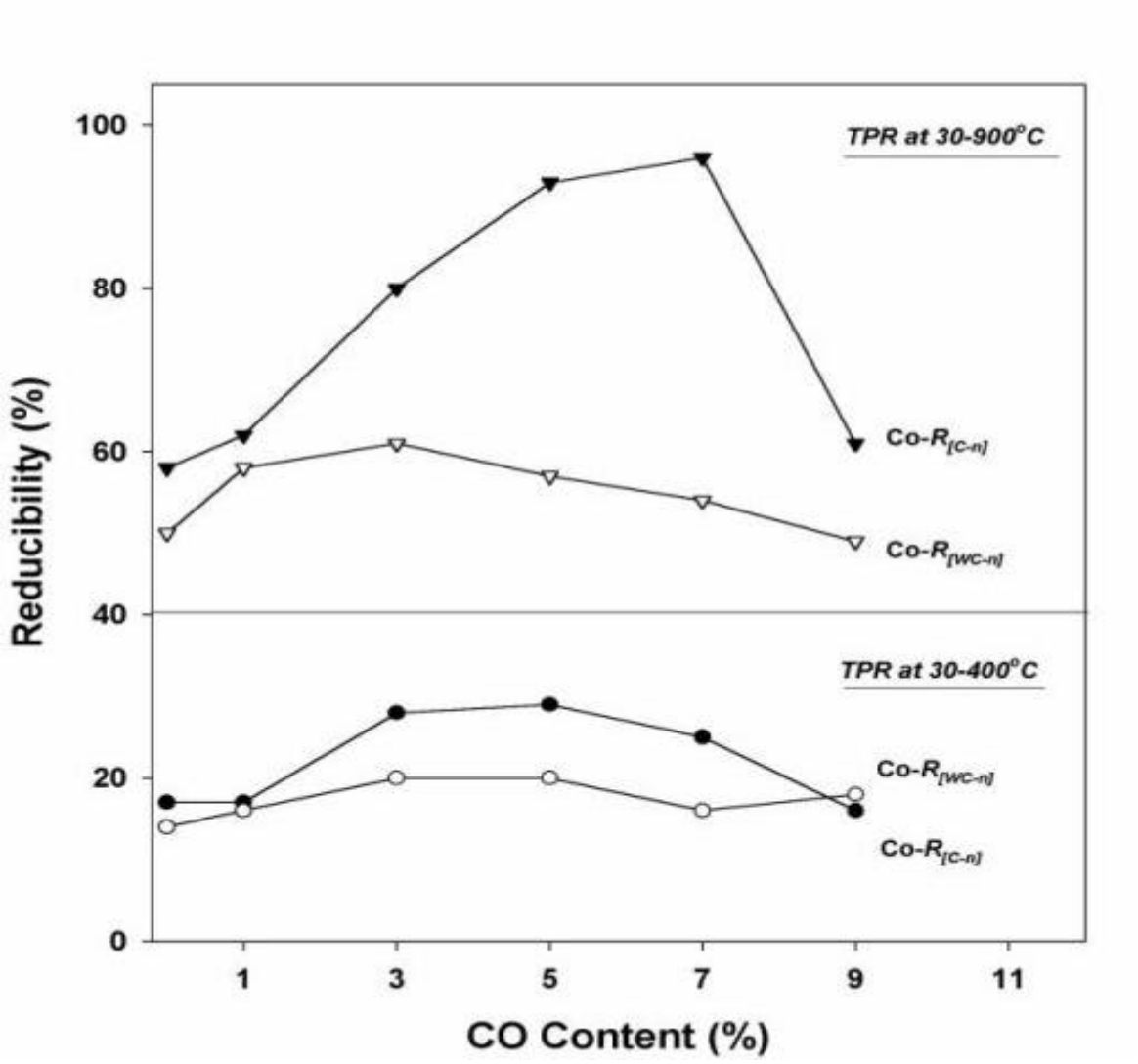

Figure 7.12 Effect of CO Addition during Reduction on reducibility of Co Catalysts

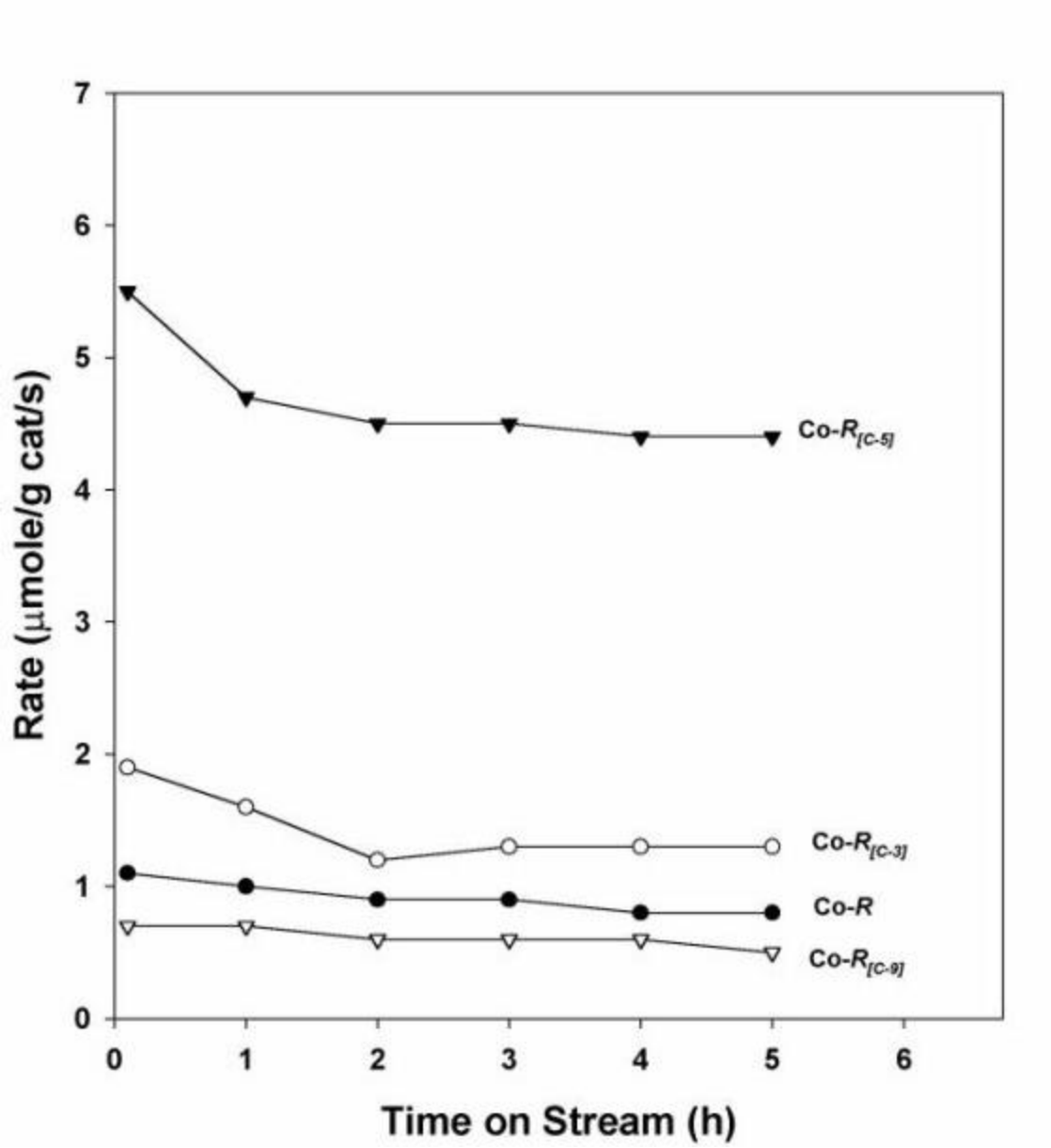

Figure 7.13 Effect of CO Addition during Reduction at Low Partial Pressure of H_2O

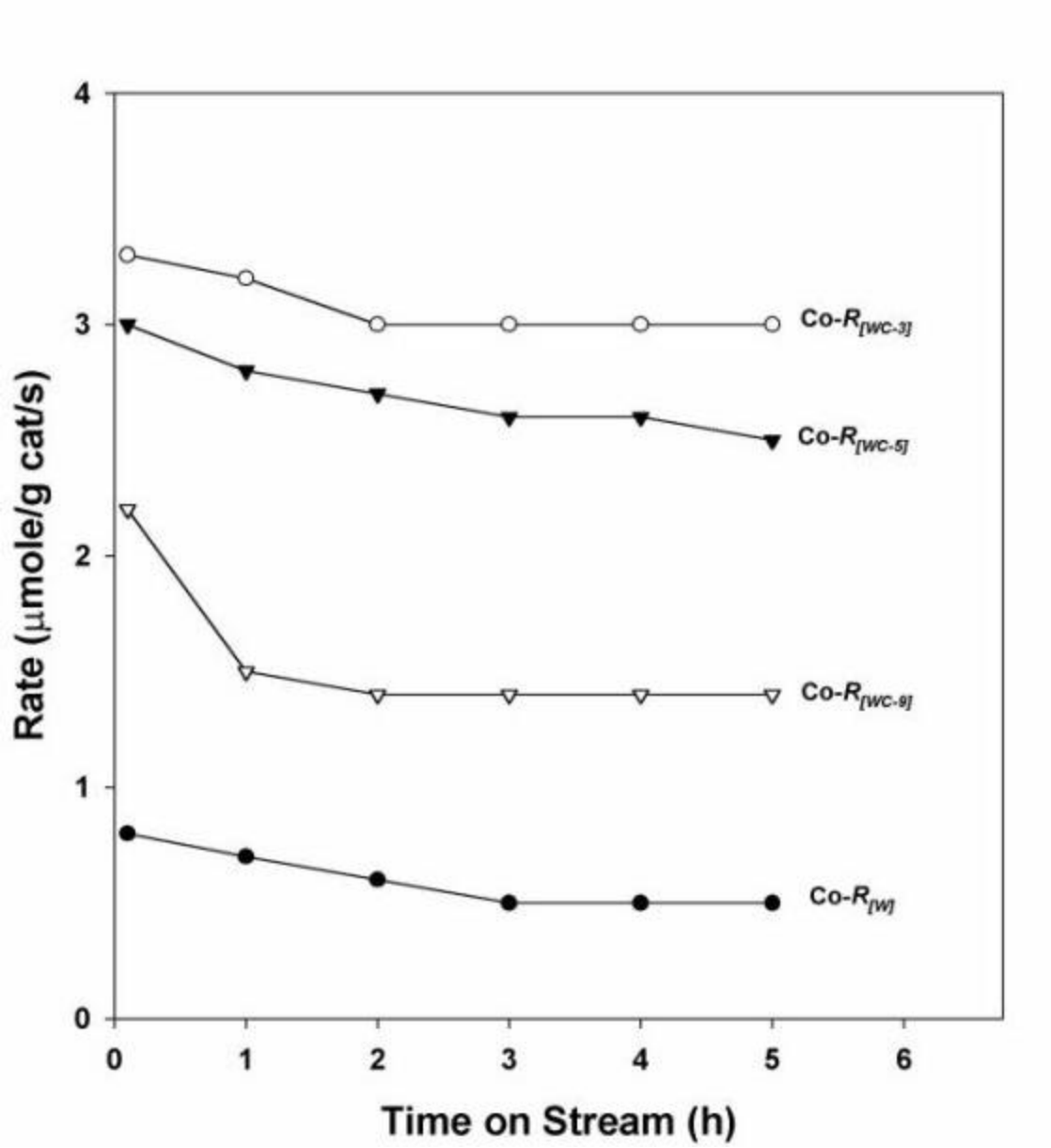

Figure 7.14 Effect of CO Addition during Reduction at High Partial Pressure of H_2O

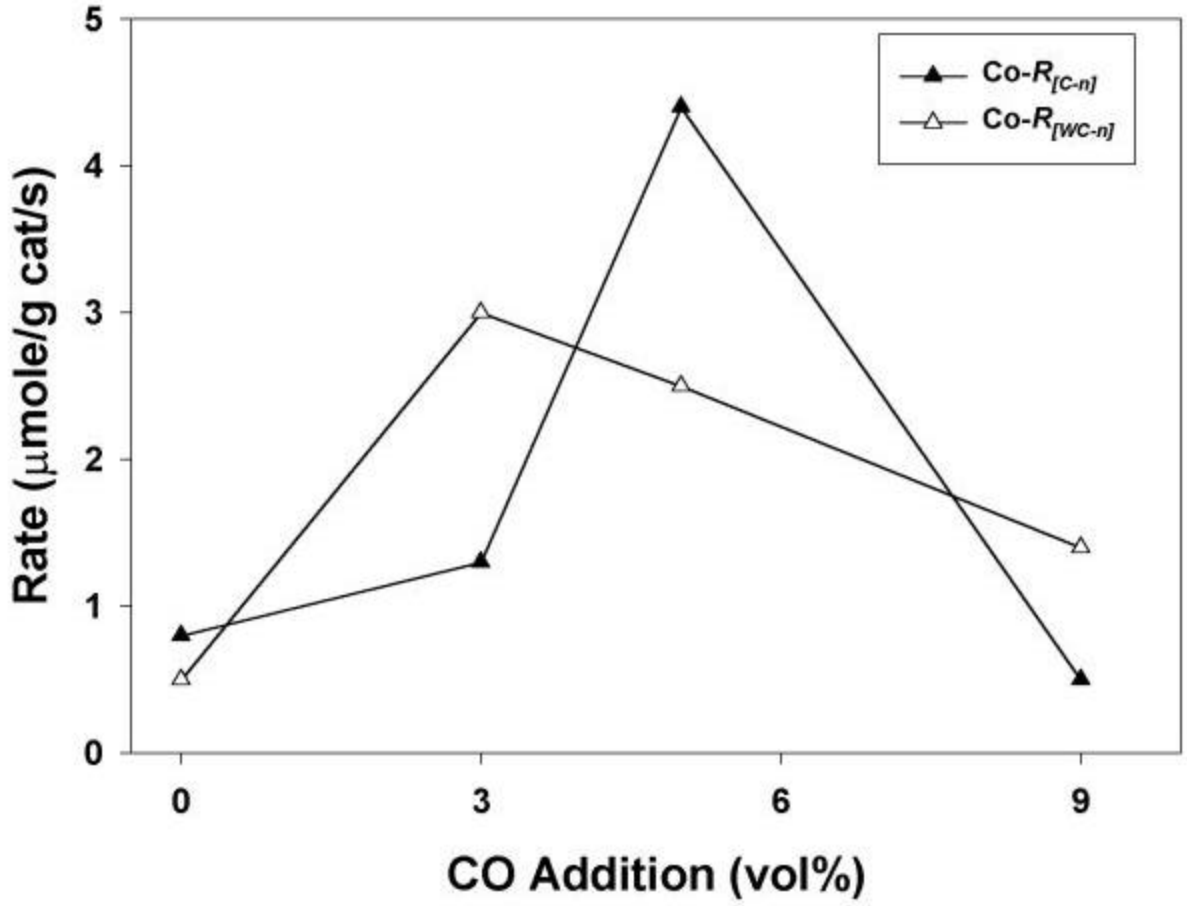

Figure 7.15 Effect of CO Addition on Steady-State Rate

8.0 EFFECT OF COPPER PROMOTION

8.1 Introduction

Aluminas are widely used as catalyst supports or carriers because of their high surface areas and high thermal resistance. However, in our previous TPR study on CoRu/γ-Al_2O_3[1], it was found that water vapor produced during reduction can increase the amount of non-reducible (at temperatures $\leq$ 900°C) Co "aluminate" formation, resulting in a lower reducibility of the catalysts. It is very difficult to physically remove all water vapor from the reduction or reaction process in term of an industrial scale. Thus, the idea of minimizing or blocking the Co "aluminate" formation was also introduced.

In order to stabilize the catalyst activity, many articles were reported on the effects of promoters such as Ru[2-4], Zr[5-6], La[7], Rh[8-10], B[11], and Pt[12] on Co-based catalysts. Although the effects of promoters have been known (such as they can increase the reducibility of Co, preserve the activity by preventing the formation of coke, exhibit cluster and ligand, act as a source of hydrogen spillover, or enhance overall Co dispersion), no major research has been focused on minimizing or blocking the amount of Co-SCF. Any means by which Co-SCF can be diminished could potentially lead to more robust catalysts. Therefore catalyst promoters, which preferentially form surface compounds with the supports offer potentially ways to block Co-SCF.

A formation of metal-aluminates (such as Ni, Co, Cu, and Fe) from α and γ-alumina supports were investigated by Bolt et al..[13] They found that the metal-aluminates formation rate

followed the sequence $CuAl_2O_4$ > $CoAl_2O_4$ > $NiAl_2O_4$ > $FeAl_2O_4$. This gave an idea of using Cu to compete with Co forming Cu "aluminate" and then the formation of Co "aluminate" can be blocked. In addition, it is known that Cu could not alloy with Co at temperature below 422°C as shown in Figure 8.1.[14]

The main objective of this study was to investigate the effect of Cu promoted Co/γ-Al_2O_3 catalysts on blocking the formation of Co "aluminate". A series of Cu promoted Co/γ-Al_2O_3 catalysts were prepared by the incipient wetness co-impregnation and sequential impregnation methods. The catalysts were then pretreated, and characterized and tested for FTS activity.

8.2 Experimental

8.2.1 Catalyst Preparation

8.2.1.1 Co/γ-Al_2O_3. The Co/γ-Al_2O_3 catalysts was prepared by the incipient wetness impregnation of γ-Al_2O_3 having a specific surface area of 209 m^2/g and an average particle size ca. 60 µm. The support precursor (vista B) was first calcined at 500°C for 10 h before impregnation in order to put it in the form of γ-Al_2O_3. Cobalt nitrate [$Co(NO_3)_2 \cdot 6H_2O$] was dissolved in de-ionized water and impregnated into the support using incipient wetness to give a final reduced catalyst with 20 wt% cobalt. The catalyst was dried at 110°C for 12 h and calcined in air at 300°C for 2 h.

8.2.1.2 Cu promoted Co/γ-Al_2O_3. The Cu promoted Co/γ-Al_2O_3 catalysts were prepared using two different methods: co-impregnation and sequential impregnation.

(i) Co-impregnation (Co-Cu/g-Al_2O_3)

The same γ-Al_2O_3 support as mentioned before was used. Cobalt nitrate [$Co(NO_3)_2$.•$6H_2O$] and copper nitrate [$Cu(NO_3)_2$•$3H_2O$] were dissolved in de-ionized water and co-impregnated into the support to produce a reduced catalyst with 20 wt% cobalt and 1-5 wt% copper. The catalysts were dried at 110°C for 12 h and calcined in air at 300°C for 2 h.

(*ii) Sequential Impregnation (Co/g-Al_2O_3-Cu)*

The same γ-Al_2O_3 support as mentioned before was used. First, a series of Cu was impregnated into the support using a solution of copper nitrate [$Cu(NO_3)_2$•$3H_2O$] in de-ionized water to produce the catalyst precursors (Cu modified γ-Al_2O_3), which have 1-5 wt% copper. The catalyst precursors were calcined at 500°C for 10 h. Cobalt nitrate ($Co(NO_3)_2$•$6H_2O$) were dissolved in de-ionized water and sequentially impregnated into the catalyst precursors as mentioned before to produce catalysts with 20 wt% of cobalt. The catalysts were dried at 110°C for 12 h and calcined in air at 300°C for 2 h.

8.2.2 Catalyst Pretreatment

The catalysts were characterized following two pretreatments. These were as follows:

(i) after the original calcination step,

(ii) after standard reduction of the calcined catalysts at 350°C for 10 h at a space velocity = 16,000 h^{-1} in H_2 and passivation with an O_2/He (5.20% of O_2) mixture at room temperature for 2 h.

8.2.3 Catalyst Nomenclature

The nomenclature used for samples in this study is the following:

a-CoCu-n-i where:

a = ***C*** refers to the catalyst samples prepared by co-impregnation method

= ***S*** refers to the catalyst samples prepared by sequential impregnation method

CoCu refers to copper promoted cobalt catalysts

n refers to wt% copper in the catalyst samples

i = ***C*** refers to the calcined catalysts samples

= ***R*** refers to the reduced and passivated catalyst samples

8.2.4 Catalyst Characterization

8.2.4.1 X-ray Powder Diffraction (XRD). XRD was performed to determine the bulk crystalline phases of the catalysts following different pretreatment conditions. X-ray powder diffraction patterns of samples were collected using a XRD diffractometer, Scintag XDS-2000 with monochromatized Cu-K_α radiation (λ = 1.54439 Å). The spectra were scanned at a rate of 2.4 degree/min. from 2θ = 20 to 80 degrees.

8.2.4.2 Raman Spectroscopy. The Raman spectra of the samples were collected by projecting a continuous wave laser of Helium-Neon (He-Ne) red (632.816 nm) through the samples exposed to air at room temperature. A scanning range between 0 to 1000 cm^{-1} with a resolution of 2 cm^{-1} was applied. The data were analyzed using the Renishaw WiRE (Windows-based Raman Environment) software, which allows Raman spectra to be captured, calibrated, and analyzed

using system 2000 functionality via the Galactic GRAMS interface with global imaging capacity.

8.2.4.3 SEM and EDX. SEM and EDX were performed to study the morphology of catalysts and elemental distribution, respectively. A Hitachi S3500N SEM was used having the back scattering electron (BSE) mode at 15 kV and a working distance (the distance between a sample and the electron beam) of 15 mm. After the SEM micrographs were taken, EDX was then performed to analyze the elemental concentration on catalyst surface (using INCA software).

8.2.4.4 Hydrogen Chemisorption. Static H_2 chemisorption at 100°C on the reduced cobalt catalysts was used to determine the number of reduced surface cobalt metal atoms. This is related to the overall activity of the catalysts during FTS. Gas volumetric chemisorption at 100°C was performed using the method described by Reuel and Bartholomew.[15] The experiment was performed in a Micromeritics ASAP 2010 using ASAP 2010C V3.00 software.

8.2.4.5 Temperature Programmed Reduction (TPR). TPR was performed to determine the reducibility and reduction behavior of the catalyst samples. TPR was carried out in an Altamira AMI-1 system using 50 mg of catalyst and temperature ramp from 30ºC to 900ºC at 5ºC/min. The reduction gas was 5% H_2 in Ar. A cold trap (-70ºC) was placed before the detector to remove water produced during the reaction. A thermal conductivity detector (TCD) was used to determine the amount of hydrogen consumption. The amount of hydrogen consumption was calibrated using TPR of silver oxide (Ag_2O) at the same conditions. The reduced and passivated

catalyst samples were re-calcined in-situ at the original calcination condition before performing TPR.

8.2.5 Reaction

FTS was carried out at 220°C and 1 atm total pressure. A flow rate of H_2/CO/Ar = 60/30/10 cc/min in fixed bed reactor under differential conditions was used. Thermocouples at the top and at the bottom of the catalysts bed assured precise temperature control during pretreatment and reaction. Typically, 0.2 g of the pretreated catalyst sample was re-reduced in situ in flowing H_2 (50 cc/min) at 350°C for 10 h prior to FTS. In order to avoid exotherms and hot spots that lead to rapid catalyst deactivation, the reaction was initiated in a controlled manner by gradually increasing the reactant concentrations over a period of 2 h. After the start-up, samples were taken in 3-h. intervals and analyzed by GC. Steady state was reached after 24 h in all cases.

8.3 Results

8.3.1 X-ray Diffraction (XRD)

XRD patterns of the calcined C-CoCu (top) and S-CoCu (bottom) catalyst samples are shown in Figure 8.2. All of them were completely identical. The diffraction peaks at 31.3°, 36.8°, 59.4°, and 65.4° are those of Co_3O_4. No XRD peaks of CuO were detected probably due to it being in a highly dispersed form. After reduction, the diffraction peaks for CoO (not shown) at 42.6° and 61.8° were seen. No peaks of Co metal were seen due to overlap with those for γ-Al_2O_3. No peaks of $CoAl_2O_4$ (spinel) were detected for any of the catalyst samples.

8.3.2 Raman Spectroscopy

Raman spectra for C-CoCu catalysts after different pretreatment conditions, CoO, Co_3O_4 (spinel), and $CoAl_2O_4$ (spinel) are shown in Figures 8.3 (for the calcined samples) and 8.4 (for the reduced and passivated samples). The Raman spectra for the S-CoCu (not shown) sample are identical to those for the C-CoCu catalysts. After calcination, the Raman bands of Co_3O_4 were observed at 198, 480, 519, 619, and 690 cm^{-1} in all the C-CoCu samples, the same result as seen from XRD. The intensity of these bands decreased with increasing the amount of Cu loading. No Raman bands of CuO were detected. After reduction, broad Raman bands between 400-750 cm^{-1} were seen for the unpromoted Co catalyst (Co-*R* sample). However, these peaks were not observed for the reduced Cu-promoted Co catalysts after the pretreatments used in this study. Instead, the Raman bands at 198, 480, 519, 619, and 690 cm^{-1} were present, which can be assigned to Co_3O_4 present on catalyst surface after the samples were exposed to air rather than CoO (detected in the bulk by XRD) since Raman is more of a surface technique. It can be also seen that the intensity of these bands decreased with increasing the amount of Cu loading. No Raman bands of $CoAl_2O_4$ (spinel) were detected.

8.3.3 SEM and EDX

Some of SEM micrographs of Cu promoted Co catalysts are shown in Figures 8.5 to 8.6. The term "granule" is used here to refer to the overall catalyst particles composed of Co, Cu, and γ-Al_2O_3. The term "patches" will be used to refer to entities rich in Co supported on the catalyst granules. In all the SEM figures, the white or light spots on the catalyst granules represent high concentrations of cobalt and its compounds while the darker areas of the granules indicate the support with minimal/no cobalt present. There was no significant change in morphology of the

catalysts samples, especially at the differences in Cu loading and the preparation methods (co-impregnation or sequential impregnation). SEM micrographs for C-CoCu-*C* and S-CoCu-*C* are shown in Figures 8.5 and 8.6, respectively. Figure 8.6 shows the SEM micrograph of the calcined Cu (5%)/γ-Al_2O_3 catalyst precursor before sequential impregnation with Co. In all SEM micrograph figures as mentioned before, the catalyst granule is shown at the top and the higher magnification of the same catalyst granule is shown at the bottom.

EDX gave more information about the elemental concentration and distribution. All main elements (Al, O, Co, and Cu) were detected. Some of the elemental distributions on cross sectional areas of catalyst granules are shown in Figures 8.7 to 8.9. The distribution of O and Al is high because they are main components of the catalyst granule. However, it can be observed that Co and Cu also were well distributed all over the catalyst granules. Figure 8.8 shows the elemental distribution for the calcined 5 wt% Cu /γ-Al_2O_3 catalyst precursor, which indicates a Cu well distributed before sequential impregnation with Co.

8.3.4 Hydrogen Chemisorption

The H_2 chemisorption results for all catalyst samples are shown in Table 8.1 and Figure 8.10. The overall dispersion of reduced metal (Co and Cu) in the catalyst samples is given. The results indicate that the overall metal dispersion increased with Cu promotion (5.0 to 7.9% for C-CoCu-*R* and 5.8 to 10.3% for S-CoCu-*R*). The overall dispersion increased with increasing the amount of Cu loading. A higher overall dispersion was observed for the CoCu catalysts prepared by the sequential impregnation method at the same amount of Cu loading.

8.3.5 Temperature Programmed Reduction (TPR)

TPR profiles for all calcined catalyst samples are shown in Figure 8.11. As can be seen in the figure, one reduction peak for Cu (5%)/γ-Al_2O_3 was obtained. It was located at ca. 250°C. This is assigned to the reduction of CuO to Cu metal.[16]

There were three major reduction peaks for unpromoted Co-*C* located at ca. 200°C, 300°C, and between 400-700°C (maximum at 500°C). These peaks have been related to the following reduction steps: $Co_3O_4 \rightarrow CoO$, $CoO \rightarrow$ Co metal, and Co_XO_Y-$Al_2O_3 \rightarrow$ Co metal.[12, 17-18]

For C-CoCu-*C* samples with differences in the amount of Cu loading, there were three peaks for C-CoCu01-*C* (1%Cu). These peaks were located at the same positions as seen for the unpromoted Co-*C*. However, the reduction peak (maximum at 500°C) was diminished by increasing the amount of Cu loading from 2 to 5 wt%. Thus, there were only two peaks left for C-CoCu02-05-*C* located at ca 200°C and 300°C.

The same phenomenon as mentioned for C-CoCu-*C* was also observed for S-CoCu-*C*. Three peaks of reduction are seen for S-CoCu01-*C*. The reduction peak at maximum ca. 500°C was also diminished by increasing the amount of Cu loading from 2 to 5%. However, a broad shoulder at the reduction peak at ca. 300°C can be clearly seen for S-CoCu-*C*, whereas it could not be seen a broad shoulder for C-CoCu-*C* samples. This caused an increase in the reducibilities for S-CoCu-*C* samples compared to those for C-CoCu-*C* samples.

The reducibilities of catalyst samples based on both the reduced Co and Cu are shown in Table 8.1 and Figure 8.12. They ranged between 63 to 71% for C-CoCu-*C* samples and 82 to 98% for S-CoCu-*C* samples. It can be seen that Cu promotion enhances the reducibility of the catalysts prepared by a sequential impregnation method. Additionally, the Cu promoted Co

catalysts prepared by the sequential impregnation method gives higher reducibilities of the catalysts compared to those prepared by the co-impregnation method.

8.3.6 Fischer-Tropsch Synthesis (FTS)

FTS was performed to determine the overall activity and product distribution of the Co catalysts with Cu promotion during FTS. The results are shown in Table 8.2 and Figure 8.13. It can be seen that Cu promotion causes a decrease in the overall activity of Co catalysts. It was also observed that the probability of chain-growth was slightly decreased with Cu promotion.

8.4 Discussion

In this study the Cu promoted Co/γ-Al_2O_3 catalysts were prepared by two different methods: co-impregnation and sequential impregnation. The amount of Cu loading was varied as well. The characteristics of the catalyst samples were identified and compared with the unpromoted Co catalysts. It can be observed from XRD, Raman spectroscopic, SEM, and EDX results that all these mentioned techniques cannot differentiate all the differences of the catalysts samples in this study. However, they still provide some useful information about the catalyst properties.

XRD was performed to determine the bulk crystalline phases of the catalysts sample after various pretreatments. After calcination, only Co_3O_4 peaks were detected for both unpromoted and Cu-promoted Co catalysts. There was no change in XRD patterns for all calcined catalyst samples upon the differences in the amount of Cu loading (up to 5 wt% Cu) and the preparation methods. No XRD peaks of CuO can be seen at all due to a highly dispersed form. After reduction, Co_3O_4 were reduced to CoO, Co metal, and Co species strongly interacted with the

support. However, only XRD peaks of CoO were detected. This indicates that besides CoO, other Co or Cu compounds were present in highly dispersed forms. Raman spectroscopic results were also in accordance with those of XRD. However, additional information was obtained from the Raman spectroscopy.

Although the Raman bands at 198, 480, 519, 619, and 690 cm^{-1} of Co_3O_4 were observed in all calcined catalyst samples, the intensity of the bands was diminished by increasing the amount of Cu loading for samples both prepared by the co-impregnation and the sequential impregnation methods. This is suggested that the amount of Cu loading affects the appearance of Co_3O_4 in the calcined samples. This is probably due to the fact that a highly dispersed CuO layer may cover the layers of Co_3O_4 phases resulting in a gradually decrease in the intensity of the Raman bands of Co_3O_4. The same phenomenon was also observed for the reduced and passivated catalyst samples. It was found that broad Raman bands between 400-750 cm^{-1} were seen for the unpromoted Co catalyst after reduction. These bands were assigned to a highly dispersed Co "aluminate" or Co species strongly interacted with the support. However, the broad Raman bands between 400-750 cm^{-1} were clearly not seen for the Cu-promoted Co catalysts after reduction. This is because of two possibly reasons: (i) the effect of a highly dispersed Cu layer covering as mentioned before and/or (ii) Cu competes with Co to form a highly dispersed Cu-aluminate, instead[13] resulting in a decrease in the amount of Co "aluminate" present. It is clear that $CoAl_2O_4$ (spinel) was not formed in all reduced catalyst samples at the reduction condition used in this study.

SEM and EDX gave information about the catalyst morphologies and elemental distribution, respectively. This may provide more information about the arrangement of Co and Cu compounds as the effect of Cu layer covering as mentioned above. However, SEM does not

differentiate Co and Cu compounds leading to the observation of only a combination for both Co and Cu compound "patches". There was no significant change in the catalyst morphologies upon changing the amount of Cu loading and the preparation methods. EDX mapping indicated a good elemental distribution for all elements-not surprising for O and Al because they are main elements of catalyst granules. However, Co and Cu were also well distributed all over the catalyst granules as seen by EDX mapping.

It is clear that Cu promotion causes an increase in the overall metal dispersion. This may be because of two possible reasons. First, Cu itself is active for H_2 chemisorption as shown in Table 8.1 (the overall Cu dispersion for 5 wt% Cu/γ-Al_2O_3 = 12.8%) resulting in an increase in the amount of H_2 uptake for the Cu-promoted Co catalysts. However, the term "synergetic" promotion[19-20] can not be applied for this case due to the amount of H_2 uptake of the CoCu catalysts was less than the sum of that for the separated Co and Cu catalysts. Secondly, Cu promotion may prevent the formation of Co "aluminate" leading to an increase in the amount of Co atoms available for H_2 chemisorption. In addition, it should emphasize that the Cu-promoted Co catalysts prepared by a sequential impregnation method. This indicates that a sequential impregnation method is significantly more effective for the Cu-promoted Co catalyst preparation based on the H_2 chemisorption results. However, this assumption is definitely incomplete without the TPR results.

It can be seen that the reducibilities of the Co catalysts dramatically increases with Cu promotion for CoCu catalysts only prepared by a sequential impregnation method. Again, the term "synergetic" promotion cannot be applied for the increased reducibilities for the same reasons as mentioned before. Based on the reducibilities, it also indicates a sequential impregnation method is more effective for the Cu-promoted Co catalyst preparation. This is

because of two possibly reasons: (i) Cu itself has 46% reducibility based on TPR results for 5 wt% Cu/γ-Al_2O_3 (as shown in Table 8.1) and (ii) Cu can probably facilitate the reduction of Co catalysts by lowering the reduction temperature of Co species strongly interacted with the support, i.e. Co "aluminate" resulting in the disappearance of the reduction peak at max. ca. 500°C for the unpromoted Co catalysts, and/or Cu can probably block the formation of Co "aluminate" by competing with Co to form Cu "aluminate" instead.[13] Considering, the TPR profiles as shown in Figure 8.10, it can be seen that the highest reduction peak at max. ca. 500°C disappeared with increasing the amount of Cu loading. Thus, two reduction peaks were observed when the amount of Cu loading $\geq$ 2 wt%. This is assigned that the lower temperature peak is related to the reduction of bulk Co_3O_4 like Co species whereas the higher temperature peak is involved with the reduction of the Co species strongly interacted with the support. Comparing the TPR profiles for the CoCu catalysts prepared by different methods, it can be seen that the position of the two peaks was quite the same. However, there was a significant change in the higher temperature peak (ca. 300°C) shape upon the different preparation methods. This is obviously demonstrated by Figure 8.14 with a comparison plot between the TPR profiles for C-CoCu05-*C* and S-CoCu05-*C*. It indicates that a broad shoulder between 300-500°C can be observed only in the TPR profiles for the Cu-promoted Co catalysts prepared by a sequential impregnation method. This broad shoulder causes an increase in the amount of H_2 consumption, then the reducibility. This confirms that the Cu-promoted Co catalysts prepared by a sequential impregnation method are more effective based on the obtained reducibilities as well as the overall metal dispersion as mentioned before. The use of metals to modify the support properties has been known for years.[4,21-28]

For the sequential impregnation used in this study, where a series of Cu was first impregnated into the support, dried, and calcined before sequential impregnated with Co, it was found that CuO can disperse as Cu^{2+} on alumina.[29] Alumina is a spinel with cationic vacancies that can be filled with metal ion such as Cu^{2+}, Co^{+2}, Fe^{2+}, and Ni^{2+}[13] migrating into the alumina matrix. Thus, after calcination at high temperatures ca. 500-700°C, a solid state reaction can cause a formation of Cu aluminate.[30] This Cu-modified alumina support provides two possible advantages for the followed Co impregnation by: (i) providing the more stable alumina support with partially forms aluminate compounds with Cu[31] and (ii) limiting the cationic vacancies occupied by Cu leading to an inhibition of the Co migration into such the occupied sites, resulting in a decrease in the amount of Co aluminate formed.

It should be remembered that the co-impregnation method used in this study was performed based upon the idea of using Cu as a promoter to compete with Co to form metal aluminate due to the Cu aluminate formation rate is faster.[13] However, a decrease in the reducibility was observed, the value was a little lower compared to that for the unpromoted Co catalyst.

Although the reducibility and the overall metal dispersion of the catalysts dramatically increase with Cu promotion, the overall activity for both initial and steady-state during FTS are lower than that those for unpromoted Co catalysts. This is because Cu may act as surface decoration[32-34] on the active Co metal surface resulting in a decrease in Co metal active sites available for catalyzing CO hydrogenation.

In this present study, Cu promotion affected the characteristics of Co catalysts depending upon the amount of Cu loading and the preparation method. The formation of Cu "aluminate" and Co "aluminate" could not be detected by XRD and Raman spectroscopy, probably due to

only a small amount of them being present and/or being present in a highly dispersed form. SEM does not differentiate the different between Co and Cu compounds. The distribution for all elements obtained by EDX is well distributed all over the catalyst granules. Considering all characterization techniques used in this study, H_2 chemisorption and TPR were the most powerful techniques for the investigation of Cu-promoted Co catalysts.

8.5 Conclusions

The metal reducibility and dispersion of the Cu-promoted Co catalysts can be increased with Cu promotion based on H_2 consumed. It was found that the effect of Cu promotion depended upon both the amounts of Cu loading and the preparation method. The results indicate that a sequential impregnation is more effective for the preparation of Cu-promoted Co catalysts. This is because it provides a more stable alumina support, which probably partially forms Cu "aluminate", prior to sequentially impregnation with Co. Thus, the cationic vacancies are limited due to such formation resulting in an inhibition of Co "aluminate" formation.

The effect of Cu promotion can be explained by three possible reasons: (i) Cu is active for H_2 chemisorption by itself, (ii) Cu^{2+} ion can migrate into alumina matrix and form Cu aliminate, which is more thermally stable, and (iii) Cu can significantly compete with Co to form metal-aluminate with a higher formation rate. However, based on reaction, FTS rate decreased with Cu addition probably due to a loss of active reduced surface Co atom exposure by Cu coverage.

Table 8.1: Reducibility and H_2 Chemisorption Results of Cu-Promoted Co/γ-Al_2O_3

Catalyst Samples	Cu/Co Atom Ratio	Metal Reducibility (30^o to $900^\circ C$)[a,b,c] (%)		*[R]* samples	
		[C]	*[RC]*	Total H_2 Chemisorption[d] (mmole H_2/g cat)	Overall Metal Dispersion[e] (%)
Co-20	0	80	58	59	3.5
Cu-05	NA	46	-	50	12.8
C-CoCu-01	0.047	63	43	89	5.0
C-CoCu-02	0.093	69	34	130	7.0
C-CoCu-03	0.140	69	38	145	7.5
C-CoCu-04	0.186	71	23	156	7.7
C-CoCu-05	0.233	65	22	165	7.9
S-CoCu-01	0.047	89	66	103	5.8
S-CoCu-02	0.093	89	62	156	8.4
S-CoCu-03	0.140	96	78	178	9.2
S-CoCu-04	0.186	98	75	187	9.3
S-CoCu-05	0.233	82	78	215	10.3

[a] The **[*R*]** samples were re-calcined **[*RC*]** at 300°C in air for 2 h before TPR measurement.

[b] The metal reducibility was based on the calibration of Ag_2O (100% reducibility).

[c] Measurement error = ±5%.

[d] Error = ±5% of measurement of H_2 chemisorption.

[e] The metal dispersion was calculated from [(2 x total H_2 chemisorption) x 100/no. of moles of both Co and Cu in the catalyst sample].

Table 8.2 Reaction Rate and Product Distribution during FTS

Catalyst Samples	**Rate[a] (mmole/g cat/s)**		**Product Distribution (%)**				
	Initial	**SS**	**C_1**	**C_2-C_4**	**C_5-C_{12}**	**C_{13+}**	a
Co/Al-*C*	3.0	2.1	14.2	48.0	35.9	1.9	0.63
S-CoCu-02-*C*	1.8	1.0	16.6	51.0	31.3	1.1	0.58
S-CoCu-03-*C*	1.9	0.9	13.6	47.1	37.1	2.2	0.60
S-CoCu-05-*C*	1.9	0.9	22.2	55.2	22.3	0.3	0.52

[a] FTS was carried out at 220°C, 1 atm, and $H_2/CO = 2$ ($H_2/CO/Ar = 60/30/10$ cc/min).

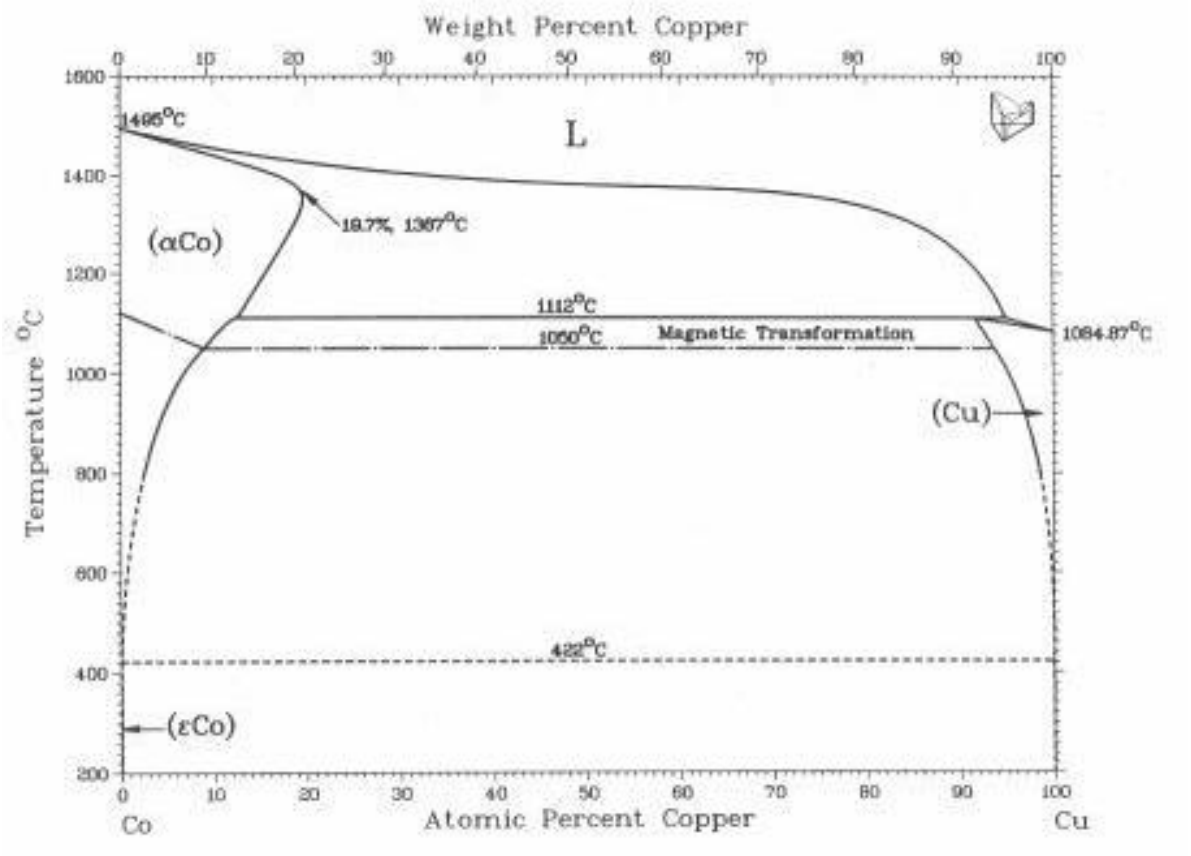

Figure 8.1 Binary Alloy Co-Cu Phase Diagram[30]

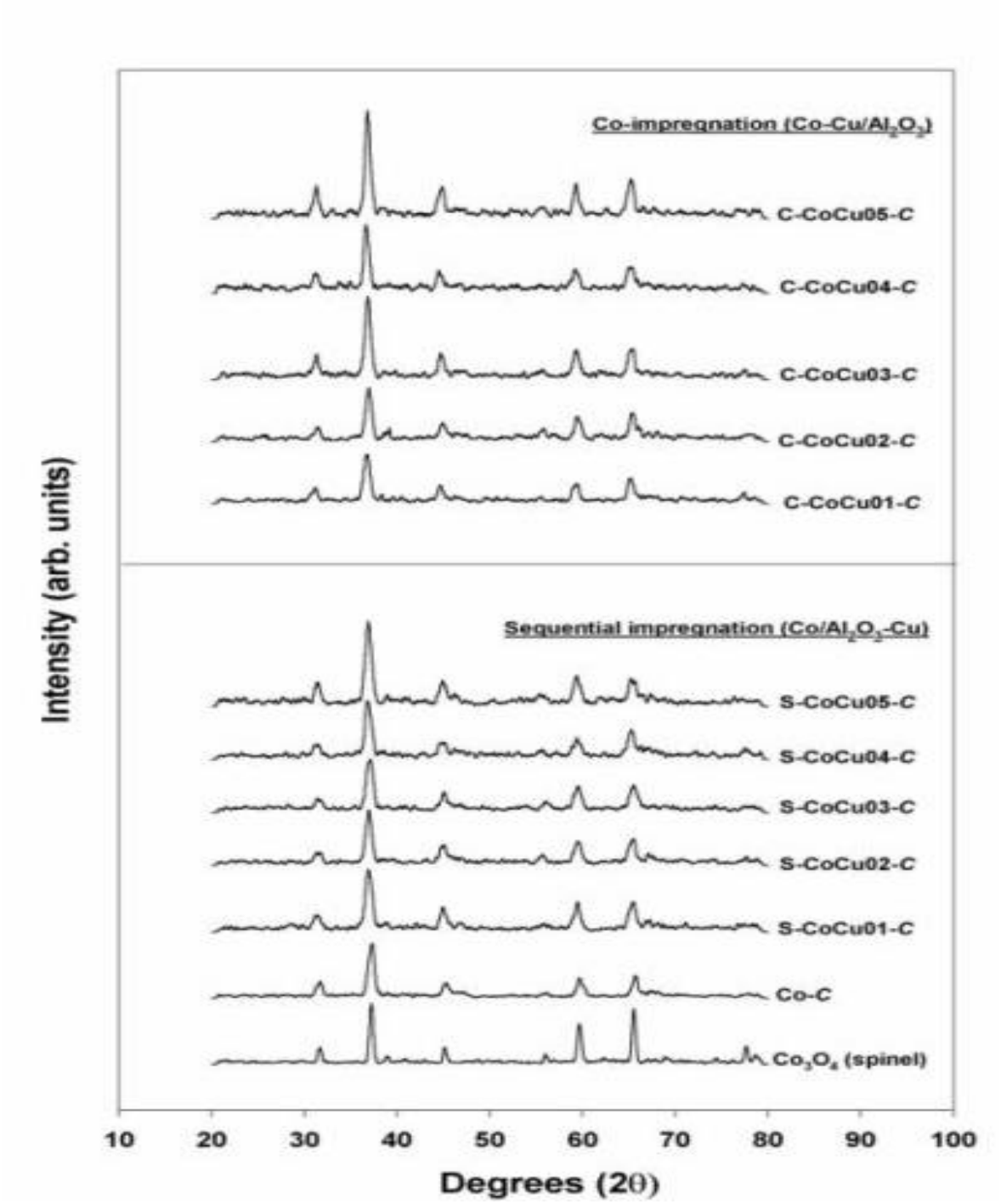

Figure 8.2 XRD Patterns of Co_3O_4 (spinel), Calcined Co, and CoCu Catalysts

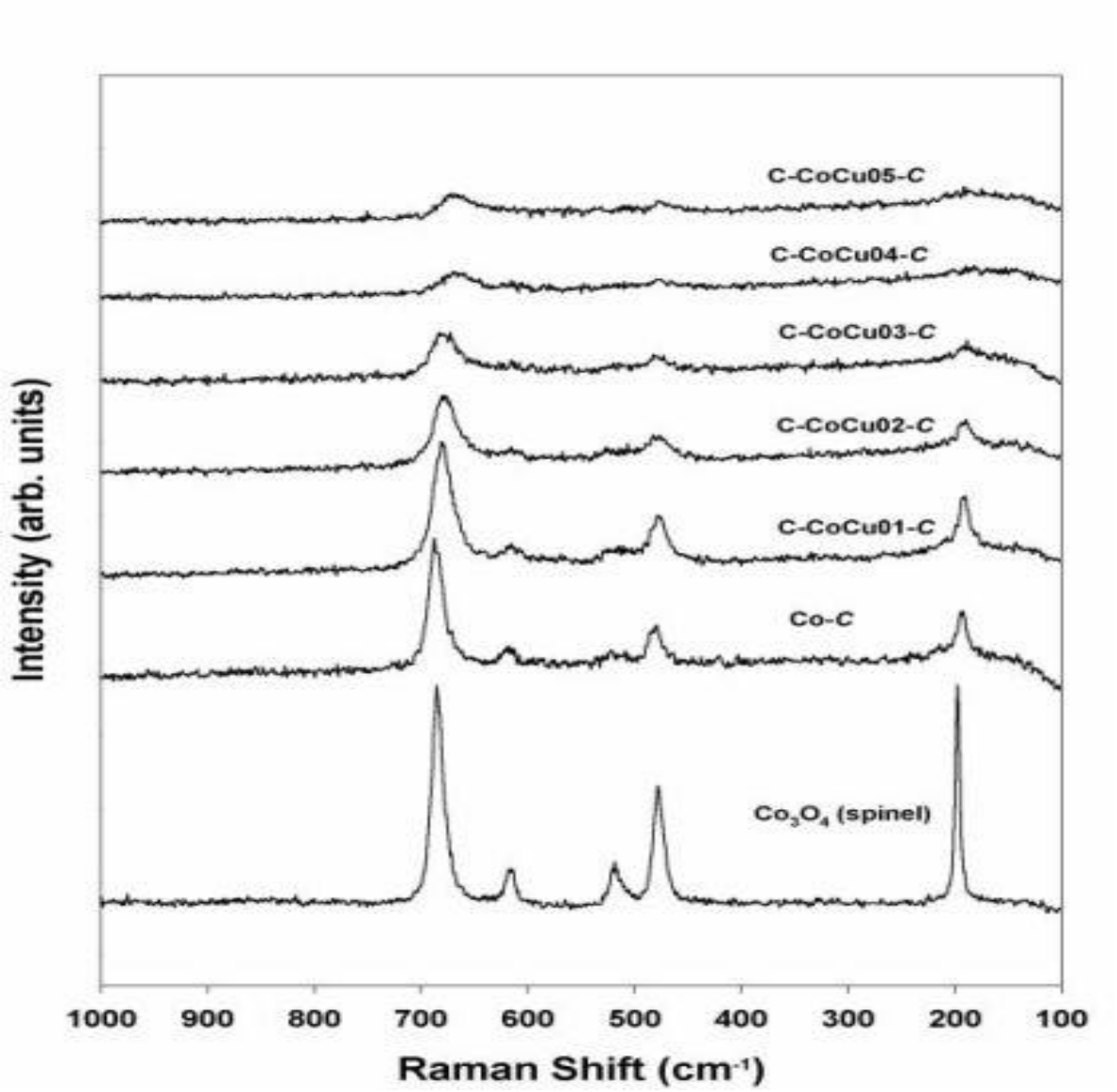

Figure 8.3 Raman Spectra of Co_3O_4 (spinel), Calcined Co, and CoCu Catalysts

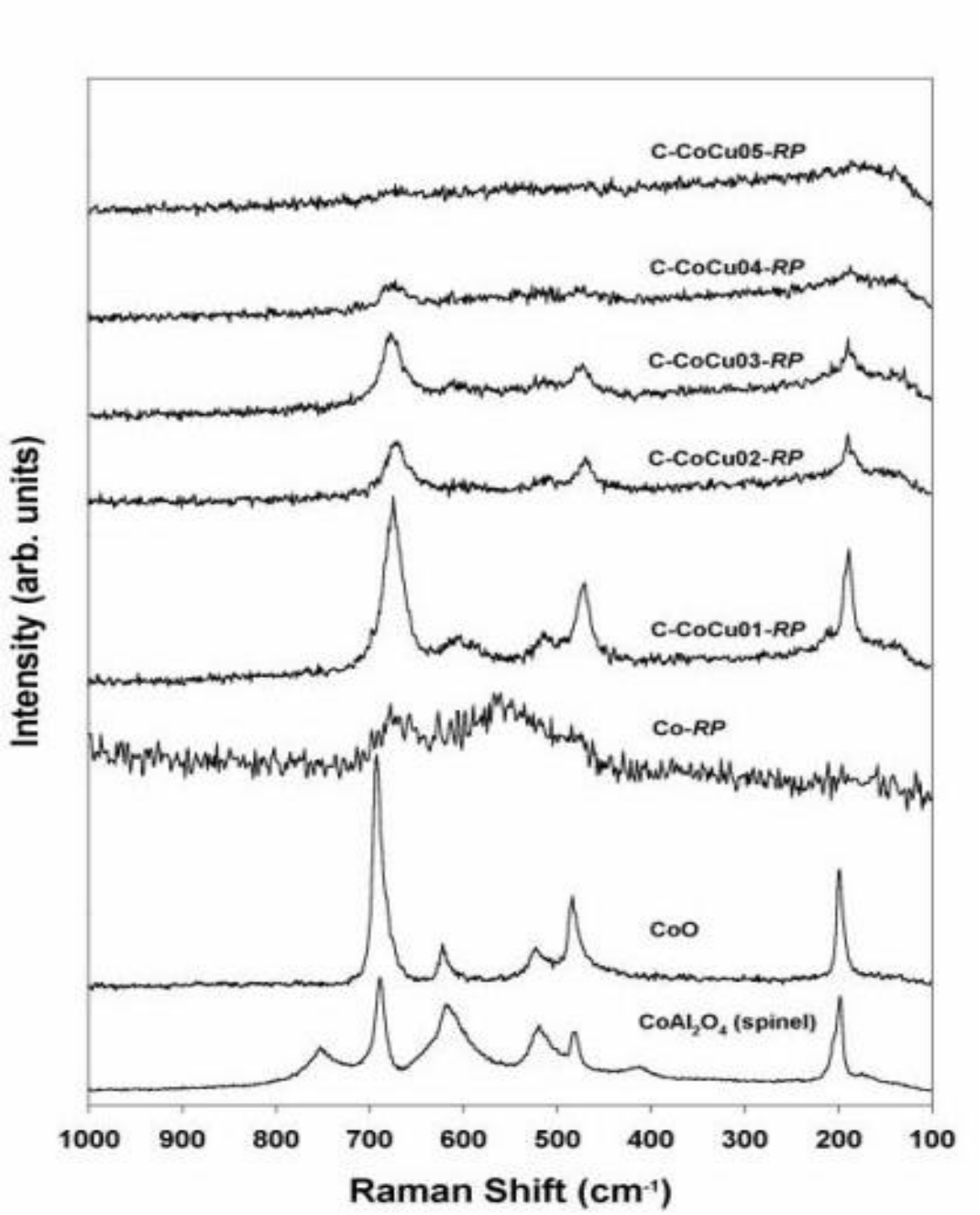

Figure 8.4 Raman Spectra of CoO, $CoAl_2O_4$ (spinel), Co-*RP*, and the Reduced and Passivated C-CoCu Catalysts

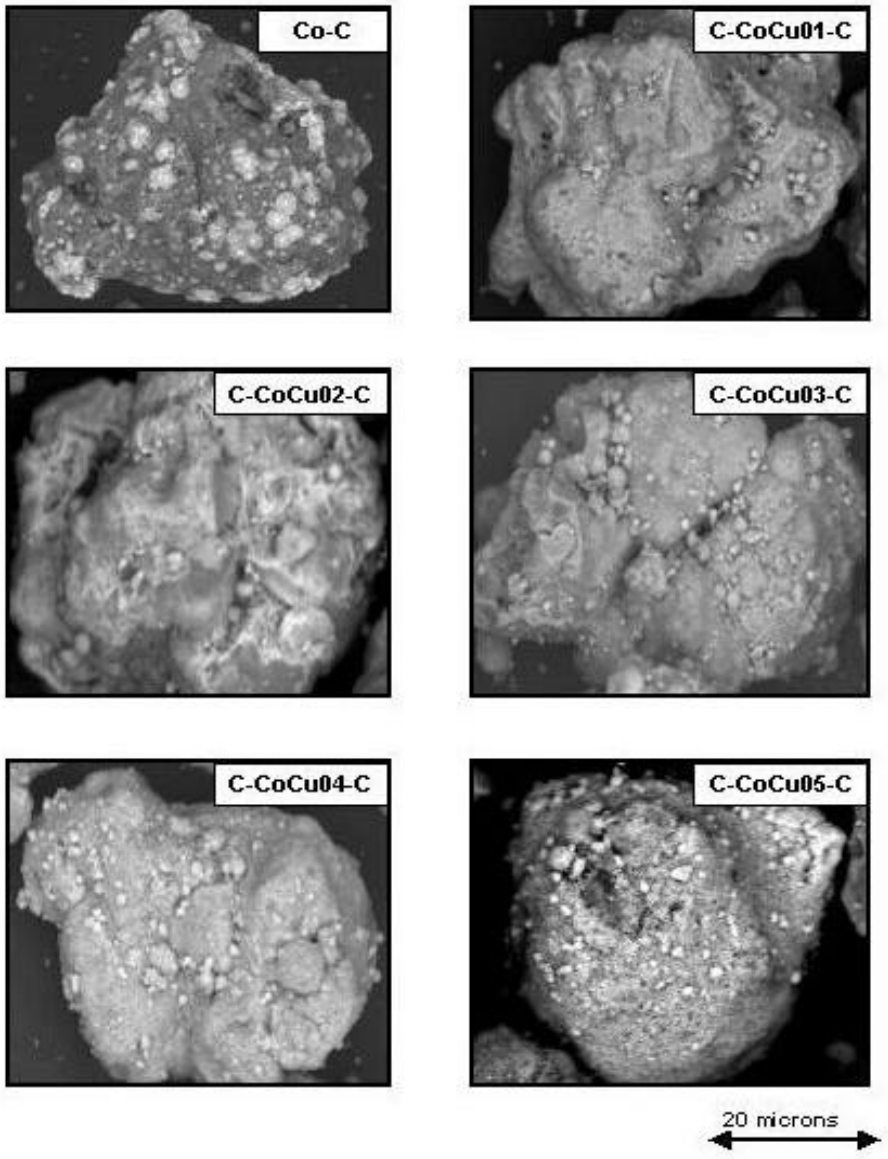

Figure 8.5 SEM Micrographs of Co-*C* and C-CoCu-*C* (external surface)

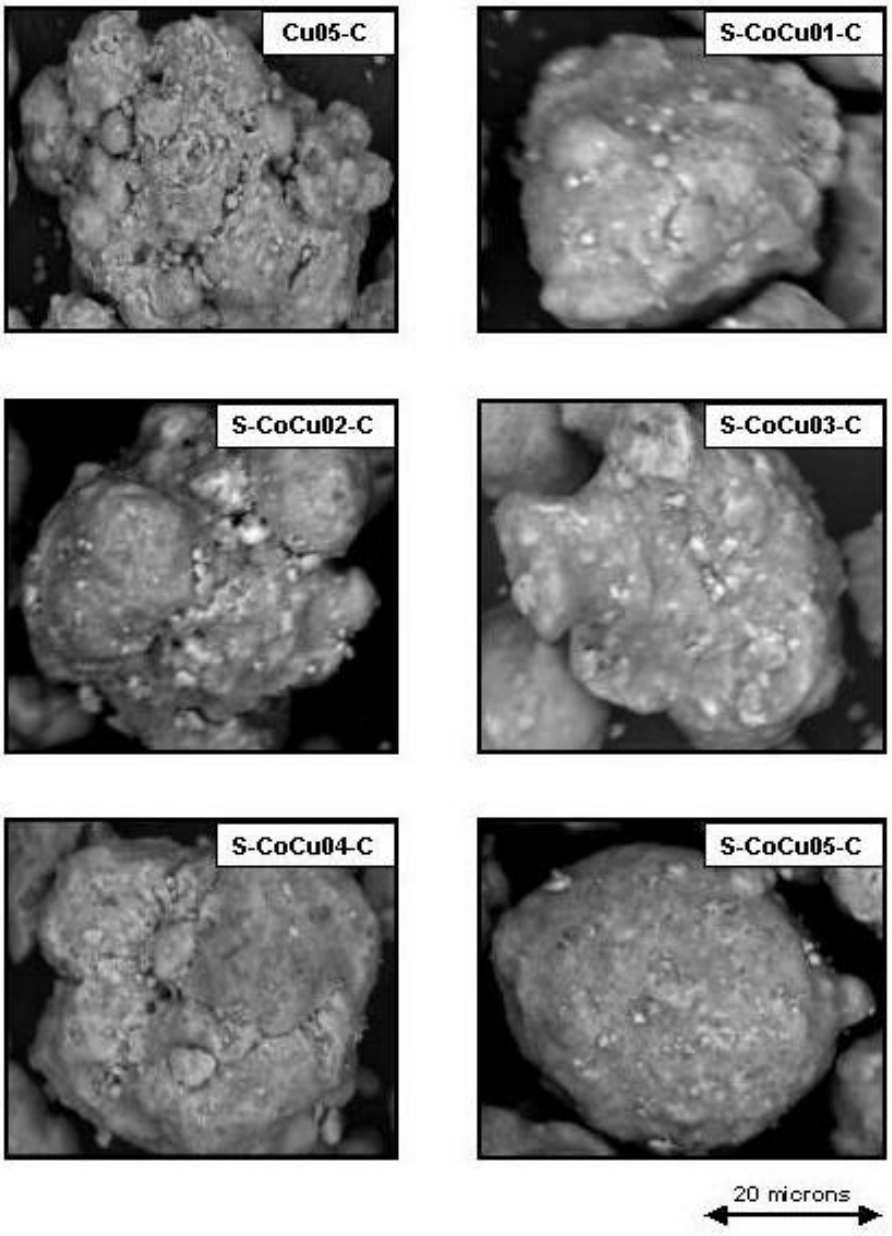

Figure 8.6 SEM Micrographs of Cu05-*C* and S-CoCu-*C* (external surface)

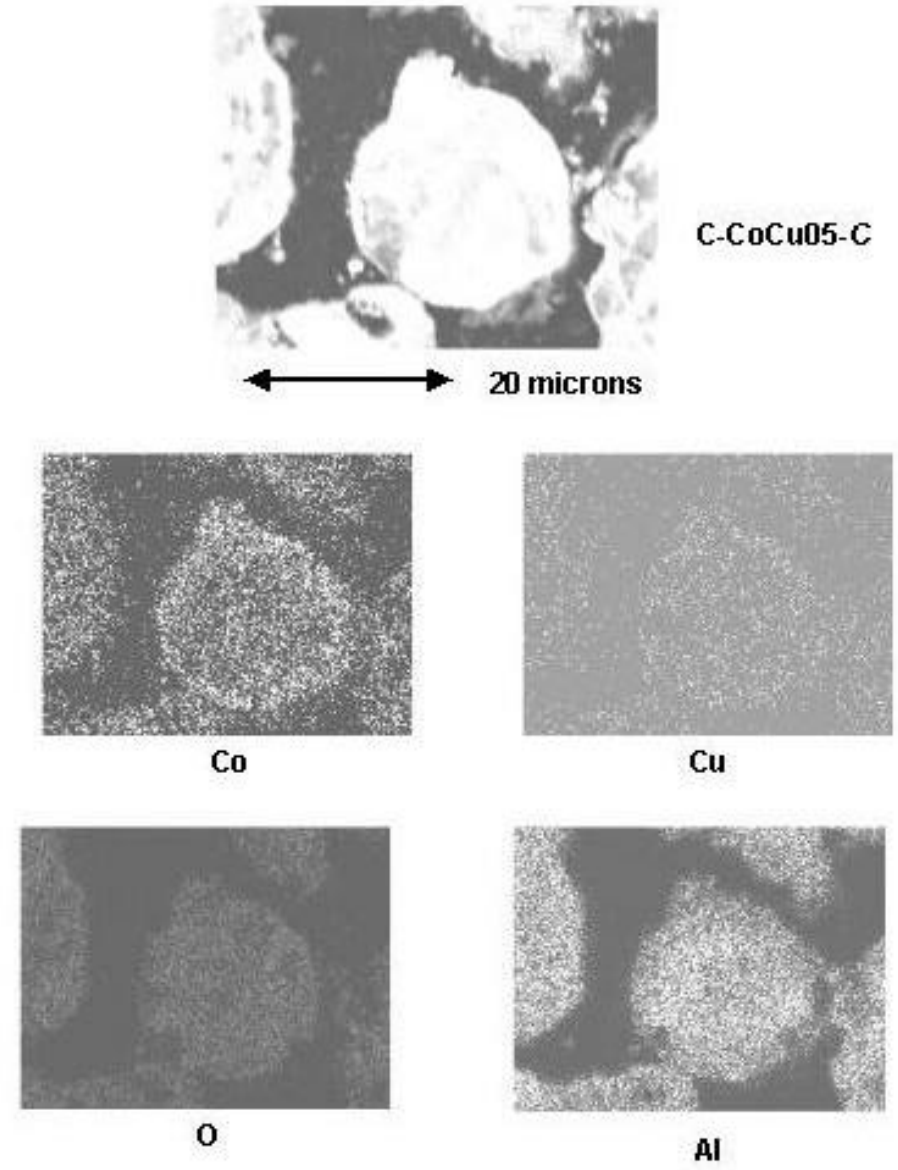

Figure 8.7 EDX Mapping of the cross-section of a C-CoCu05-*C* Catalyst Granule

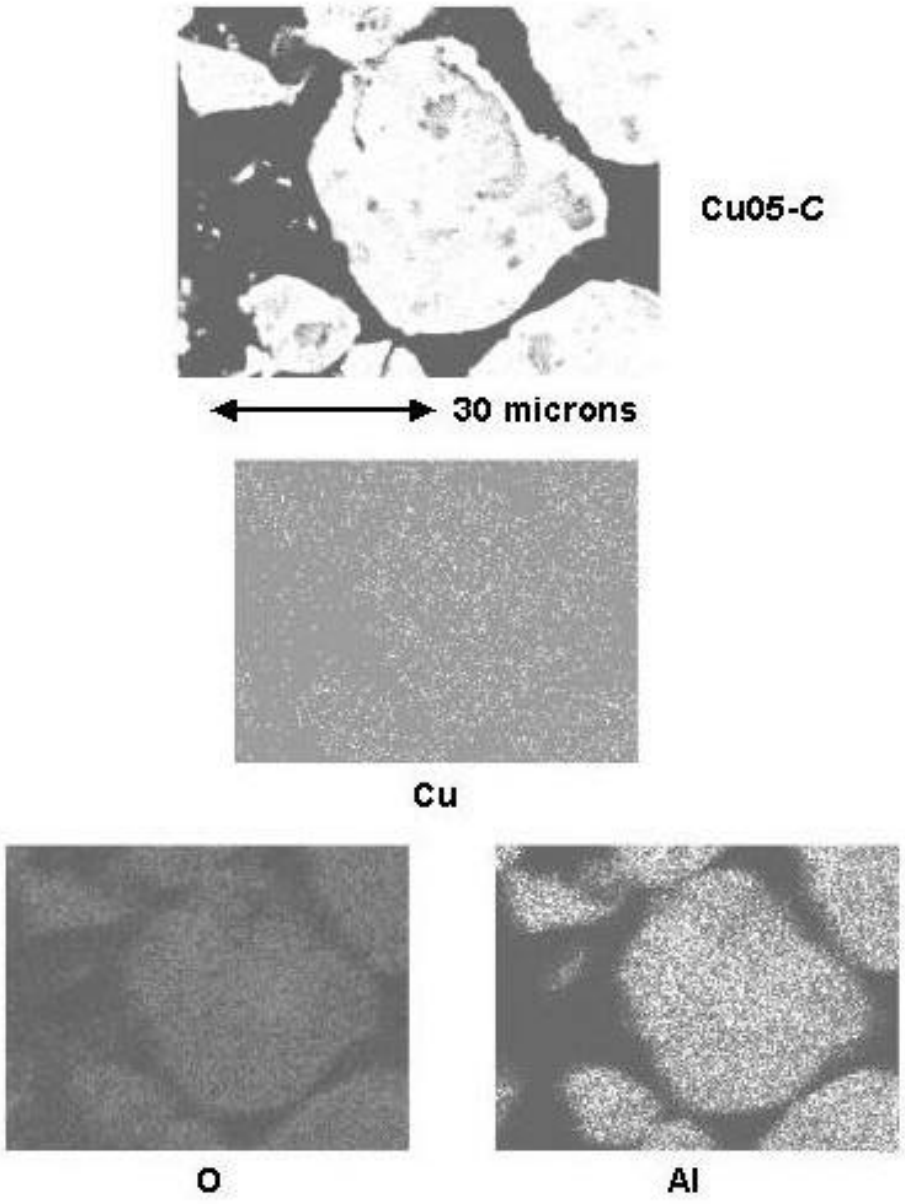

Figure 8.8 EDX Mapping of the cross-section of a Cu05-*C* Catalyst Precursor Granule

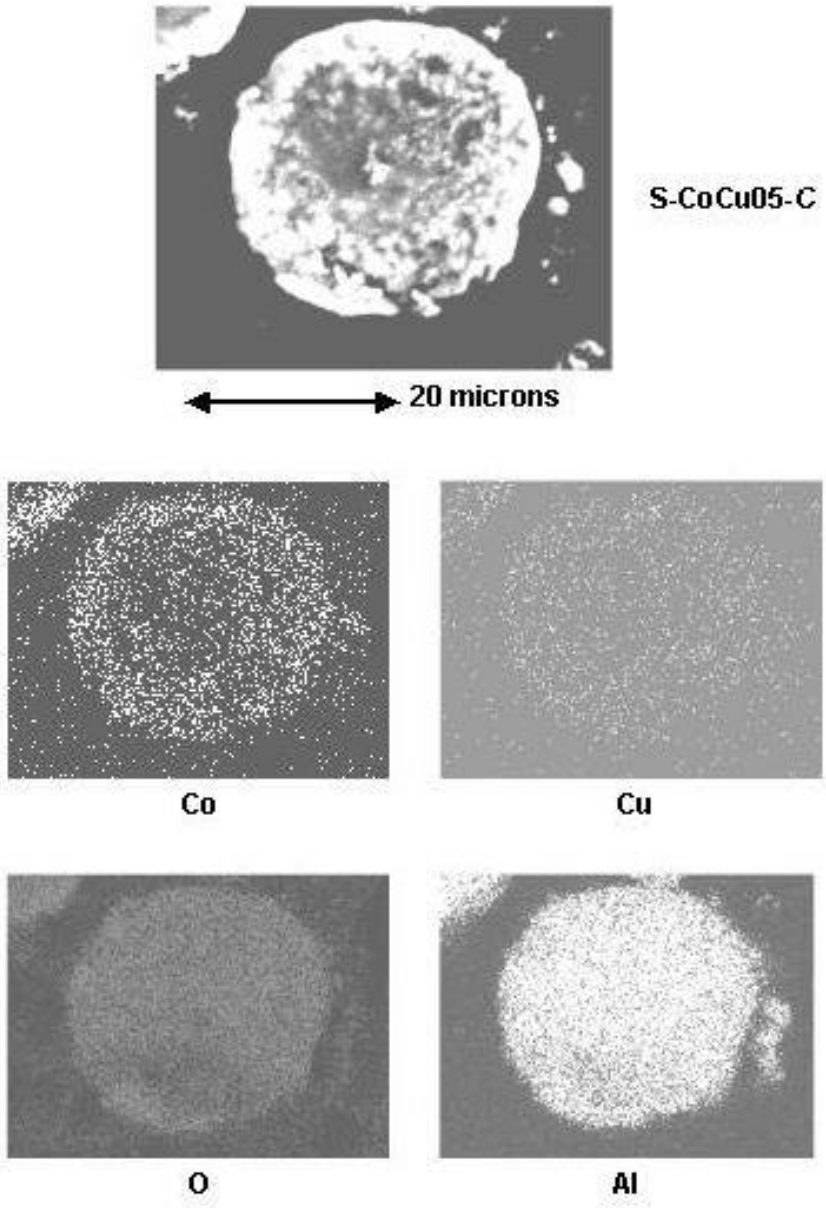

Figure 8.9 EDX Mapping of the cross-section of a S-CoCu05-*C* Catalyst Granule

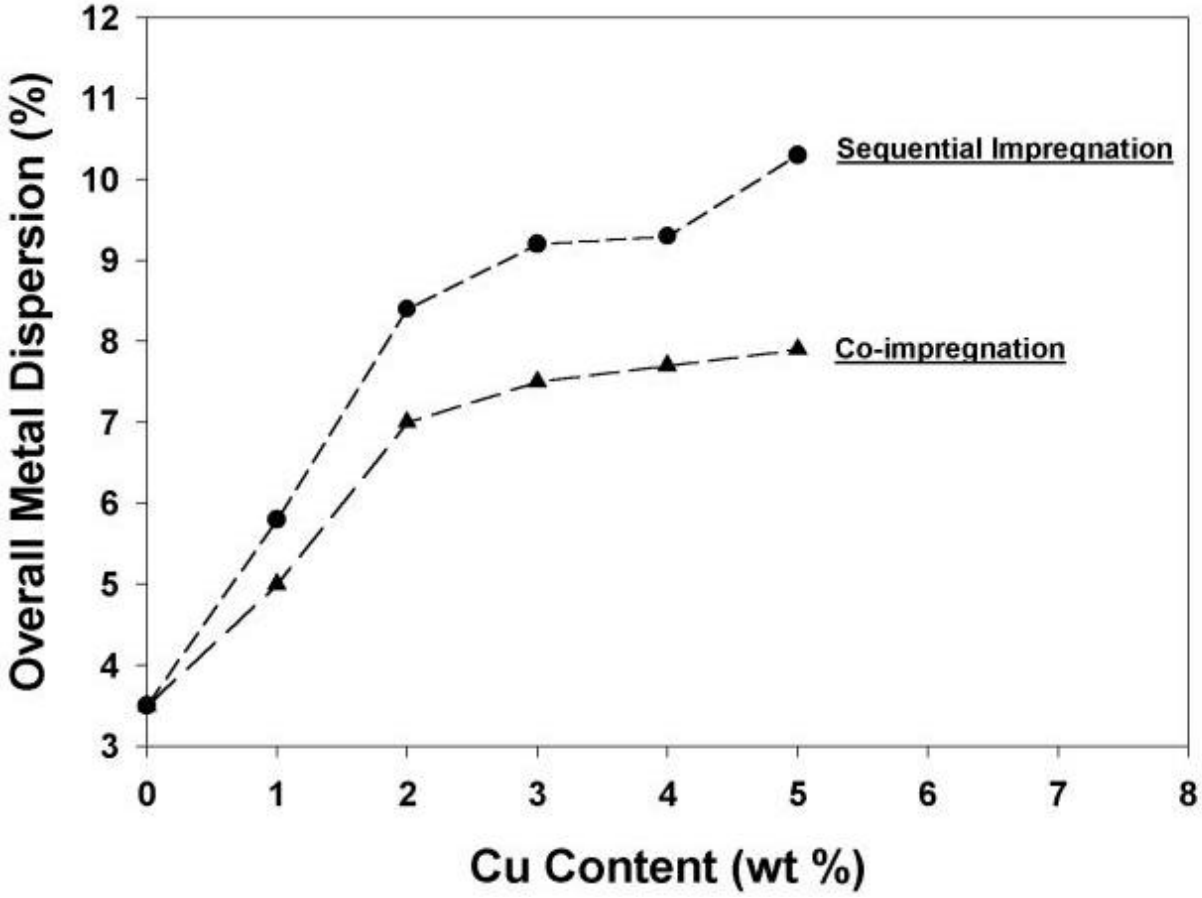

Figure 8.10 Effect of Cu Promoter on the Overall Metal Dispersion

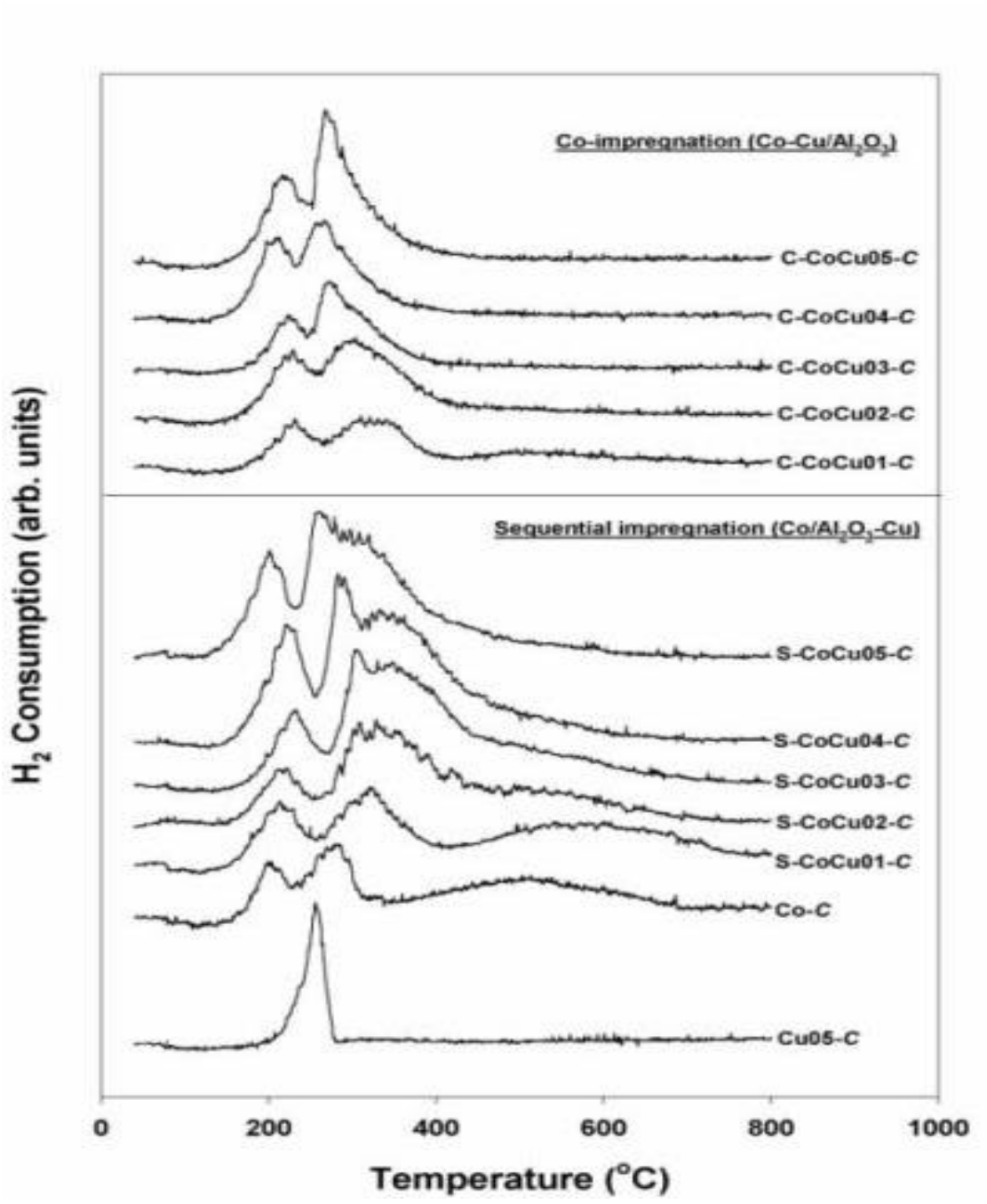

Figure 8.11 TPR Profiles of Co-*C*, Cu05, and Calcined CoCu Catalysts

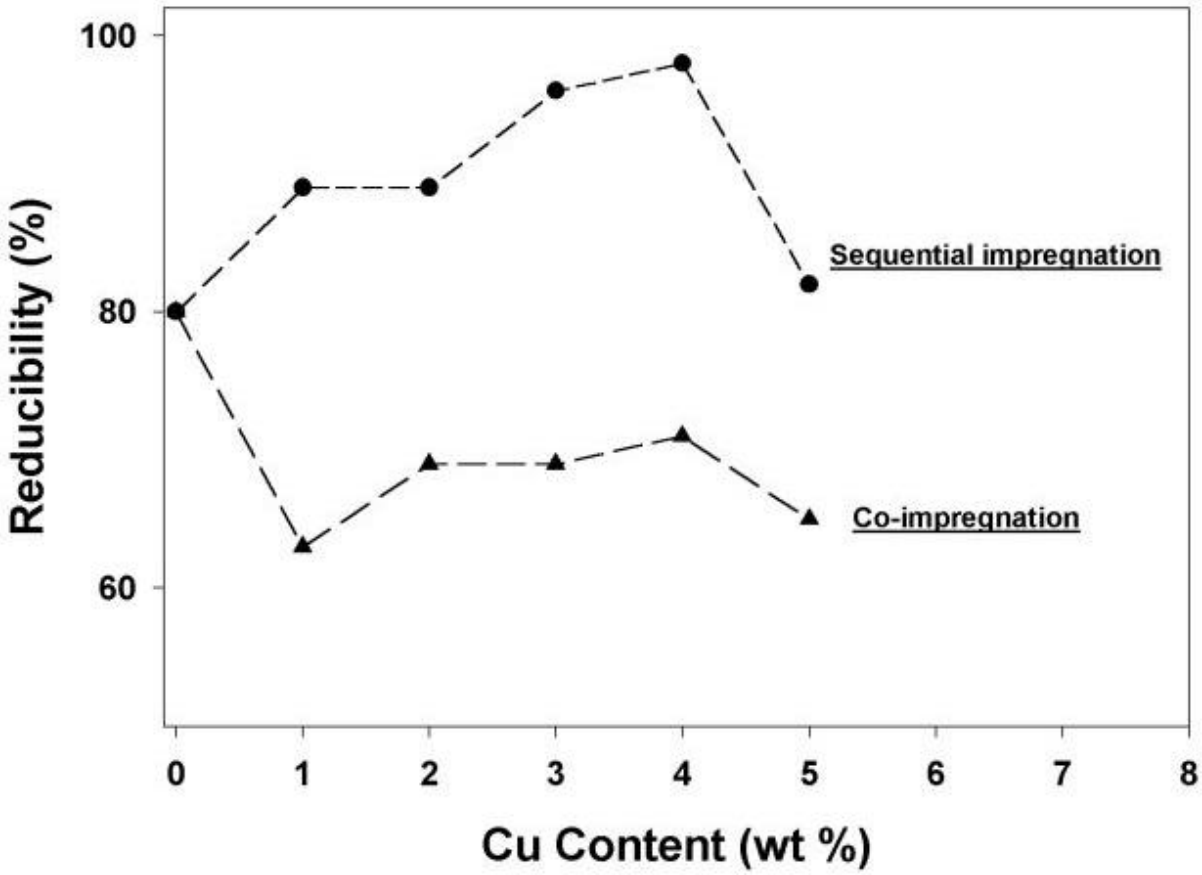

Figure 8.12 Effect of Cu Promotion on Reducibility of the Catalysts

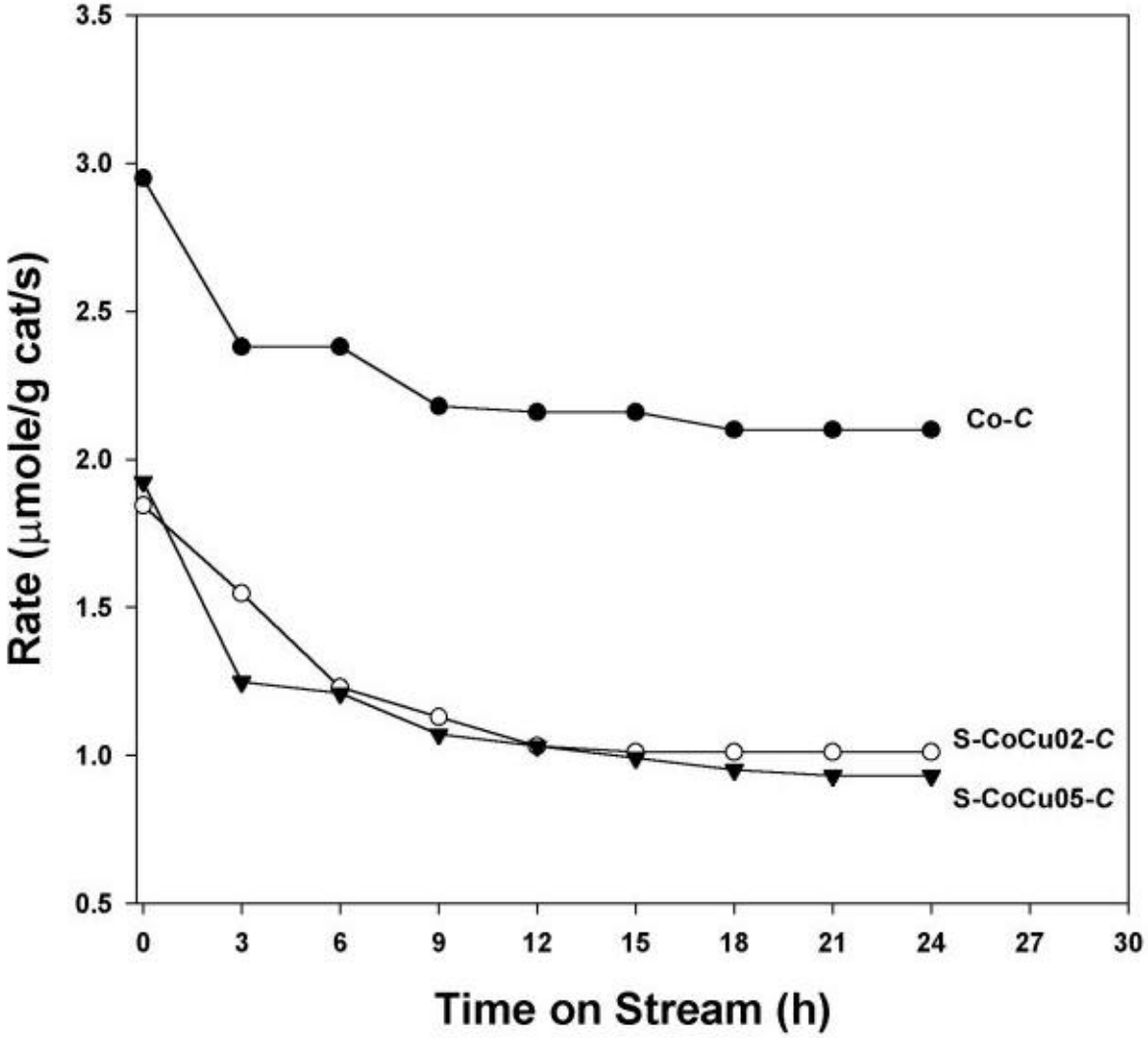

Figure 8.13 Effect of Cu Promotion on Reaction Rate During FTS

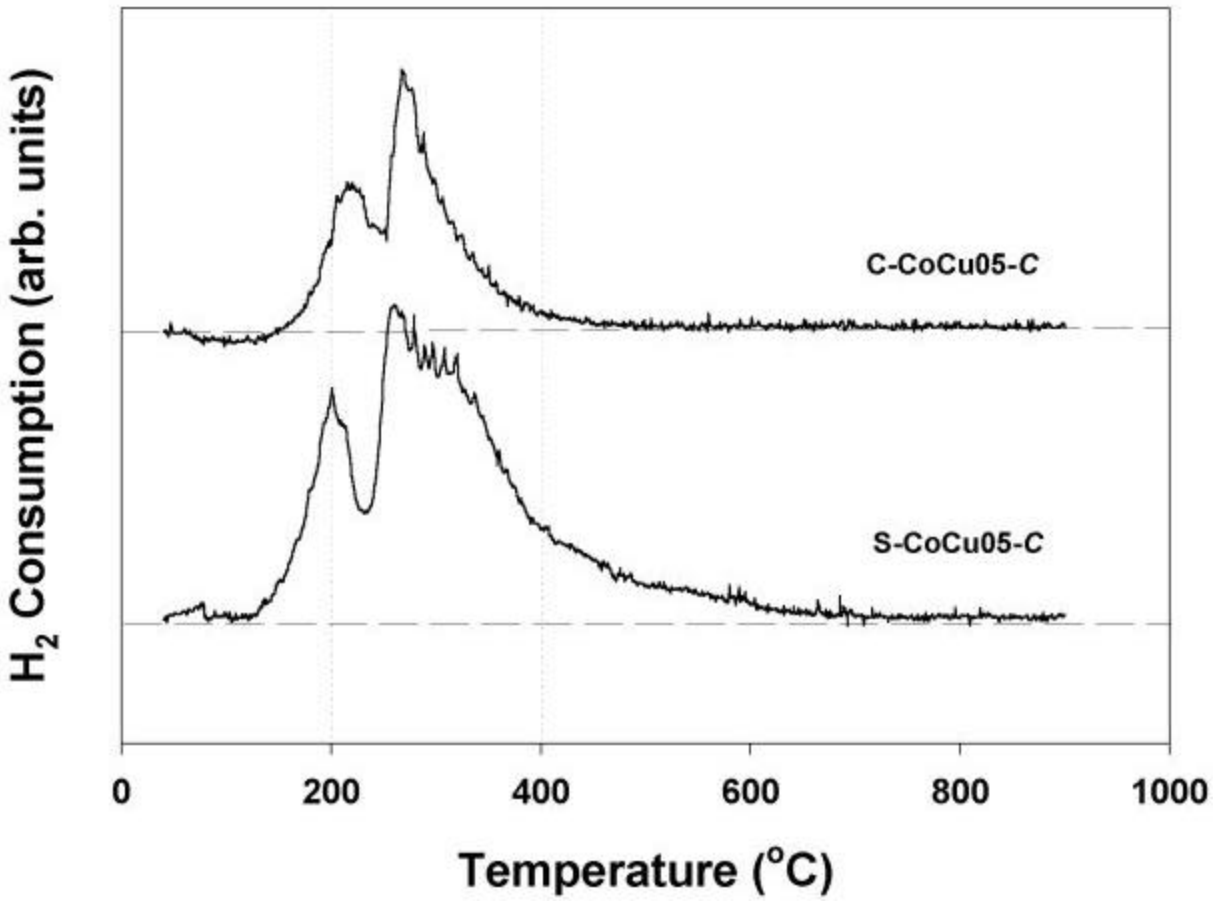

Figure 8.14 Comparison of TPR Profiles for Cu Promotion Catalysts

9.0 EFFECT OF ZIRCONIA-MODIFIED ALUMNA SUPPORT

9.1 Introduction

In order to increase catalyst activity, many promoters such as Ru[1-3], Zr[4-5], La[6], Rh[7-9], B[10], and Pt[11] have been investigated for Co catalysts. It has been proposed that various of these promoters can increase the reducibility of Co, preserve the activity by preventing the formation of coke, exhibit cluster and ligand effects, act as a source of hydrogen spillover, and enhance the dispersion. The use of additives to specifically modify the metal-support interaction has also been investigated. It has been found that metal dispersion, chemical state, as well as catalyst activity are affected by changing the interaction between the metal catalytic phase and the support as a result of modification using B, Ge, Ga, and Zn.[10, 12-20]

A number of FTS patents by Shell[21-22] have involved Zr promotion of Co/SiO_2. Ali et al.[4] investigated Zr promotion of Co/SiO_2 catalysts for FTS and found that Zr is basically a rate promoter. Rohr et al.[5] investigated the effect of adding Zr to an alumina support for Co FTS catalysts. They found that at 5 bar and a H_2:CO ratio of 9:1, Zr-modified alumina-supported Co exhibited an increase in the activity and selectivity to C_{5+} hydrocarbons. Steady-state isotopic transient kinetic analysis (SSITKA) showed that the intrinsic activity of Co/Al_2O_3 was not greatly affected by Zr modification.[5] Although, Zr modification appears to increase the rate of FTS rate on Co catalysts [4,5], no studies have specifically addressed how Zr promotes the reaction. Understanding how Zr modifies catalyst properties could lead to the design of more robust and active Co catalysts.

This investigation focused on studying the impact of Zr modification of Co/γ-Al_2O_3 catalysts. A series of Co/γ-Al_2O_3-Zr catalysts were prepared with a range of Zr concentrations. Since the presence of water vapor during reduction is known to increase Co-aluminate formation, the impact of Zr loading on the reducibility of Co in the absence and presence of water vapor was investigated. The effect on the reaction rate and product distribution during FTS was also measured. SSITKA of CO hydrogenation was performed to obtain a better understanding of the effect of Zr modification on the intrinsic activity and surface coverage of reaction intermediates.

9.2 Experimental

9.2.1 Materials

9.2.1.1 Co/γ-Al_2O_3. The Co/γ-Al_2O_3 catalyst was prepared by the incipient wetness impregnation of γ-Al_2O_3. The support precursor (Al_2O_3, Vista B) was first calcined at 500°C for 10 h before impregnation in order to put it in the form of γ-Al_2O_3 having a specific surface area of 209 m^2/g and average particle size ca. 60 μm. Cobalt nitrate [$Co(NO_3)_2 \cdot 6H_2O$] was dissolved in de-ionized water and impregnated into the support using incipient wetness to give a final catalyst with 20 wt% cobalt. The catalyst was dried at 110°C for 12 h and calcined in air at 300°C for 2 h.

9.2.1.2 Co/γ-Al_2O_3-Zr. The Zr-modified alumina-supported Co catalysts (Co/γ-Al_2O_3-Zr) were prepared by the sequential impregnation method. The same support (γ-Al_2O_3) as mentioned before was used. First, Zr was impregnated into the support using a solution of zirconium (IV) n-propoxide (70 wt% in n-propanol, Alfa Aesar) to produce Zr-modified alumina supports

having 2, 5, and 11 wt% of ZrO_2. The Zr-modified supports were then calcined at 350°C for 2 h prior to impregnation of cobalt. Cobalt nitrate was then used to impregnate the Zr-modified supports to produce catalysts with 20 wt% cobalt using the same procedure as given above.

9.2.2 Catalyst Pretreatment and Nomenclature

The catalysts were characterized following these three pretreatments:

i) the original calcination step;

ii) standard reduction of the calcined catalysts at 350°C for 10 h using a high space velocity (16,000 h^{-1}) of H_2 followed by passivation with an O_2/He (5.20% of O_2) mixture at room temperature for 2 h;

iii) standard reduction of the calcined catalysts at 350°C for 10 h using a high space velocity (16,000 h^{-1}) of a mixture of H_2 and 3 vol% water vapor followed by passivation with an O_2/He (5.20% of O_2) mixture at room temperature for 2 h.

The nomenclature used for samples in this study is the following:

Co/Al-Zr-n-i

where;

n refers to wt% ZrO_2 in the catalyst samples.

i = ***C*** refers to the calcined catalyst samples.

= ***RP*** refers to the reduced and passivated catalyst samples.

= $\boldsymbol{R_WP}$ refers to the samples reduced in the presence of 3 vol% water vapor and then passivated.

The catalyst compositions are shown in Table 9.1.

9.2.3 Catalyst Characterization

9.2.3.1 X-ray Powder Diffraction (XRD). XRD was performed to determine the bulk crystalline phases of the catalysts following different pretreatment conditions. X-ray powder diffraction patterns of samples were collected using a Scintag XDS-2000 X-ray diffractometer with monochromatized Cu-K_α radiation (λ = 1.54439 Å). The spectra were scanned at a rate of 2.4 degree/min from 2θ = 20 to 80 degrees.

9.2.3.2 Raman Spectroscopy. The Raman spectra of the samples were collected by projecting a continuous wave laser of helium-neon (He-Ne) red (632.816 nm) through the samples exposed to air at room temperature. A scanning range between 100 to 1000 cm^{-1} with a resolution of 2 cm^{-1} was applied. The data were analyzed using Renishaw WiRE (Windows-based Raman Environment) software which allows Raman spectra to be captured, calibrated, and analyzed using system 2000 functionality via the Galactic GRAMS interface with global imaging capacity.

9.2.3.3 SEM and EDX. SEM and EDX were performed to study the morphologies of the catalyst samples and their elemental distributions, respectively. A Hitachi S3500N SEM was used in the back scattering electron (BSE) mode at 15 kV with a working distance (the distance between a sample and the electron beam) of 15 mm. After the SEM micrographs were taken, EDX was performed to determine the elemental concentration on the catalyst surface (using INCA software).

9.2.3.4 Hydrogen Chemisorption. Static H_2 chemisorption on the re-reduced cobalt catalyst samples at 100°C was performed using the method described by Reuel and Bartholomew[23] and was used to determine the number of reduced surface cobalt metal atoms. This is related to the overall activity of the catalyst during FTS. Chemisorption was conducted in a Micromeritics ASAP 2010 and analyzed using ASAP 2010C V3.00 software. Prior to H_2 chemisorption, the reduced and passivated catalyst samples were evacuated to 10^{-6} mm Hg at 100°C for 15 min, reduced in flowing H_2 (50 cc/min) at 100°C for 15 min, reduced at 350°C in flowing H_2 for 10 h, and then evacuated at 350°C for 90 min to desorb any hydrogen.

9.2.3.5 Temperature Programmed Reduction (TPR). TPR was performed to determine the reducibility and reduction behavior of the catalyst samples. TPR was carried out in an Altamira AMI-1 system using 50 mg of catalyst and a temperature ramp from 30ºC to 800ºC at 5ºC/min. The reduction gas was 5% H_2 in Ar. A cold trap (-70ºC) was placed before the detector to remove water produced during the reaction. A thermal conductivity detector (TCD) was used to determine the amount of hydrogen consumed. The hydrogen consumption was calibrated using TPR of silver oxide (Ag_2O) at the same conditions. The reduced and passivated catalyst samples were re-calcined *in situ* at 300°C for 2 h before performing TPR.

9.2.4 Reaction

FTS was carried out at 220°C and 1 atm total pressure. A flow rate of H_2/CO/Ar = 60/30/10 cc/min in a fixed-bed reactor under differential reaction conditions was used. Thermocouples at the top and the bottom of the catalyst bed ensured precise temperature control

during pretreatment and reaction. Typically, 0.2 g of the pretrea0ted catalyst sample was re-reduced *in situ* in flowing H_2 (50 cc/min) at 350°C for 10 h prior to FTS. In order to avoid exotherms and hot spots that lead to rapid catalyst deactivation, the reaction was initiated in a controlled manner by gradually increasing the reactant concentrations over a period of 2 h. After the start-up, samples were taken in 3 h intervals and analyzed by gas chromatography. Steady state was reached after 24 h in all cases.

9.2.5 Steady-State Isotopic Transient Kinetic Analysis (SSITKA)

SSITKA was performed using a differential fixed-bed glass microreactor. Hydrogenation of CO was carried out at 220°C and 1.8 atm. A flow rate of H_2/CO/He = 20/2/8 cc/min was used. A relatively high H_2/CO ratio of 10 was used to minimize deactivation due to carbon deposition during reaction. Thermocouples at the top and at the bottom of the catalyst bed assured precise temperature control during pretreatment and reaction. Typically, 15 mg of a calcined catalyst sample was re-reduced *in situ* in flowing H_2 (30 cc/min) at 350°C for 10 h prior to the reaction. As the reaction began, reactor effluent samples were taken at 1 h intervals and analyzed by GC. Generally, steady-state was reached after 5 h in all cases. During steady-state, transients of methane and CO were obtained by switching the flow of ^{12}CO/Ar to ^{13}CO without disturbing the stability of the reaction. A trace (5%) of Ar in the ^{12}CO was used to account for the gas phase hold-up of the system. The decay or increase of isotopically marked species was monitored by an online Leybold-Inficon Auditor-2 quadruple mass spectrometer. Average surface residence times for the carbon in CH_4 and CO were calculated from these transient studies. The number of surface intermediates, which gave rise to CH_4 and the amount of reversibly chemisorbed CO were also calculated.

9.3 Results

9.3.1 X-ray Diffraction

XRD patterns for the calcined Co catalysts (with and without Zr modification) and Co_3O_4 (spinel) are shown in Figure 9.1. They had identical XRD patterns. The diffraction peaks at 31.3°, 36.8°, 45°, 55°, 59.4°, and 65.4° are those of Co_3O_4. Peaks for γ-Al_2O_3 were also evident. No peaks of ZrO_2 or any other Zr compound, however, were detected. This indicates that ZrO_2 was present in a highly dispersed form.[4] It will be assumed from this point that Zr was in the form of ZrO_2. After reduction and passivation, only XRD peaks of CoO (at 37°, 42.6° and 61.8°) and γ-Al_2O_3 were evident. No Co metal peaks were seen due to its high dispersion and their overlap with those for γ-Al_2O_3. No XRD peaks of $CoAl_2O_4$ (spinel)[24] could be detected either for any of the catalyst samples.

9.3.2 Raman Spectroscopy

Raman spectra for the calcined catalyst samples and Co_3O_4 are shown in Figure 9.2. After calcination, the Raman bands at 198, 480, 519, 619, and 690 cm^{-1} were observed in all catalyst samples. These can be assigned to Co_3O_4. The Raman spectrum for γ-Al_2O_3 was essentially flat. The Raman band (at 642 cm^{-1}) for ZrO_2[25] was not seen for any of the catalyst samples. Raman spectra of the reduced and passivated catalyst samples are shown in Figure 9.3. Raman bands for all reduced and passivated catalyst samples with Zr modification were identical, but different from those for the reduced and passivated Co catalyst without Zr modification (Co/Al-*RP*), as seen in Figure 9.3. Only two very broad Raman bands at ca. 690 and 560 cm^{-1} were detected for Co/Al-*RP* and this has been correlated to the formation of a highly dispersed Co "aluminate"

phase.[24] Similar results can be observed for the samples reduced with 3 vol% added water vapor (*R*$_W$*P* samples) as shown in Figure 9.4. Strong Raman bands at 690, 480 and 198 cm^{-1} were observed for the reduced and passivated catalyst samples with Zr modification. These bands can be assigned to Co_3O_4 (see Figures 9.3 and 9.4), present on the Co surface after the samples were passivated and exposed to air, rather than CoO (detected in the bulk by XRD) since Raman is more of a surface technique. No peaks for $CoAl_2O_4$ (spinel) were detected in any of the samples.

9.3.3 SEM and EDX

The typical particle/granule morphologies of the calcined catalyst samples are shown in Figure 9.5. In all the Co catalyst micrographs, the white or light spots represent high concentrations of Co and its compounds and the gray areas represent the alumina or Zr-modified alumina support with no/minimal Co present. There was no significant change in morphology between the alumina and Zr-modified alumina supports. However, it can be seen in Figure 9.5 that Co on the Zr-modified alumina supports was more dispersed (i.e., had smaller SEM-visible Co patches/particles that were more scattered) than on the unmodified alumina support.

EDX gave useful information about the elemental distribution on the cross sectioned calcined catalyst granules. Figure 9.6 shows the typical elemental distribution for a cross section of a granule of Zr-modified alumina support. EDX mapping indicated that all elements in the modified support were well distributed throughout the catalyst granules. This was also true for the catalyst after Co loading, as shown in Figure 9.7.

9.3.4 Temperature Programmed Reduction (TPR)

In order to eliminate residual $Co(NO_3)_2$ and its impact on the TPR spectra and the calculation of reducibility[24], all TPR results are reported after initial reduction and re-calcination at 300°C (Figure 9.8). There were two major peaks for Co/Al-*C* located at ca. 350°C, and between 400-700°C (maximum at 600°C). These peaks have been related to the following reduction steps: $Co_3O_4 \rightarrow CoO$ and $CoO \rightarrow$ Co metal (ca. 350°C), and Co_XO_Y-$Al_2O_3 \rightarrow$ Co metal (between 400-700°C), respectively.[3,11,24,26-27]

There were also three major peaks for the Co catalysts with Zr modification located at 320°C and between 500-800°C (maximum at 700°C). It would appear that the broad peak with its maximum ca. 600°C was shifted about 100°C higher with Zr modification. This indicates that Zr modification caused changes in reduction behavior of the Co catalysts. There was an apparent decrease in both peak locations for the Zr-modified catalysts with Zr loading. The TPR profile for the Zr-modified support [11 wt% ZrO_2-Al_2O_3 (without Co)] showed no reduction peak. Thus, the support would appear not to have been reducible during TPR. However, one might ask what is the possibility that Co impregnated into the Zr-modified supports can activate hydrogen to partially reduce ZrO_2 as a result of spillover. If that happened, any additional H_2 consumed by ZrO_2 would lead to an overestimation of Co reducibility. In order to answer this question, TPR of alumina and modified supports containing 5 wt% Pt were studied. All the PtO_2 on alumina was reducible at temperatures 30-400°C (maximum at 200°C) as shown in Figure 9.9. While the addition of Zr resulted in a shift of the second reduction peak to higher temperature, there was no evidence for any additional consumption of H_2. Thus, it is concluded that, during TPR, activation of H_2 by reduced Pt or Co was not sufficient to cause any significant reduction of ZrO_2.

Figure 9.10 shows TPR profiles of the Co/Al and Co/Al-Zr-05 catalysts after reduction with and without added water vapor. These catalysts had been re-calcined prior to TPR. The two-peak reduction TPR profiles were observed for the *RWPC* samples. However, water vapor present during standard reduction resulted in a shift of the second TPR reduction peak to even higher temperature for both the unmodified and Zr-modified catalysts.

The reducibilities of Co/γ-Al_2O_3 and Co on Zr-modified γ-Al_2O_3 after various pretreatments are shown in Table 9.2. While the reducibilities during TPR to 800^{o}C are interesting, the amount of reduction during TPR from 30 to 400^{o}C is more important since it is related to the reducibilities of these Co catalysts during standard reduction at 350^{o}C.[28] It can be seen that the reducibility of alumina-supported Co increased significantly with Zr modification.

9.3.5 H_2 Chemisorption

H_2 chemisorption results are shown in Table 9.2. The overall dispersion of reduced Co in the catalyst samples is also given. The Co metal dispersions of the catalysts ranged between 3.5 to 3.8%. The results indicate that the amount of adsorbed H_2 was not dramatically changed with Zr modification, although there was perhaps a slight increase. The Zr-modified support [11 wt% ZrO_2/γ-Al_2O_3 (without Co)] was inactive for H_2 chemisorption.

9.3.6 Reaction Rate

FTS was performed to determine the overall activity and product distribution of the Co catalysts with and without Zr modification. The results are shown in Table 9.3 and Figure 9.11. It can be seen that the presence of ZrO_2 (2-11 wt%) as a support modifier increased by approximately a factor of two both the initial and steady-state FTS rates. TOF based on H_2

chemisorption also increased by approximately a factor of two with Zr modification due to the increase in rate, since the amount of H_2 adsorbed was essentially constant. Considering the product distribution, it can be observed that the addition of the Zr modifier resulted in a slight increase in the Anderson-Schulz-Flory (ASF) chain-growth probability (α). As also seen in Table 9.3, it appears that the amount of carbon deposited on the catalysts during FTS for 24 h decreased with Zr modification. The reaction rates on the unmodified and Zr-modified catalysts after various pretreatments are shown in Table 4. It is obvious that the rate on the calcined samples (reduced prior to FTS) was higher than on the reduced and passivated samples (re-reduced prior to FTS). Moreover, the rate on the reduced and passivated samples decreased with the addition of water vapor during standard reduction (again re-reduced prior to FTS), although less so on the Zr-modified catalyst.

9.3.7 SSITKA

Steady-state isotopic transient kinetic analysis was used to determine *in situ* surface reaction parameters. SSITKA enables one to calculate the surface concentration of reaction intermediates and pseudo-first order rate constant (k_p).[2,6,29] During steady-state reaction, the surface residence times (τ) for CO and CH_4 were determined by integrating the areas between the transient curves for Ar and labeled CO or CH_4, respectively. The pseudo-first order rate constant (k_p), a measure of intrinsic site activity for methanation, was calculated by taking the inverse of the residence time of CH_4. The method used to calculate these parameters is described extensively by Shannon and Goodwin.[29]

Table 9.5 shows the SSITKA results for Co catalysts with and without Zr modification. The surface reaction residence time for the CH_4 intermediates (τ_M) remained unchanged with Zr

modification. Thus, there was no change in the intrinsic activity ($1/\tau_M$) of the methane producing sites. This indicates that the mean activity of the sites producing methane was not affected by Zr modification. The surface residence time for CO (τ_{CO}) was also found to show no significant difference. The surface abundance of intermediates leading to the formation of methane (N_M), however, was almost twice as much upon Zr modification. The surface coverages for methane intermediates (θ_M) were found to be low (< 0.2), as is typical, but this was somewhat higher with Zr modification.

9.4 Discussion

It is obvious that Zr modification resulted in significant differences in the properties of alumina-supported Co. It was found that the reducibility for TPR from 30-800°C (Table 9.2) increased with Zr modification (ZrO_2 = 2-11 wt%). The reducibility achieved during TPR from 30-400°C (related to the reducibility during standard reduction at 350°C for alumina-supported Co catalysts)[28] also increased with Zr modification, although the amount of Zr added did not seem to have a great impact.

It is known from our previous work[24] that a high partial pressure of water vapor during reduction results in a lower reducibility for an unpromoted Co catalyst. Water present in the H_2 reduction gas (such as naturally occurs as a byproduct of metal catalyst reduction) decreases the reducibility of Co catalysts due to the formation of non-reducible (at temperatures ≤ 900°C) Co "aluminate" [24,28], as is apparent in Table 9.2 for the unpromoted Co catalyst. This was also true for the Zr-modified samples. The reducibility (30-400°C) of Co/Al-Zr-05-*RPC* decreased from 37% to 18% (Table 9.2) when water was added during standard reduction (R_W*PC* sample).

However, it is obvious that the reducibility was still higher than that of unpromoted Co catalyst reduced also in the presence of water vapor (Co/Al-*RWPC* sample). In addition, as seen in Figures 9.3 and 9.4, there was no Raman evidence for the formation of Co "aluminate" of the Zr-modified catalysts. This suggests that Zr modification decreased the impact of water vapor during reduction, possibly by partially blocking Co "aluminate" formation.

In general, most authors have reported reducibilities during TPR of Co catalysts in the calcined form. For catalysts prepared with Co nitrate, TPR measurement of reducibilities of catalysts initially only calcined can result in an over estimation of the amount of Co reduced due to the consumption of H_2 by Co nitrate.[3,24] In order to eliminate this error, the residual nitrate has to be removed either by prolonging the initial calcination period from 2 to 14 h[3], or by reduction at 350°C followed by re-calcination prior to TPR measurement. After the elimination of the Co nitrate peak at ca. 200°C,[3,24] only two reduction peaks remain.[3,24] This is the reason why reducibilities of the reduced, passivated, and re-calcined samples are reported in this study as they provide more accurate values of reducibility.

As reported by Rohr et al.[5], reducibilities of Co/γ-Al_2O_3 during TPR to 900°C were not changed with Zr modification. Our measurements of reducibility were lower than those of Rohr et al., and we found that during TPR to 800°C our Zr-modified catalysts exhibited slightly higher reducibilities than the unmodified one. The difference between our results and those of Rohr et al. was probably due to the fact that we eliminated the contribution from residual Co nitrate and TPR was performed to 800°C. Probably because of the former, we were better able to detect important reducibility differences upon Zr modification.

In the present study, dramatic changes in the characteristics of the Raman bands for the reduced and passivated catalyst samples with the Zr modification were observed. Basically, the

Co "aluminate" bands were no longer present upon Zr modification. Only Raman bands for Co_3O_4 at 690, 480, and 198 cm^{-1} were evident on the reduced and passivated Zr-modified samples (Figure 9.3). Similar results were also found even when water vapor was added during standard reduction, as shown in Figure 9.4. This suggests that Zr modification decreases the amount of Co "aluminate" formed, even in the presence of water vapor. It should also be noted that XRD did not detect any differences upon Zr modification. The XRD results were typical for reduced Co/γ-Al_2O_3 catalysts.[3,24,28] The Co "aluminate" formed has been concluded to be too dispersed to be detected by XRD.[24]

One of the most critical parameters determining the catalytic activity of Co FTS catalysts besides Co reducibility is H_2 chemisorption. However, it was found that the H_2 chemisorption on the Co catalysts was not dramatically affected by Zr modification; there was only a slight increase in the amount of H_2 chemisorption (Table 9.2).

Considering the unpromoted Co catalyst, its TOF was ca. $2x10^{-2}$ s^{-1} - typical for Co catalysts under these conditions. Due to the large increases in FTS rate without any changes in H_2 chemisorption, the calculated TOFs at steady-state based on H_2 chemisorption were found to be larger by a factor of two with Zr modification. Since TOF is basically related to the intrinsic activity by definition, it might appear that Zr modification caused an increase in the intrinsic activity for alumina-supported Co catalysts. However, this conclusion is rendered doubtful based on the SSITKA results.

Our SSITKA results confirm those of Rohr et al. that the intrinsic activity was not affected by Zr modification, as indicated by the constant values of the intrinsic pseudo-first order activity ($k_p = 1/\tau_M$). The SSITKA results show that there was an increase in the number of active reaction intermediates (N_M) with Zr modification. Thus, the higher activity of the Co catalysts

with Zr modification is due either to a greater concentration of active sites or a higher occupancy of the sites during reaction. It is known that the number of active intermediates on Co surface obtained by SSITKA during CO hydrogenation is only a small fraction ($\theta < 0.2$) of the number of Co metal surface atoms measured by H_2 chemisorption.[2] It should also be noted that the number of reaction intermediates is a better measure of the true number of active sites than that is the number of reduced Co atoms obtained by H_2 chemisorption. Without any change in intrinsic activity, it is unlikely that an increase in surface coverage (θ) alone can explain the rate change, suggesting an increase in the number of active Co sites. Clearly, the reducibility of Co/γ-Al_2O_3 was increased by Zr modification, and it might be expected that H_2 chemisorption would also increase significantly. Given the consistency of the site activity ($1/\tau_M$), it is possible that TOF_H is in error (or at least variable) due to an incomplete chemisorption of H_2. The standard conditions for H_2 chemisorption on Co has been chosen to maximize activated chemisorption while minimizing hydrogen spillover. The conditions used, while appropriate for most Co catalysts, may not be appropriate for these Zr-modified ones.

9.5 Conclusions

Zr modification of the alumina support had a significant impact on the properties of Co/γ-Al_2O_3 catalysts. The overall catalytic activity during FTS doubled upon Zr modification. Most of this increase appears to have been due to an increase in reducibility. The increase in reducibility appeared to have been caused by a decrease in the amount of Co-SCF, as seen by Raman spectroscopy. Zr modification may have caused: (i) a stabilization of the alumina support by limiting its defect sites, thus blocking Co "aluminate" formation, and/or (ii) a

minimization of the impact of water vapor on modifying the surface properties of alumina, thereby decreasing the ease of Co migration into the alumina. SSITKA showed that the number of active reaction intermediates (N_M) increased with Zr modification while the intrinsic activity ($1/\tau_M$) remained constant. Thus, in summary, Zr modification increased Co reducibility and, probably, the number of exposed Co sites active for CO hydrogenation. Considering the variation in TOF_H but the lack of variation in $1/\tau_M$ (a measure of intrinsic activity), it is likely that TOF_H is in error due to errors in measuring accurately by H_2 chemisorption the number of reduced Co surface atoms. The standard H_2 chemisorption procedure of Reuel and Bartholomew[37], thus, may not be suitable for Zr-modified Co catalysts.

Table 9.1 Catalyst Compositions

Catalyst Samples	**Compositions (wt %)**			
	Co	**ZrO_2 (Zr)**	**g-Al_2O_3**	**Total**
Co/Al	20	0	80	100
Co/Al-Zr-02	20	2.2	77.8	100
Co/Al-Zr-05	20	5.4	74.6	100
Co/Al-Zr-11	20	10.8	69.2	100

Table 9.2 Reducibility and H_2 Chemisorption Results

Catalyst Samples	Zr/Co Atom Ratio	Reducibility[a,b,c]						Chemisorption	
		(30-800°C)			(30-400°C)[d]			Total H_2 Chemisorption[e] (mmole H_2/g cat.)	% Co Dispersion[f]
		C	RPC	R_WPC	C	RPC	R_WPC		
Co/Al	0	80	58	50	29	17	14	59	3.5
Co/Al-Zr-02	0.05	81	64	-	60	38	-	59	3.5
Co/Al-Zr-05	0.13	90	67	58	63	37	18	64	3.8
Co/Al-Zr-11	0.26	98	65	-	62	39	-	64	3.8
Al-Zr-11	NA	0	0	0	0	0	0	0	0

[a] The ***RP*** and ***R_WP*** samples were re-calcined at 300°C in air for 2 h before TPR measurement.

[b] The reducibility was based on a calibration with Ag_2O (100% reducibility).

[c] Error = ±5% of measurement of reducibility.

[d] The reducibility during TPR between 30-400°C is related to the reducibility of the catalysts during standard reduction.[(28)]

[e] Error = ±5% of measurement of H_2 chemisorption.

[f] %Co dispersion (%) = [2 x (total H_2 chemisorption/g cat)/ (no. μmole Co total /g cat)] x 100%.

Table 9.3 FTS Reaction Rate and Product Distribution

Catalyst Samples	Rate[a,b] (mmole/g cat/s)		TOF_H^C x 10^3 (s^{-1})		Product Distribution (%)					Carbon Content (%)[d]
	Initial	SS	Initial	SS	C_1	C_2-C_4	C_5-C_{12}	C_{13+}	a	
Co/Al-***R***	3.0	2.2	25	19	14.2	48.0	35.9	1.9	0.63	0.42
Co/Al-Zr-02-***R***	6.5	3.6	55	31	11.0	42.5	42.5	4.0	0.66	-
Co/Al-Zr-05-***R***	7.5	3.6	59	28	11.3	43.1	41.9	3.7	0.66	0.14
Co/Al-Zr-11-***R***	6.5	3.8	51	30	11.1	42.7	42.3	3.9	0.68	-

[a] FTS was carried out at 220°C, 1 atm, and H_2/CO ratio = 2 (H_2/CO/Ar = 60/30/10 cc/min). Catalyst samples were reduced (*R*) after pretreatments prior to the reaction.

[b] Error ±5%.

[c] Based on total H_2 chemisorption.

[d] Carbon content on the used catalyst samples after FTS for 24 h was analyzed using combustion/coulometric titration by Galbraith Laboratories, Inc.

Table 9.4 Effect of Pretreatment on Reaction Rate during FTS

Catalyst Samples	Rate [a,b] (μmole/g cat/s)	
	Initial	**Steady-State**
Co/Al-***R***	3.0	2.2
Co/Al-***RPR***	2.6	1.4
Co/Al-$\boldsymbol{R_W PR}$	2.2	0.6
Co/Al-Zr05-***R***	7.5	3.6
Co/Al-Zr05-***RPR***	6.5	2.2
Co/Al-Zr05-$\boldsymbol{R_W PR}$	5.0	1.8

[a] FTS was carried out at 220°C, 1 atm, and H_2/CO ratio = 2 (H_2/CO/Ar = 60/30/10 cc/min). Catalyst samples were reduced after pretreatments prior to the reaction.

[b] Error ±5%.

Table 9.5 SSITKA Results for CO Hydrogenation (H_2/CO = 10, T =220^{o}C, and P = 1.8 atm)

Catalyst Samples	**CO Conversion (%)**	**Rate CH_4 Formation (μmole/g cat/s)**	t_{CO}[a] **(s)**	N_{CO}[b] **(μmole/g cat)**	t_M[a] **(s)**	N_M[b] **(μmole/g cat)**	q_M[c]	k_p[d] **(s^{-1})**	TOF_H[e] **(s^{-1})**
Co/Al	3.6	2.6	1.0	39	3.6	10	0.08	0.28	0.02
Co/Al-Zr11	7.0	4.9	1.0	41	3.5	17	0.13	0.28	0.04

[a] Standard deviation = ± 0.2 s.

[b] Standard deviation = ± 0.6 μmole/g cat.

[c] θ_M is the surface coverage of carbonacious intermediates = N_M/(total adsorbed H).

[d] $k_p = 1/\tau_M$, pseudo-first-order rate constant.

[e] Based on total H_2 chemisorption

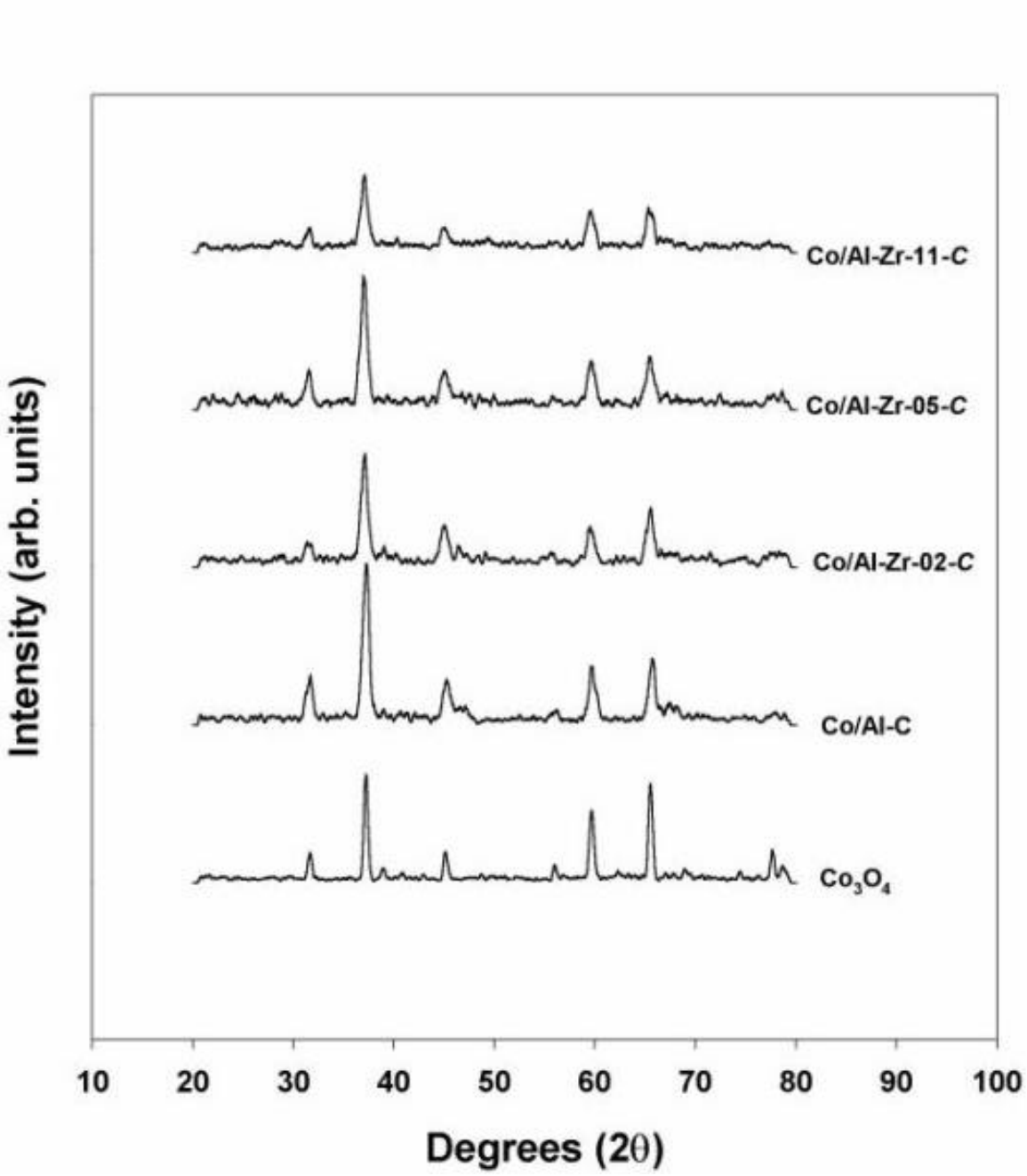

Figure 9.1 XRD Patterns of Co_3O_4, Co-*C*, and Co/Al-Zr-i-*C* Catalysts

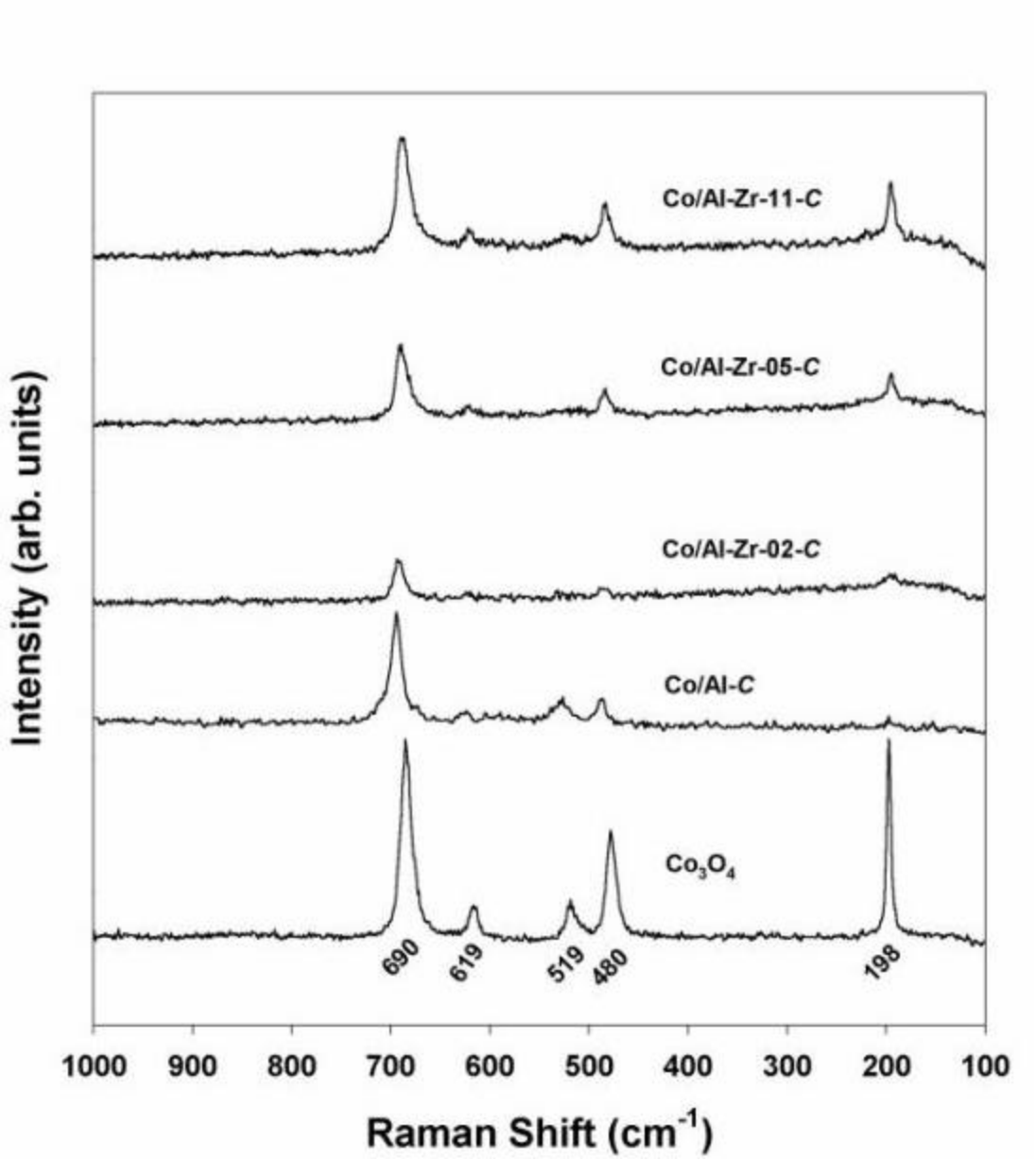

Figure 9.2 Raman Spectra of Co_3O_4 and Co/Al-Zr-i-*C* Catalysts

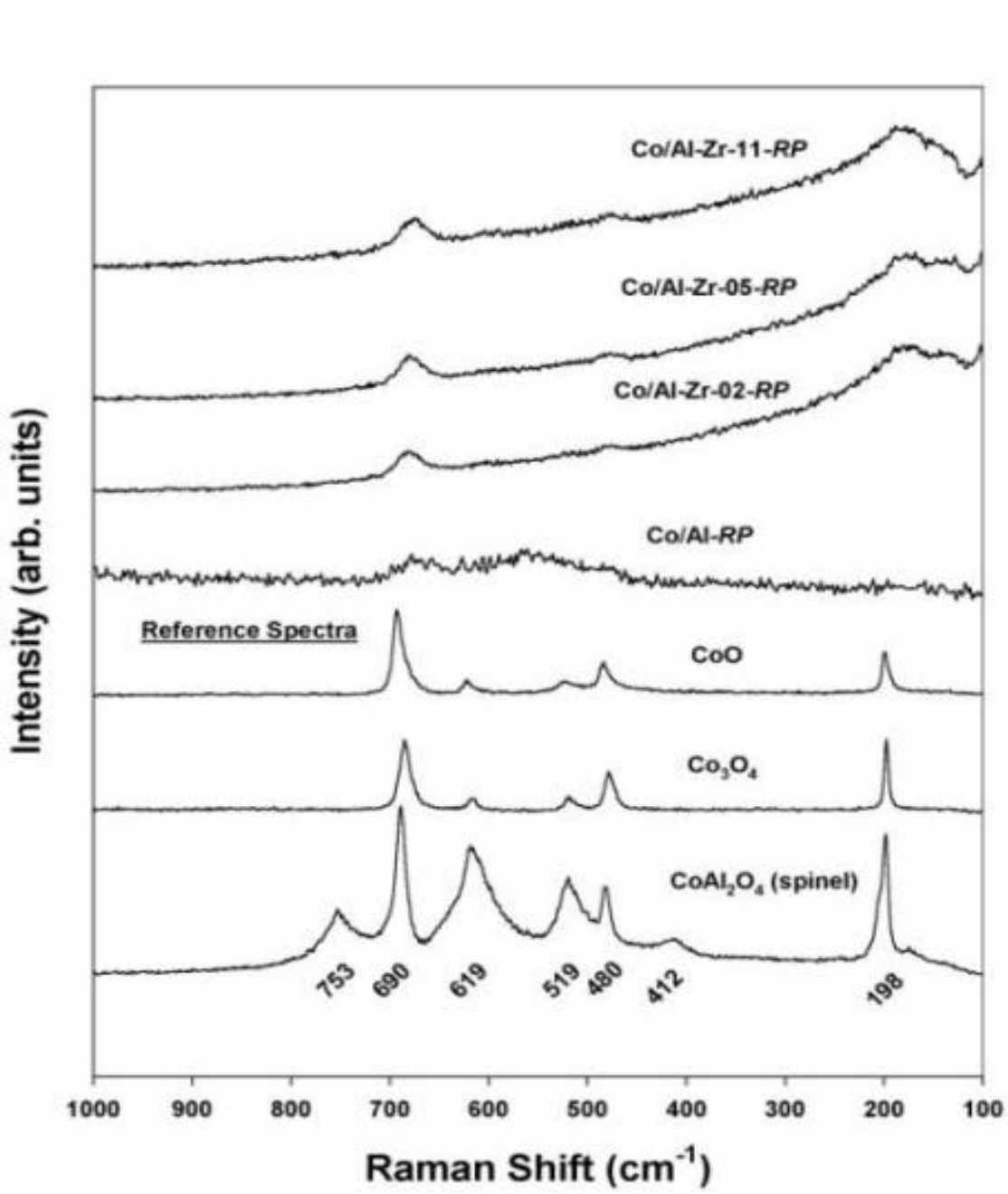

Figure 9.3 Raman Spectra of reduced and Passivated Co/Al-Zr-i Catalysts

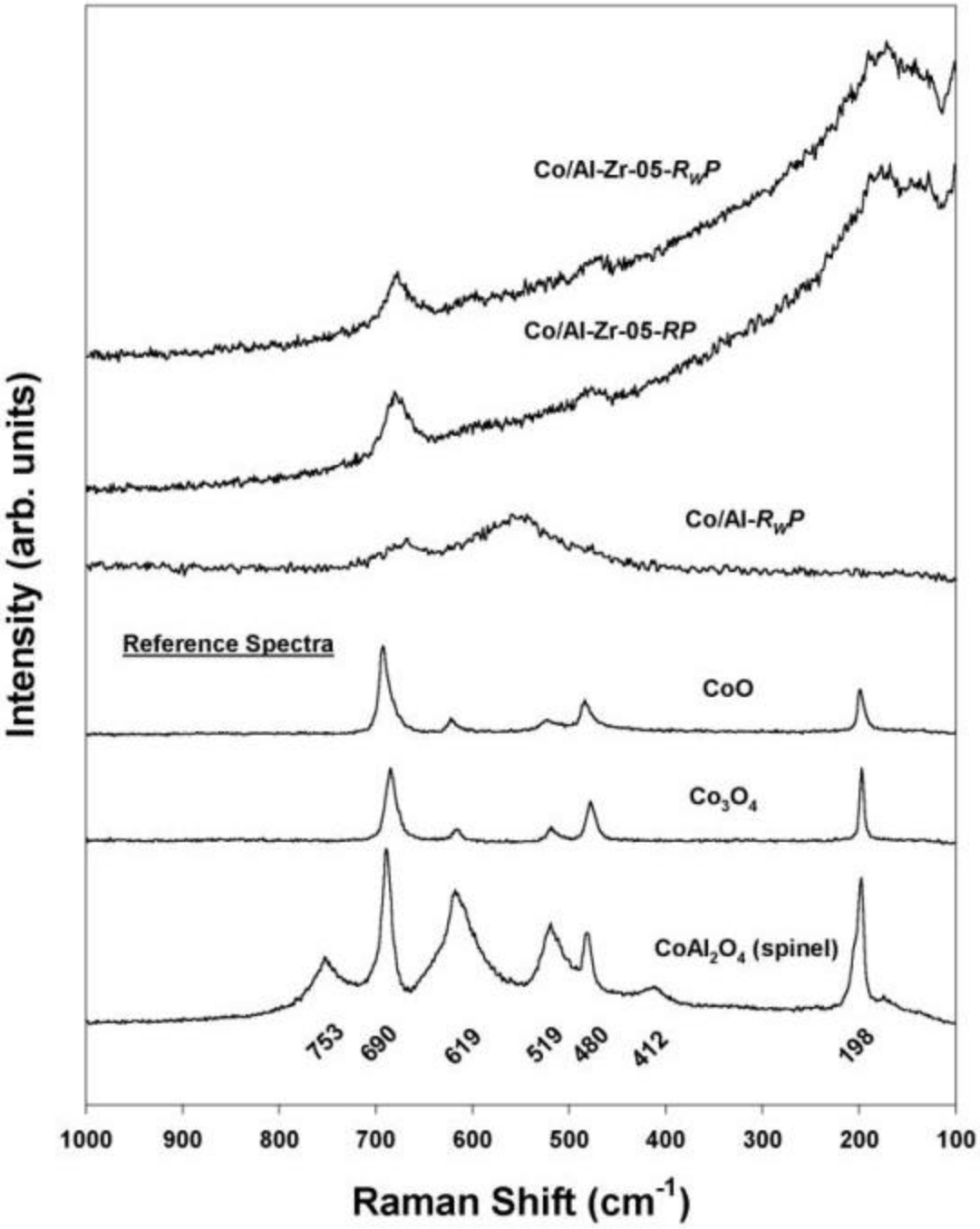

Figure 9.4 Raman Spectra of Co/Al-Zr-05-*RP* and R_WP Samples

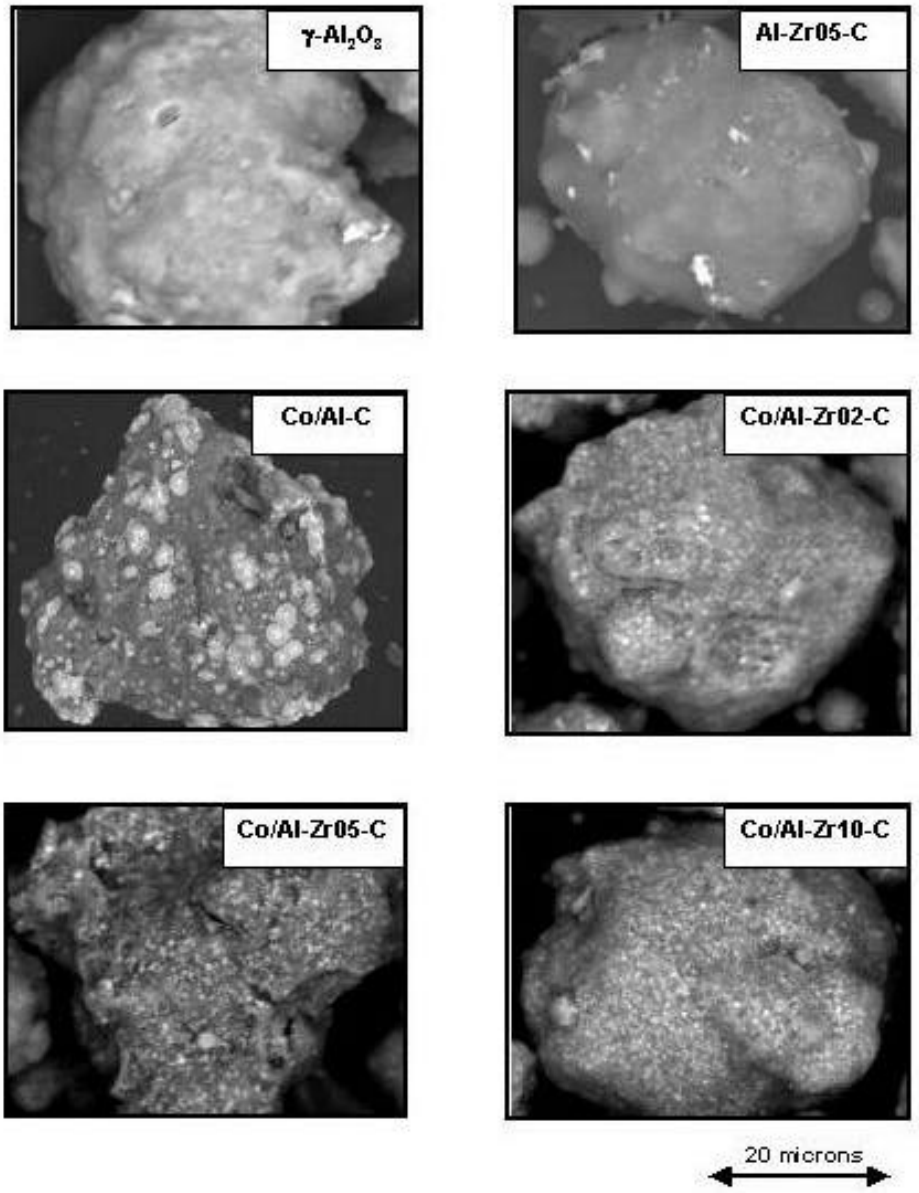

Figure 9.5 SEM Micrographs of Supports and Zr Modification Catalyst Granules

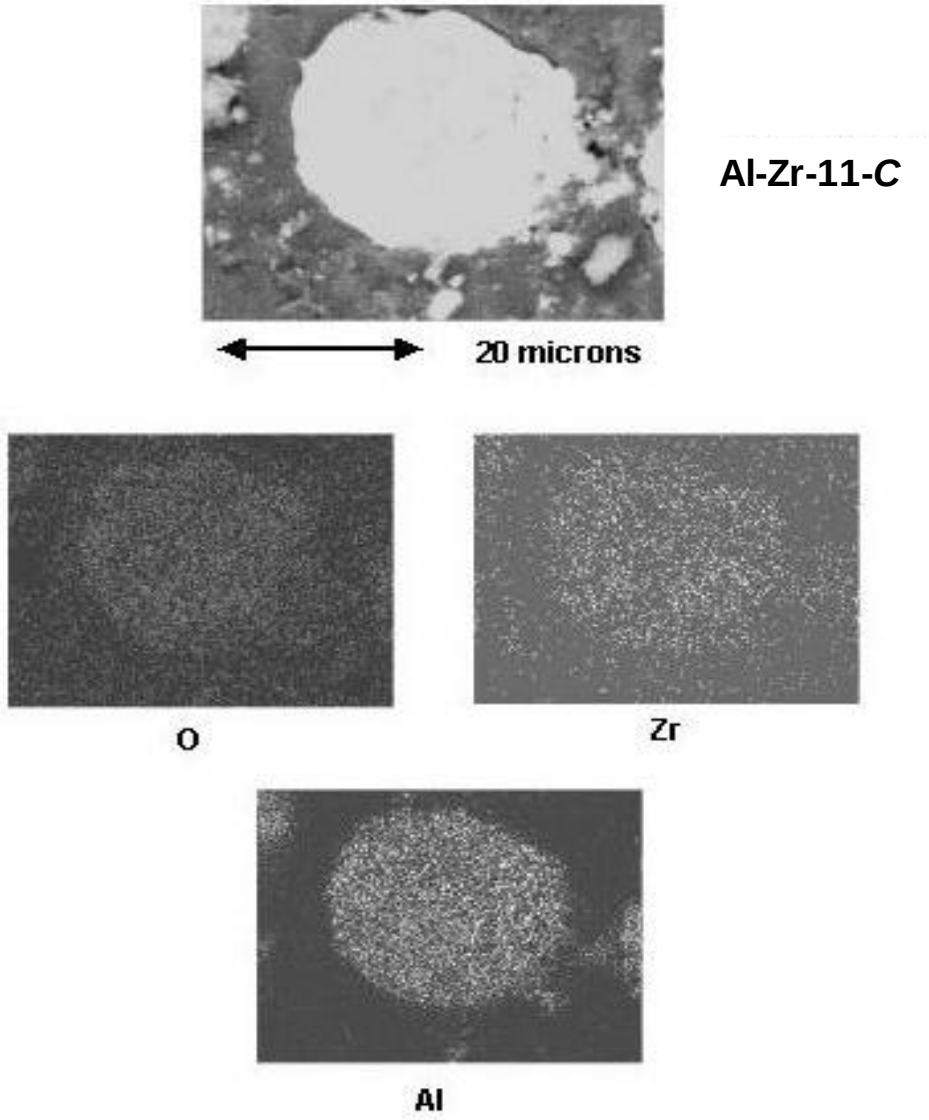

Figure 9.6 EDX Mapping of the Calcined Al-Zr-11-*C* Catalyst Precursor Granule (cross section)

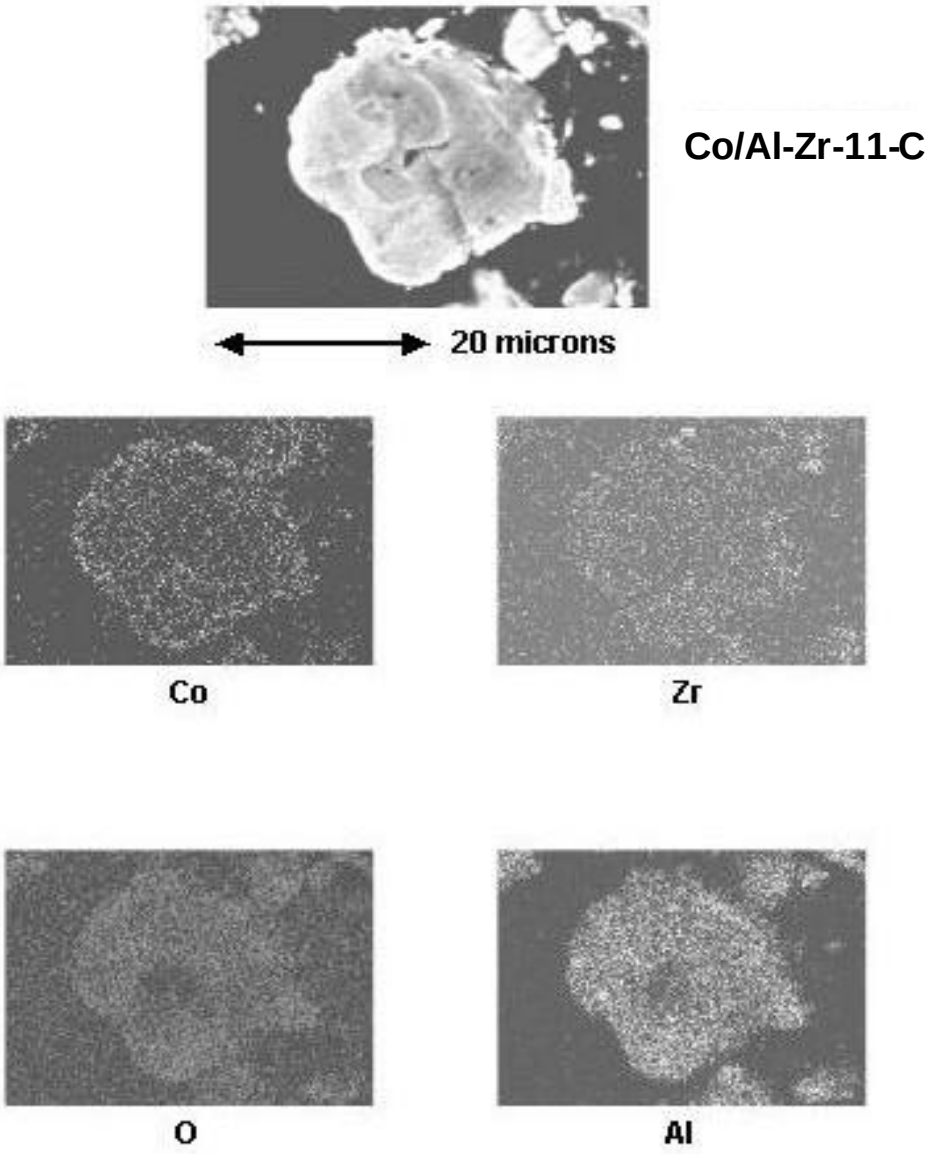

Figure 9.7 EDX Mapping of the Calcined Co/Al-Zr-11 Catalyst Granule

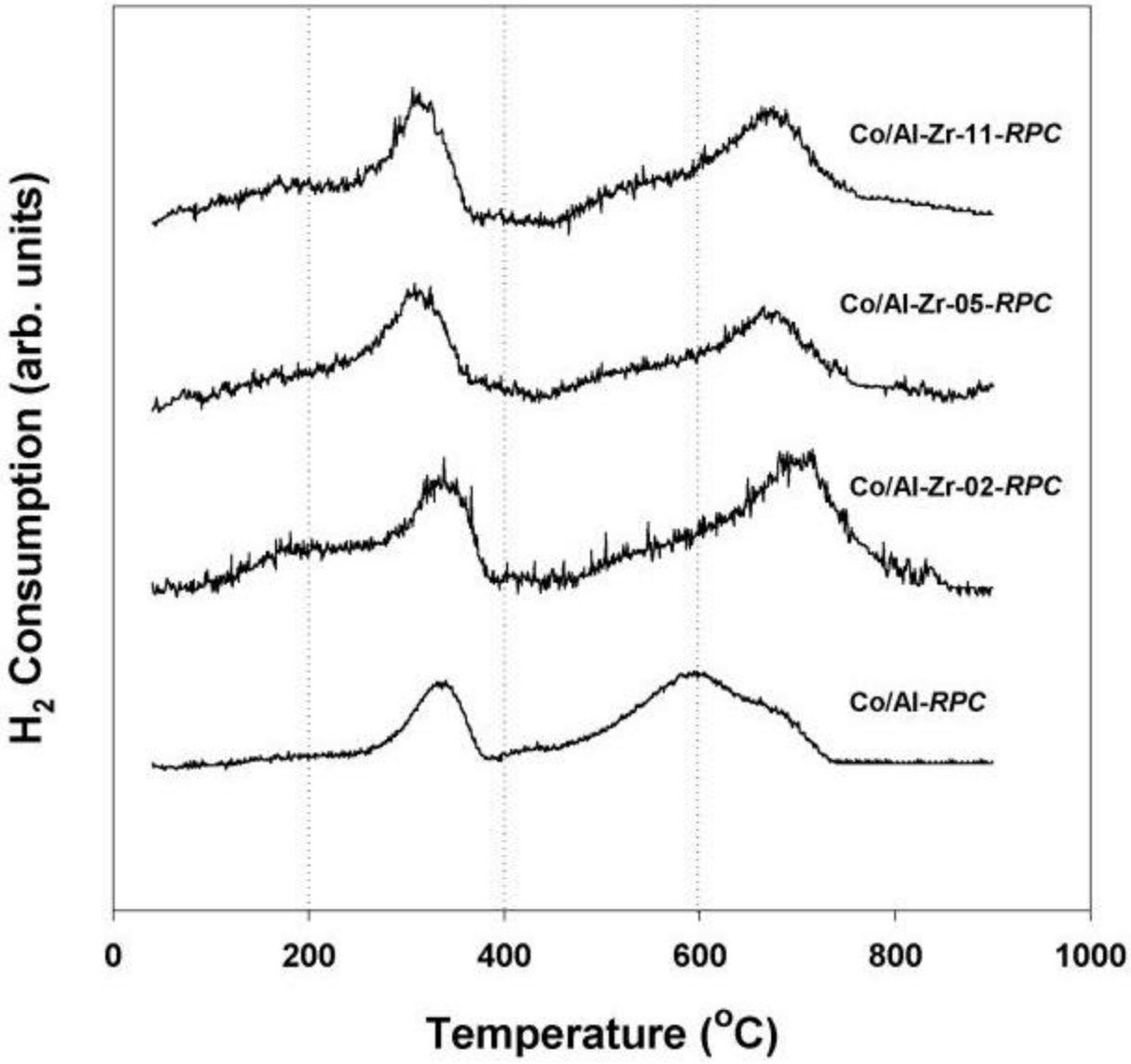

Figure 9.8 TPR Profiles of Co/Al-Zr-*RPC* Catalysts

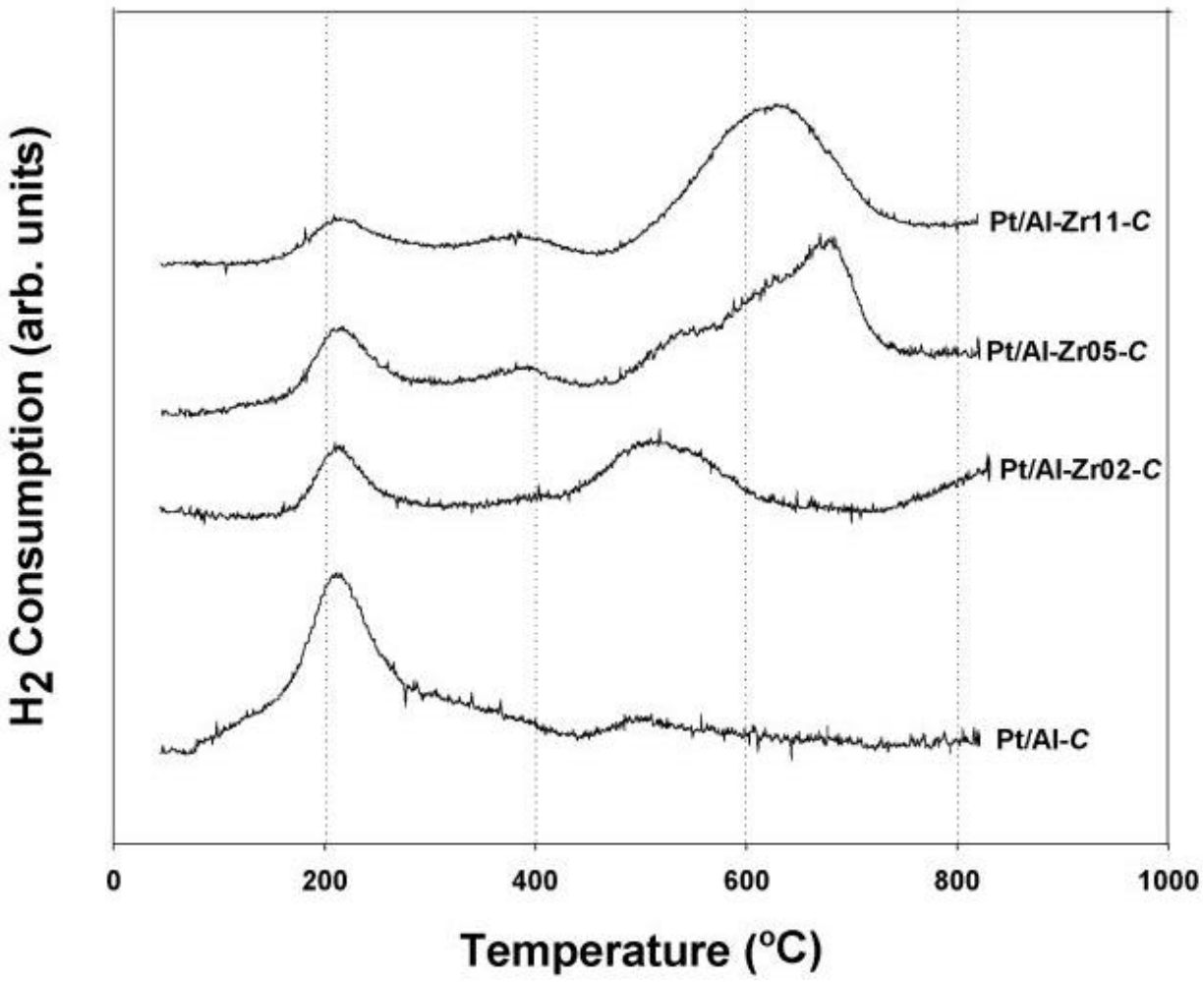

Figure 9.9 Effect of Pt on the Activation of ZrO_2

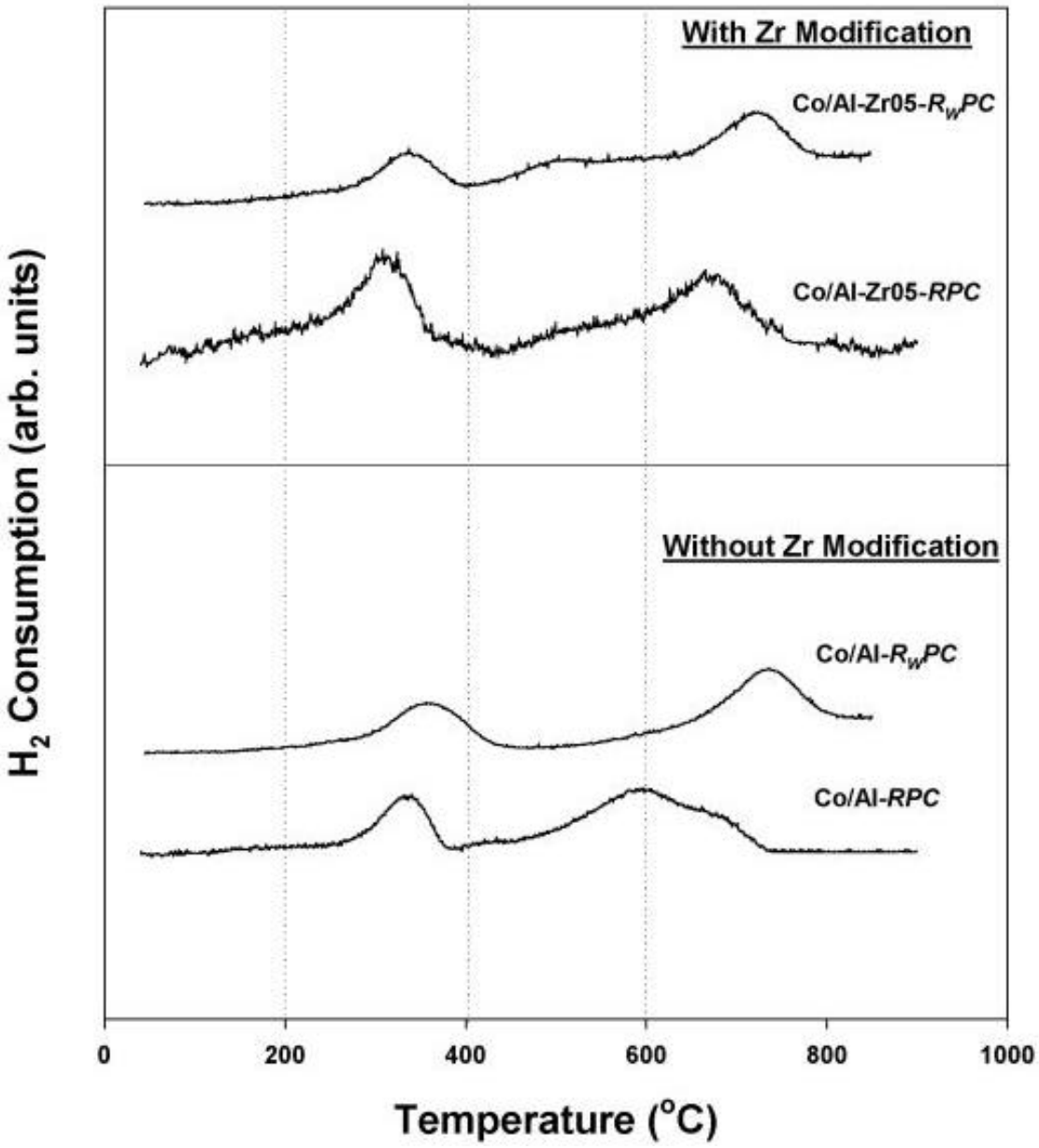

Figure 9.10 Effect of Water on TPR Behavior of Zr Modification Catalysts

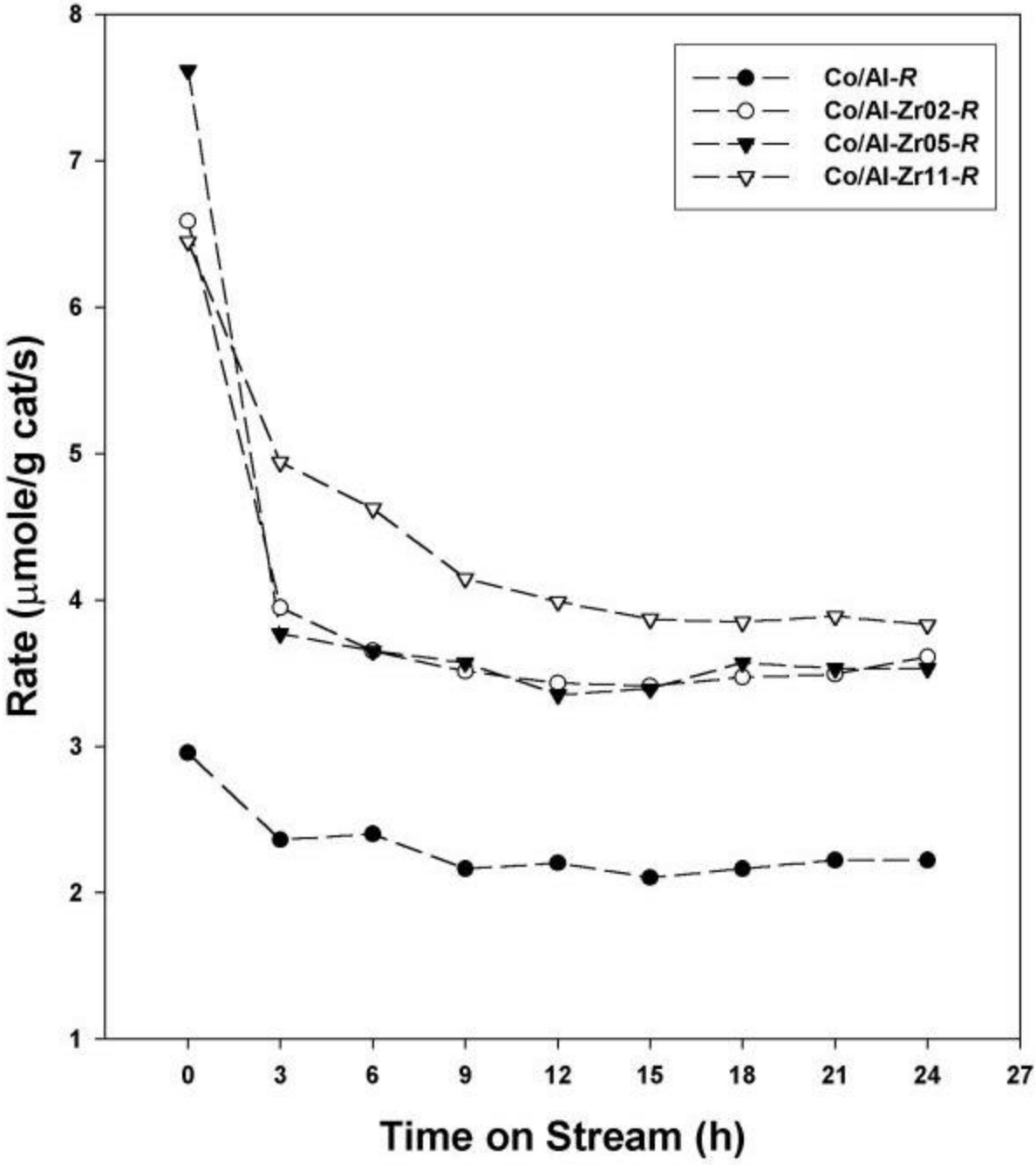

Figure 9.11 A Plot of Reaction Rate and TOS

10.0 SUMMARY

The presented studies focused on developing a better understanding of the nature of Co-support compound formation (Co-SCF) and how this compound formation can be minimized in order to stabilize the catalyst activity. Many characterization techniques were used to identify Co-SCF. Reaction rate during CO hydrogenation of the various pretreated catalyst samples was also measured to determine the catalyst activity.

The first portion of the dissertation focused on developing a better understanding of Co-SCF. It is very important to first fully understand the nature of Co-SCF prior to applying strategies to minimize this formation. Water vapor present during reduction has a major impact on alumina-supported Co catalysts resulting an increase in the amount of non-reducible Co "aluminate" (at temperatures $\leq 900^{o}C$) formed. This Co "aluminate" formed caused changes in the characteristics of Co catalysts, especially their reducibilities and overall activity during FTS. It is concluded that water vapor present during reduction possibly increases the amount of Co able to migrate into the alumina matrix forming a highly dispersed Co "aluminate" resulting in two broad Raman bands between 400-750 cm^{-1}. This surface Co "aluminate" formed is different from $CoAl_2O_4$ (spinel).

The addition of Ru promoter to Co catalysts increases both the overall Co dispersion and reducibility. It is suggested that the Ru promoter not only facilitates the reduction of Co a lower temperatures, but also decreases the formation of Co strongly interacting with the alumina and non-reducible Co "aluminate" by minimizing the impact of water vapor on this formation. It is highly possible that this minimization is due to the effect of reduction at lower temperatures.

One of strategies to minimize Co-SCF was to change the reduction gas compositions. The addition of carbon monoxide (CO) during standard H_2 reduction of Co/γ-Al_2O_3 catalyst produced specific activities about four times greater than when the catalyst was reduced without CO addition. Most of this increase appears to have been due to increases in Co reducibility and dispersion. In general, initial and steady-state rates of CO hydrogenation, Co reducibility, and Co dispersion went through a maximum for 3-5 vol% CO added during H_2 reduction. Carbon deposition was detected upon increasing the amount of added CO. The effect of CO addition may be due to one or more of possibly three reasons: (i) CO may help to prevent the formation of Co species strongly interacting with the support, thereby facilitating its reduction, (ii) CO may decrease sintering of the Co metal resulting in an increase in Co dispersion, and (iii) CO may block Co "aluminate" formation by minimizing the impact of water vapor even at low partial pressures. The effect of metal promoters, such as copper (Cu) and zirconia (Zr) on Co-SCF was also investigated.

Cu promotion resulted in increases in both metal reducibility and dispersion for Cu-promoted Co/γ-Al_2O_3 catalysts. It was found that the effect of Cu promotion depended upon both the amounts of Cu loading and the preparation method. The results indicate that a sequential impregnation is more effective for the preparation of Cu-promoted Co catalysts. However, based on reaction, FTS rate decreases with Cu addition probably due to a loss in active reduced surface Co atom exposure by Cu coverage.

Zr modification of the alumina support had a significant impact on the properties of Co/γ-Al_2O_3. The overall catalytic activity during FTS doubled upon Zr modification. Most of this increase appears to have been due to an increase in reducibility. The increase in reducibility appeared to have been caused by a decrease in the amount of non-reducible Co "aluminate", as

seen by Raman spectroscopy. Zr modification may have caused: (i) a stabilization the alumina support by limiting its defect sites, thus blocking Co "aluminate" formation, and/or (ii) a minimization of the impact of water vapor on modifying the surface properties of alumina, thereby decreasing the ease of Co migration into the alumina. Steady-state isotopic transient kinetic analysis (SSITKA) showed that the number of active reaction intermediates (N_M) increased with Zr modification while the intrinsic activity ($1/\tau_M$) remained constant.

APPENDIX

Appendix: Reducibility and Dispersion Calculation

A1. Reducibility Calculation

The area of peaks during TPR can be obtained based on 1 g of the calcined catalysts. For supported Co catalysts, it can be assumed that the major species of calcined Co catalysts is Co_3O_4. Based on 20 wt% of Co in the catalyst sample. The amount of H_2 that can be consumed by Co_3O_4 is calculated as follow:

MW: Co = 58.93 g/mole

Co_3O_4 = 240.79 g/mole

Based on 1 g of 20 wt% Co/γ-Al_2O_3

1 g of the reduced catalyst contains 0.2 g of Co = 0.00339 mole

Co_3O_4/Co = 1/3

Co_3O_4 = 1/3*Co mole

Co_3O_4 = [(1/3)*(0.00339)] mole

$Co_3O_4 + 4\ H_2 \rightarrow 3\ Co + 4\ H_2O$

Co_3O_4/H_2 = 1/4 mole

$H_2 = 4*Co_3O_4$ mole = [4*0.00113] mole

Thus, the amount of H_2 that can be consumed at 100% reducibility is 0.00452 mole.

Note: for Cu-promoted Co catalysts, the calcined form of Cu is CuO. Using the same method, it is found that 1 g of 5 wt% Cu/γ-Al_2O_3 can consume 0.00079 mole of H_2 (at 100% reducibility).

A2. Dispersion Calculation

A stoichiometry of $H/Co_s = 1$[(1)] (the amount of adsorbed H_2 is known from the experiment) and an average Co atom surface space of 6.62 $Å^2$ [(2)], the hydrogen chemisorption measurement is used to calculate the metal surface area per gram of catalyst, S:

$$S = [Co_s] \times (6.62\ Å^2) \times (10^{-20}\ m^2/Å^2)$$

Co_s = No. of Co surface atoms per gram catalyst

= No. of moles of H atoms adsorbed/g cat. = $(H_{2total} \times 2 \times 6.02 \times 10^{23})$

The dispersion (D) can be calculated by:

$$D\ (\%) = [(Co_s)/Co_{total}) \times 100]$$

Assuming that the metal particles to be cubic with 5 sides exposed to the gas phase, the relationship:

$$d_P = [5/(S' \times \rho_{Co})]$$

S' = Cobalt surface area per gram reduced cobalt in catalyst

For a 20 wt% Co catalyst

$$S' = S \times [(1\ \text{gram catalyst}/(0.2\ \text{gram cobalt} \times \text{reduced fraction of } Co^0)]$$

ρ_{Co} is the density of the Co which is 8.9 g/cc.

BIBLIOGRAPHY

BIBLIOGRAPHY

Chapter 1

1. Kogelbauer, A., Weber, J.C., and Goodwin, J.G., Jr., *Catal. Lett*. **34**, 259 (1995).
2. Schanke, D., Hilmen, A.M., Bergene, E., Kinnari, K., Rytter, E., Adnanes, E., and Holmen, A., *Catal. Lett*. **34**, 269 (1995).
3. Zhang, Y., Wei, D., Hammache, S., and Goodwin, J.G., Jr., *J. Catal*. **188**, 218 (1999).
4. Riva, R., Miessner, H., Vitali, R., and Piero, G.D., *Appl. Catal. A*. **196**, 111 (2000).
5. Bechara, R., Balloy, D., Dauphin, J.Y., and Grimblot, J., *Chem. Mater.* **11**, 1703 (1999).
6. Kraum, M., and Baerns, M., *Appl. Catal. A.* **186**, 189 (1999).
7. Ernst, B., Libs, S., Chaumette, P., and Kiennemann, A., *Appl. Catal. A* **186**, 145 (1999).
8. Jablonski, J.M., Wolcyrz, M., and Krajczyk, L., *J. Catal*. **173**, 530 (1998).
9. Ernst, B., Bensaddik, A., Hilaire, L, Chaumette, P., and Kiennemann, A., *Catal. Today* **39**, 329 (1998).
10. Ming, H., and Baker, B.G., *Appl. Catal. A.* **123**, 23 (1995).
11. Schanke, D., Hilmen, A.M., Bergene, E., Kinnari, K., Rytter, E. Adnanes, E., and Holmen, A., *Energy & Fuels* **10 (4)**, 867 (1996).
12. Chin, R.L., and Hercules, D.M., *J. Phys. Chem*. **86**, 360 (1982).
13. Backman, L.B., Rautiainen, A., Krause, A.O.I., and Lindblad, L., *Catal. Today* **43**, 11 (1998).
14. Greegor, R.B., Lytle, F.W., Chin, R.L., and Hercules, D.M., *J. Phys. Chem*. **85**, 1232 (1981).

15. Withers, H.P., Jr., Elierzer, K.F., and Mitchell, J.W., *Ind. Eng. Chem. Res.* **29**, 1807 (1990).

16. Iglesia, E., *Appl. Catal.A.* **161**, 59 (1997).

17. Brady, R.C., and Pettit, R.J., *J. Am. Chem Soc.* **103**, 1287 (1981).

Chapter 2

1. Satterfield, C.N., *Heterogeneous Catalysis in Industrial Practice,* 2nd, McGraw-Hill Inc. (1996).
2. Gormley, R. J., Zarochak, M.F., Deftenbaugh, P.W., and Rao, K.R.P.M., *Appl. Catal. A.* **161**, 263 (1997).
3. Iglesia, E., *Appl. Catal A.* **161**, 59 (1997).
4. Brady, R.C., and Pettit, R.J., *J. Am. Chem. Soc.* **103**, 1287 (1981).
5. Anderson, R.B., *The Fischer-Tropsch Synthesis (Academic Press, Orlando),* (1984).
6. Schanke, D., Hilmen, A.M., Bergene, E., Kinnari, K., Ryther, E., Adnanes, E., and Holmen, A., *Catal. Lett.* **34**, 269 (1995).
7. Chin, R.L., and Hercules, D.M., *J. Phys Chem.* **86**, 360 (1982).
8. Belambe, A.R., Oukaci, R., Goodwin, J.G., Jr., *J. Catal.* **166**, 8 (1997).
9. Hilmen, A.M., Schanke, D., and Holmen, A., *Catal. Lett.* **38**, 146 (1996).
10. Van de Loosdrencht, J., van der Harr, M., van der Kraah, A.M., van Dillen, A.J., Gens, J.W., *Appl. Catal A.* **150**, 365 (1997).
11. Schanke, D., Hilmen, A.M., Bergene, E., Kinnari, K., Rytter, E., Adnanes, E., and Holmen, A., *Energy & Fuels* **10 (4)**, 867 (1996).
12. Reuel, R.C., and Bartholomew, C.H., *J. Catal*. **85**, 63 (1984).
13. Reuel, R.C., and Bartholomew, C.H., *J. Catal.* **85**, 78 (1984).

14. Arnoldy, P., and Monlijn, J.A., *J. Catal.* **93**, 38 (1985).

15. Kogelbauer, A., Weber, J.C., and Goodwin, J.G., Jr., *Catal. Lett.* **34**, 259 (1995).

16. Iglesia, E., Soled, S.L., Fiato, R.A., and Via, G.H., *J. Catal.* **143**, 345 (1993).

17. Ho, S.W., Houalla, M., and Hercules, D.M., *J. Phys. Chem.* **94**, 6396 (1990).

18. Martens, J.H.A., Blik, V.H.F.J., and Prins, R., *J. Catal.* **97**, 200 (1986).

19. Keyser, M.J., Everson, R.C., and Espinoza, R.L., *Appl. Catal.A.* **171**, 99 (1998).

20. Noronha, F.B., Schmal, M., Nicot, C., Moraweck, B., and Freety, R., *J. Catal.* **168**, 42 (1997).

21. Bessell, S., *Appl. Catal. A.* **126**, 235 (1995).

22. Barthilomew, C.H., *Std. Surf. Sci. Catal.* **64**, 158 (1991).

23. Anderson, R.B., *The Fischer-Tropsch Synthesis (Academic Press, Orlando),* (1984).

24. Somojai, G.A., *Introduction to the Surface Chemistry and Catalyst*, John Wiley, Chap. 7 (1994).

25. Blik, V.H.F.J., and Prins, R., *J. Catal.* **97**, 188 (1986).

26. Goodwin, J.G., Jr., *Prep. Acs. Div. Petr. Chem.* **36 (1),** 156 (1991).

27. Kogelbauer, A, Goodwin, J.G., Jr., and Oukaci, R., *J. Catal.* **160**, 125 (1996).

28. Vada, S., Hoff, A., Adnanes, E., Schanke, D., Holmen, A., *Topics Catal.* **2**, 155 (1995).

29. Zhang, Y., Wei, D., Hammache, S., and Goodwin, J.G., Jr., *J. Catal.* **188**, 281 (1999).

30. Ali, S., Chen, B., and Goodwin, J.G., Jr., *J. Catal.* **157**, 35 (1995).

31. Haddad, G.J., Chen, B., and Goodwin. J.G., Jr., *J. Catal.* **160**, 43 (1996).

32. Blik, V.H.F.J., KÖningsberger, D.C., and Prins, R., *J. Catal.* **97**, 210 (1986).

33. Martens, J.H.A., Blik, V.H.F.J., and Prins, R., *J. Catal.* **97**, 200 (1986).

34. Schanke, D., Vada, S., Blekkan, E.A., Hilmen, A.M., Hoff, A., and Holmen, A., *J. Catal.* **156**, 85 (1995).

35. Tahenchi, K., Matsuzaki, T., Arakawa, H., Hanaoka, T., and Sugi, Y., *Appl. Catal.* **48**, 149 (1989).

36. Cimino, A., Logcono, M., and Schiavello, M., *J. Phys. Chem.* **79**, 243 (1975).

37. Pettit, F.S., Randklev, E.H., and Felten, E.J., *J. Am. Ceram. Soc.* **49**, 199 (1966).

38. Armijo, J.S., *Oxid. Met.* **1**, 171 (1969).

39. Minford, W.J., and Stubican, *J. Am. Ceram. Soc.* **57**, 363 (1974).

40. Hirato, K., and Komatsu, W., *J. Am. Ceram. Soc*. **60**, 105 (1977).

41. Schmalzried, H., *Solid Sate Reactions*, 2nd ed. Verlag Chemie, Weinheim, (1981).

42. Bolt, P.H., Habraken, F.H.P.M., and Geus, J.W., *J. Solid State Chem.* **135**, 59 (1998).

43. Lycourghiotis, A., Defosse, C., Delannay, F., Lemaitre, J., and Delmon, B., *J. Chem. Soc. Faraday* **76**, 1677 (1980).

44. Houalla, M., Lemaitre, J., and Delmon, B., *J. Chem. Soc. Faraday* **78**, 1389 (1982).

45. Houalla, M., Belannay, F., and Delmon, B., *J. Phys. Chem*. **85**, 1704 (1981).

46. Kordulis, C., Volisotis, S., Lycourghiotis, A., Vattia, D., and Delmon, B. *Appl. Catal. A.* **11**, 179 (1984).

47. Lycourghiotis, A., Vattis, D., and Aroni, P., *J. Phys. Chem.* **120**, 211 (1980).

48. Lo Jacono, M., Schiavello, M., DeBeer, V.H.J., and Minelli, G., *J. Phys. Chem*. **81**, 1583 (1977).

49. Muralidhar, G., Massoth, F.E. and Shabtai, J., *J. Catal.* **85**, 44 (1984).

50. Massoth, F.E., Muralidhar, G., and Shabtai, J., *J. Catal.* **85**, 53 (1984).

51. Lopez, F., Medina, H., Martinez, N., and Mitchell, P.C. H., *React. Kinet. Catal. Lett.* **22**, 253 (1983).

52. Chin, R.L., and Hercules, D.M., *J. Catal.* **74**, 121 (1982).

53. Fierro, J., Agudo, A., Grange, P., and Delmon, B., in "proceedings, 8th International Congress on Catalysis, Berlin, 1984, Vol.II, p. 363.

54. Stranick, M.A., Houalla, M., and Herculea, D.M., *J. Catal*. **104**, 396 (1987).

55. Rohr, F., Lindvag, O.A., Holmen, A., and Blekkan, E.A., *Catal. Today* **58**, 247 (2000).

56. Sharma, B.K., Sharma, M.P., Roy, S.K., Kumar, S., Tendulkar, S.B., Tembe, S.S., and Kulkarni, B.D., *Fuel* **77 (15),** 1763 (1998).

57. Marion, M.C., Garbowski, E., Primet, M., *J. Chem. Soc. Faraday Trans*. **86**, 3027 (1990).

58. Artizzu, P., Garbowski, E., Primet, M., Brulle, Y., and Saint-Just, J., *Catal. Today* **47**, 83 (1999).

Chapter 5

1. Kogelbauer, A., Goodwin, J.G., Jr., and Oukaci, R., *J. Catal.* **160**, 125 (1996).
2. Belambe, A.R., Oukaci, R., and Goodwin, J.G., Jr., *J. Catal.* **166**, 8 (1997).
3. Iglesia, E., Soled, S.L., and Fiato, R.A., *J. Catal.* **137**, 212 (1992).
4. Blik, V.H.F.J., Köningsberger, D.C., and Prins, R., *J. Catal.* **97**, 210 (1986).
5. Martens, J.H.A., Blik, V.H.F.J., and Prins, R., *J. Catal.* **97**, 200 (1986).
6. Schanke, D., Vada, S., Blekkan, E.A., Hilmen, A., Hoff, A., and Holmen, A.,*J. Catal.* **156**, 85 (1995).
7. Takeuchi, K., Matsuzaki, T., Arakawa, H., Hanaoka, T., and Sugi, Y., *Appl. Catal. A.* **48**, 149 (1989).

8. Vada, S., Hoff, A., Adnanes, E., Schanke, D., and Holmen, A., *Topics Catal*. **2**, 155 (1995).

9. Iglesia, E., Soled, S.L., Fiato, R.A., and Via, G.H., *J. Catal.* **143**, 345 (1993).

10. Shpiro, E.S., Tkachenko, O.P., Belyatskii, V.N., Rudnyi, Y., Telegina, N.S. Panov, S.Y., Gryaznov, V.M., and Minachev, K.M., *Kinet. Catal.* **31**, 832 (1990).

11. Goodwin, J.G., Jr., Prep. *Acs. Div. Petr. Chem*. **36 (1)**, 156 (1991).

12. Zhang, Y., Wei, D., Hammache, S., and Goodwin, J.G., Jr., *J Catal.* **188**, 281 (1999).

13. Reuel, R.C., and Bartholomew, C.H., *J. Catal.* **85**, 63 (1984).

14. Ohtsuka, H., Tabata, T., Okada, O., Sabatino, L.M.F., and Bellussi, G., *Catal. Today* **42**, 45 (1998).

15. Li, J., and Coville, N.J., *Appl. Catal. A.* **181**, 201 (1999).

16. Sexton, B.A., Hughes, A.E., and Turney, T.W., *J. Catal.* **97**, 390 (1986).

17. Arnoldy, P., and Moulijn, J.A., *J. Catal.* **93**, 38 (1985).

18. Hilmen, A.M., Schanke, D., and Holmen, A., *Catal. Lett.* **38**, 143 (1996).

19. Wang, W., and Chen, Y., *Appl. Catal. A.* **77**, 223 (1991).

20. Lapidus, A., Krylova, A., Kazanskii, V., Borovknov, Z., Ratnousky, J., Zukal, A.,Jan, M.C., *Appl. Catal. A.* **73**, 65 (1991).

21. Delmon, B., and Roman, A., *J. Catal.* **30**, 333 (1973).

22. Houalla, M., Delannay, F., Matsuura, I., and Delmon, B., *J. Chem. Soc. Faraday Trans.* **176**, 2128 (1980).

23. Mile, B., Stirling, D., Zammitt, M., Lovell, A., and Webb, M., *J. Catal.* **144**, 217 (1988).

24. Van'T Blik, H.F.J., and Prins, R., *J. Catal.* **97**, 188 (1986).

25. Hurst, N.W., Gentry, S.J., Jones, A., and McNicol, B.D., *Catal. Rev. Sci. Eng*. **24(2)**, 233 (1982).

26. Betancourt, P., Rives, A., Hubaut, R., Scott, C.E., and Goldwasser, J., *Appl. Catal. A*. **170**, 307 (1998).

Chapter 6

1. CRC Press, Inc., "CRC Handbook of Chemistry and Physic", Weast, R.C., Astle, M.J., and Beyer, W.H., Boca Raton, Florida, 64th edition, p. B86-87, 1983-84.
2. Jongsomjit, B., Panpranot, J., and Goodwin, J.G., Jr., *J. Catal*. **204**, 98 (2001).

Chapter 7

1. Zhang, Y., Wei, D., Hammache, S., and Goodwin, J.G., Jr., *J. Catal*. **188**, 218 (1999).
2. Jongsomjit, B., Panpranot, J, and Goodwin, J.G., Jr., *J. Catal*. **204**, 98 (2001).
3. Reuel, R.C., and Bartholomew, C.H., *J. Catal.* **85**, 63 (1984).
4. Kogelbauer, A., Goodwin, J.G., Jr., and Oukaci, R., *J. Catal.* **160**, 125 (1996).
5. Schanke, D., Vada, S., Blekkan, E.A., Hilmen, A.M., Hoff, A., and Holmen, A., *J. Catal*. **156**, 85 (1995).
6. Arnoldy, P., and Moulijn, J.A., *J. Catal*. **93**, 38 (1985).
7. Hilmen, A.M., Schanke, D., and Holmen, A., *Catal. Lett*. **38**, 143 (1996).
8. Bahr, H.A., and Jessen, V., *Ber.* **63B 2**, 226 (1930).
9. Hadad, G.J., Chen, B., and Goodwin, J.G., Jr., *J. Catal*. **161**, 274 (1996).
10. Belambe A.R., Oukaci, R., and Goodwin, J.G., Jr., *J. Catal.* **166**, 8 (1997).
11. Anderson, J.R., *Structure of Metallic Catalysts*, Academic Press, New York (1975).

Chapter 8

1. Zhang, Y., Wei, D., Hammache, S, and Goodwin, J.G., Jr., *J. Catal*. **188**, 218 (1999).
2. Iglesia, E., Soled, S.L., and Fiato, R.A., *J. Catal.* **137**, 212 (1992).
3. Belambe, A.R., Oukaci, R., and Goodwin, J.G., Jr., *J. Catal*.**166**, 8 (1997).
4. Kogelbauer, A., Goodwin. J.G., Jr., and Oukaci, R., *J. Catal.* **160**, 125 (1996).
5. Ali, S., Chen, B., and Goodwin, J.G., Jr., *J. Catal.* **157**, 35 (1995).
6. Rohr, F., Lindvag, O.A., Holmen, A., and Blekkan, E.A., *Catal. Today* **58**, 247 (2000).
7. Haddad, G.J., Chen, B., and Goodwin, J.G., Jr., *J. Catal.* **160**, 43 (1996).
8. Blik, V.H.F.J., Köningsberger, D.C., and Prins, R., *J. Catal*. **97**, 210 (1986).
9. Martens, J.H.A., Blik, V.H.F.J., and Prins, R., *J. Catal.* **97**, 200 (1986).
10. Blik, V.H.F.J., and Prins, R., *J. Catal*. **97**, 188 (1986).
11. Stranick, M.A., Houalla, and Hercules, D.M., *J. Catal.* **104**, 396 (1987).
12. Schanke, D., Vada, S., Blekkan, E.A., Hilmen, A.M., Hoff, A., and Holmen, A., *J. Catal.* **156**, 85 (1995).
13. Bolt, P.H., Habraken, F.H.P.M., and Gens, J.W., *J. Solid State Chem.* **135**, 59 (1998).
14. Massalski, T.B., Binary Alloy Phase Diagrams, vol. 1, American Society for Metals, 1st edition, Metals Park, Ohio, 1986.
15. Reuel, R.C., and Bartholomew, C.H., *J. Catal*. **85**, 63 (1984).
16. Brands, D.S., Poels, E.K., and Bliek, A., *Appl. Catal. A.* **184**, 279 (1999).
17. Arnoldy, P. and Moulijn, J.A., *J. Catal.* **93**, 38 (1985).
18. Hilmen, A.M., Schanke, D., and Holmen, A., *Catal. Lett*. **38**, 143 (1996).
19. Iglesia, E., Soled, S.L., Fiato, R.A., and Via, G.H., *J. Catal*. **143**, 345 (1993).

20. Schwab, G.M., in "Catalysis Science and Technology" J.R. Anderson and M. Boudart, Vol. 2, Chap. 1, Springer-Verlag, New York, 1981.

21. Cimino, A., Logcono, M., and Schiavello, M., *J. Phys. Chem*. **79**, 243 (1975).

22. Lo Jacono, M., Schiavello, M., DeBeer, V.H.J., and Minelli, G., *J. Phys. Chem*. **81**, 1583 (1977).

23. Muralidhar, G., Massoth, F.E., and Shabtai, J., *J. Catal*. **85**, 44 (1984).

24. Massoth, F.E., Muralidhar, G., and Shabtai, J., *J. Catal*. **85**, 53 (1984).

25. Lopez, F., Medina, H., Martinez, N., and Mitchell, P.C.H., *React. Kinet. Catal. Lett*. **22**, 253 (1983).

26. Chin, R.L., and Hercules, D.M., *J. Catal*. **74**, 121 (1982).

27. Fierro, J., Agudo, A., Grange, P., and Delmon, B., in "Proceeding 8th International Congress on Catalysis, Berlin, 1984, Vol. II, p. 363.

28. Stranick, M.A., Houalla, M., and Hercules, D.M., *J. Catal*. **104**, 396 (1987).

29. Garbowski, E., and Primet, M., *J. Chem. Soc. Chem. Commun*. **1**, 11 (1991).

30. Marion, M.C., Garbowski, E., and Primet, M., *J. Chem. Soc. Faraday Trans*. **86**, 3027 (1990).

31. Kingery, W.D., Introduction to Ceramics, Wiley, New York, 1960

32. Chen, B., and Goodwin, J.G., Jr., *J. Catal*. **148**, 409 (1994).

33. Chen, B., and Goodwin, J.G., Jr., *J. Catal*. **158**, 228 (1996).

34. Chen, B., and Goodwin, J.G., Jr., *J. Catal*. **158**, 511 (1996).

Chapter 9

1. Iglesia, E., Soled, S.L., and Fiato, F.A., *J. Catal.* **137**, 212 (1992).
2. Belambe, A.R., Oukaci, R., and Goodwin, J.G., Jr., *J. Catal.***166**, 8 (1997).
3. Kogelbauer, A., Goodwin. J.G., Jr., and Oukaci, R., *J. Catal.* **160**, 125 (1996).
4. Ali, S., Chen, B., and Goodwin, J.G., Jr., *J. Catal.* **157**, 35 (1995).
5. Rohr, F., Lindvag, O.A., Holmen, A., and Blekkan, E.A., *Catal. Today* **58**, 247 (2000).
6. Haddad, G.J., Chen, B., and Goodwin, J.G., Jr., *J. Catal.* **160**, 43 (1996).
7. Blik, V.H.F.J., Köningsberger, D.C., and Prins, R., *J. Catal*. **97**, 210 (1986).
8. Martens, J.H.A., Blik, V.H.F.J., and Prins, R., *J. Catal.* **97**, 200 (1986).
9. Blik, V.H.F.J., and Prins, R., *J. Catal*. **97**, 188 (1986).
10. Stranick, M.A., Houalla, and Hercules, D.M., *J. Catal.* **104**, 396 (1987).
11. Schanke, D., Vada, S., Blekkan, E.A., Hilmen, A.M., Hoff, A., and Holmen, A., *J. Catal.* **156**, 85 (1995).
12. Lycourghiotis, A., Defosse, C., Delannay, F., Lemaitre, J., and Delmon. B., *J. Chem. Soc. Faraday Trans.* **76**, 1677 (1980).
13. Houalla, M., Lemaitre, J., and Delmon, B., *J. Chem. Soc. Faraday Trans.* **78**, 1389 (1982).
14. Houalla, M., Delannay, F., and Delmon, B., *J. Phys. Chem.* **85**, 1704 (1981).
15. Cimino, A., Logcono, M., and Schiavello, M., *J. Phys. Chem.* **79**, 243 (1975).
16. Lo Jacono, M., Schiavello, M., DeBeer, V.H.J., and Minelli, G., *J. Phys. Chem.* **81**, 1583 (1977).
17. Muralidhar, G., Massoth, F.E., and Shabtai, J., *J. Catal.* **85**, 44 (1984).
18. Massoth, F.E., Muralidhar, G., and Shabtai, J., *J. Catal.* **85**, 53 (1984).
19. Chin, R.L., and Hercules, D.M., *J. Catal.* **74**, 121 (1982).

20. Sharma, B.K., Sharma, M.P., Roy, S.K., Kumar, S., Tendulkar, S.B., Tembe, S.S., and Kulkarni, B.D., *Fuel* **77 (15)**, 1763 (1998).

21. Post, M.F., and Sie, S.T.B., European Patent Application 0167 215 A2, 1985.

22. Hoek, A., Joustra, A.H., Minderhould, J.K., and Post, M.F., UK Patent Application GB 2 125 062 A, 1983.

23. Reuel, R.C., and Bartholomew, C.H., *J. Catal.* **85**, 63 (1984).

24. Jongsomjit, B., Panpranot, J., and Goodwin, J.G., Jr., *J. Catal*. **204**, 98 (2001).

25. Liu, Z., Dong. L., Ji, W., and Chen, Y., *J. Chem. Soc. Faraday Trans*. **94 (8)**, 1137 (1998).

26. Arnoldy, P., and Moulijn, J.A., *J. Catal*. **93**, 38 (1985).

27. Hilmen, A.M., Schanke, D., and Holmen, A., *Catal. Lett*. **38**, 143 (1996).

28. Zhang, Y., Wei, D., Hammache, S., and Goodwin, J.G., Jr., *J. Catal*. **188**, 218 (1999).

29. Shannon, S.L., and Goodwin, J.G., Jr., *Chem. Rev*. **95**, 677 (1995).

Appendix

1. Reuel, R.C., and Bartholomew, C.H., *J. Catal*. **85**, 107 (1983).

2. Anderson, J.R., *Structure of Metallic Catalysts*, Academic Press, New York, 1975.